MODELING THE FLUID TO SOLID TRANSITION IN CEMENT PASTE, MORTAR, AND CONCRETE

A Dissertation

Presented to the Faculty of the Graduate School

of Cornell University

in Partial Fulfillment of the Requirements for the Degree of

Doctor of Philosophy

by

Chang Hoon Lee

January 2014

MODELING THE FLUID TO SOLID TRANSITION IN CEMENT PASTE, MORTAR, AND CONCRETE

Chang Hoon Lee, Ph.D.

Cornell University 2014

This research proposes a framework for modeling the fluid-to-solid transition of cement paste, mortar, and concrete by application of generalized mathematical growth models. In the general case growth models are applied to mechanisms such as ontogenesis, chemical reactions, ecological systems (such as population growth or predator-prey relationship), and so on. In this specific research the models correlate an internal growth mechanism with a variety of externally observable outcomes that include stiffening as measured by penetration resistance and compressive strength. The primary focus is on correlating or predicting the outcomes rather than on the internal growth mechanism itself, which in this case is the hydration of Portland cement. Also, the proposed framework makes it possible to predict the strength of concrete considering the strength degradation because of high concrete temperature by using five Arrhenius-type equations that can represent nonlinearity in Arrhenius plot. In addition, the growth model was applied to represent setting behaviors of paste, mortar, and concrete, and the quantitative characterization of the setting behaviors is investigated. Also, the difference in setting behaviors of sieved and prepared mortars is examined with quantifying the paste content and aggregate grading in the mortars.

BIOGRAPHICAL SKETCH

The author was born on May 10, 1975 in Seoul, Korea. After his graduation from Sun-Duk high school in 1994, the author enrolled at the Korea University in Korea. At Korea University, he majored in Civil and Environmental Engineering and obtained Bachelor's degree in 1998. In his junior and senior years of undergraduate years, he joined ROTC program and was commissioned as a second lieutenant in 1998.

The author served in Korean Army for two and half years as an engineering officer. After he retired from Korean Army as lieutenant, the author attended graduate school to achieve an Master of Science in Korea university. For Master of Science study, the author worked for developing 3-dimensional strut-and-tie model that applied to design diaphragms in prestressed concrete box girder bridges.

Following his Master of Science, the author worked at the Disaster Prevention Science and Technology as a researcher until 2005, and he performed various projects associated with concrete materials and structures. The author the moved to Ithaca, NY in 2005 to pursue doctoral studies in the School of Civil and Environmental Engineering in Cornell University.

This dissertation is dedicated to
my father, Jong-Won Lee,
my mother, Kum-Ja Kim,
and my wife, Sang-Hee Park.

Without their love, support, and faith,
this achievement would never been possible.

ACKNOWLEDGEMENTS

First and foremost, I would like to thank my greatest advisor and mentor, Professor Kenneth Hover, for his guidance of this research and his lessons about life. His enthusiasm and dedication made this work different, and his support and patience enabled me to accomplish this work. Especially, I have enjoyed having discussions with Professor Hover about countless ideas, called "rabbit hunting", and it was extremely helpful to flourish this work.

I am very thankful to Professor Mircea Grigoriu not only for serving in my committee, but also for providing me an opportunity to work on the project, "Development of Bayesian Fragility." Such experience was a great chance to learn probabilistic modeling and to improve this research in the future.

I greatly appreciate Professor Richard Hennig in Material Science and Engineering. It would have been impossible to understand the material science aspects of this research without his advice and comments.

I wish to acknowlege Professor Wilkins Aquino for his reviews and comments on this research as a committee member. Also, I thank Professor Christopher Earls and Professor Derek Warner for their advice on this research and my career.

I am very grateful to the assistants who have participated in this work. Anna Lee was always willing to help the experiments, and her carefulness and precise techniques to handle concretes were very helpful to create delicate data sets of this research. Also, I wish to thank Hannah Kiem for helping continuous setting experiments for the spring semester, 2010.

The experiments for this research would not have beeen possible without Tim Bond who always solved any technical issues and gave ideas to set up the complicated experiments. Also, I would also like to express my gratitude to

Nadine Porter for her kindness, prayer and support. She made my mind in peace whenever I was in concerns.

I owe many thanks to graduate students who accompanied me through good and difficult times. They include Alin Radu, Haoran Zhao, Sepher Saroukhani and Nathan Harris. Each of them was always ready to share ideas and to have discussion probabilities, concretes, mathematics, mechanics, software, and other random topics. I wish them all the best in their careers.

Special thanks also go to my previous advisor Dr. Young Soon Yoon in Korea University for encouraging me to pursue doctoral studies.

I greatly and truly appreciate my father Jong-Won Lee, my mother Kum-Ja Kim, and my sister Eun Kyung Lee. They always believed and encouraged me to accomplish this work. Especially, I deeply thank my dad with whole my heart for his life lessons that made me to be patient and overcome all challenges that I have confronted in the work and the life.

I have been very fortunate to meet my wife, Sang Hee Park, at Cornell, and I am very grateful for her support and patience. She is my best wife, friend, and colleague. Without her tolerance, it would have been impossible to accomplish this work.

TABLE OF CONTENTS

LIST OF TABLES

LIST OF FIGURES

CHAPTER 1

INTRODUCTION

This research proposes a framework for modeling the fluid-to-solid transition of cement paste, mortar, and concrete by application of generalized mathematical growth models. In the general case growth models are applied to mechanisms such as ontogenesis, chemical reactions, ecological systems (such as population growth or predator-prey models), and so on. In this specific research the models correlate an internal growth mechanism with a variety of externally observable outcomes that include stiffening as measured by penetration resistance and compressive strength. The primary focus is on correlating or predicting the outcomes rather than on the internal growth mechanism itself, which in this case is the hydration of Portland cement.

As the cement hydrates, (a micro-scale process that begins shortly after the mixing process is initiated), a number of external, macroscopic behaviors are observed during the ensuing hours and days. These macro-phenomena begin with a reduction in fluidity (or "workability") known as "slump-loss," as measured by ASTM C143 (Slump of Hydraulic-Cement Concrete). The rate of slump loss (and all of the mechanisms to be discussed) depends on mixture composition and temperature. About the time the concrete has very little fluidity as indicated by the slump test ("zero slump"), (which is also the time at which the slump can no longer provide useful information about the fluid to solid transition), mortar sieved from the concrete can be evaluated by measuring the pressure required to insert probes of various sizes to a prescribed depth. The primary standard for this procedure is the ASTM C403 test ("Time of Setting of Concrete Mixtures by Penetration Resistance"). About the time that it

is impractical to use the hand-held penetration device to insert a probe ("time of final setting" in the terminology of C403) it becomes possible to measure the continuing growth of compressive strength of the concrete by means of ASTM C39 ("Compressive Strength of Cylindrical Concrete Specimens"). It is generally observed that concrete gains strength rapidly in its early hours and days, with a rate of strength gain that diminishes with time. While ASTM procedures C143, C403, and C39 are very different from each other, employing equipment and techniques that are seemingly unrelated, each method provides a means of monitoring the growth of chemical and physical bonds that are developing as a result of the hydration of the Portland cement. As such, slump loss, setting, and strength gain are each manifestations of the same fundamental growth process.

The ability to understand this growth process and to make predictions for how it is affected by mixture composition and temperature are critical for the control of construction operations such concrete batching and delivery, placing, consolidation, finishing, and the subsequent provision of a favorable curing environment for the development of hardened concrete properties. Such prediction and control has been done primarily via empirical methods, developed over years of experience in many different environments. This work seeks to rationalize prediction and control on the basis of generalized growth models that provide a framework for connecting kinetics of cement hydration (via hydration rate constants, for example) to setting behavior and strength development, accompanied by a generalized form for accounting for the effects of temperature.

The dissertation therefore consists of six chapters including Chapter 1, introduction. Chapter 2 proposes a framework for predicting concrete strength con-

sidering temperature and time effects, based largely on the Bertalanffy growth model. This function has been adopted to represent concrete strength development on the basis of similarities between the growth of biological species and the development of concrete properties. The mathematical flexibility of the Bertalanffy model is introduced, and the temperature dependency of model parameters of the Bertalanffy model is represented by several functions including the Arrhenius equation with the advantage of enabling use of a nonlinear Arrhenius plot. Eventually, this research provides a closed-form function to represent the temperature dependency of the limiting strength. In addition, the proposed framework makes it possible to consider effects of strength degradation due to higher curing temperatures in the strength predictions. This is particularly applicable useful for concretes exposed to high temperature where the so-called "cross-over effect" is likely to occur, in which the strength-gain benefits of early-age high temperature curing have to be balanced against the accompanying reduction in later-age strength.

Chapter 3 continues the discussion of concrete strength as a function of time, temperature, available moisture, and the unique composition of the concrete mixture by expanding on what has been standardized as ASTM C1074 ("Estimating Concrete Strength by the Maturity Method"). As standardized by C1074, temperature sensitivity of a given mixture can be characterized by Datum Temperature (based on the Nurse-Saul method) or by Activation Energy (as proposed by Freiesleben Hansen-Pederson). While these methods and their defining parameters were independently developed, the parameters are nevertheless interdependent as a change in a concrete mixture that affects temperature sensitivity as expressed by Datum Temperature will also be reflected in a change of Activation Energy, and vice versa. Therefore, Chapter 3 further devel-

ops Carino's exploration of the relationship between Datum Temperature and Activation Energy, suggesting alternative approaches by which an appropriate value of one can be calculated from the other for any given range and profile of expected concrete temperatures.

Chapter 4 explores and quantifies the effects of experimental and procedural details in the ASTM C403 test ("Time of Setting of Concrete Mixtures by Penetration Resistance"), by focusing on the quantitative significance of the note in C403 that "initial and final setting times may be increased when using the prepared mortar." The setting time of concrete as measured by ASTM C403 is determined from the penetration resistance of mortar extracted from concrete by removing coarse aggregates larger than the $4.75\ mm$ (#4) sieve. Tests by the authors and others have shown a difference in penetration resistance obtained from mortars extracted from concrete compared with penetration resistance of mortar intentionally mixed to represent the mortar fraction of the concrete of interest, as is noted qualitatively in C403. The authors report this difference quantitatively, having observed or discovered in the literature prepared mortars with an initial setting time up to 6–16% greater than that of sieved mortar, and final setting time that is up to 3–16% greater than that of sieved mortar. In general these differences are 1 to 3 times greater than the single operator precision for acceptable range of test results, and are thus significant in the context of C403.

Chapter 5 further explores and quantifies the effects of experimental and procedural details in ASTM C403 by identifying and measuring changes in paste content and aggregate grading that are brought about by the required sieving process. This is important because setting of concrete is measured by

ASTM C403 via penetration resistance of mortar extracted from concrete by removing coarse aggregates larger than the $4.75\ mm$ (#4) sieve. However, C403 is sometimes performed on mortar prepared to represent the mortar fraction of the concrete in question, thus avoiding the time-and-labor intensive sieving operation. As discussed in Chapter 4, C403 notes that "setting times may be increased when using the prepared mortar." The authors previously reported this difference quantitatively, having observed or discovered in the literature prepared mortars with an initial setting time up to 8–14% greater than that of sieved mortar, and final setting time 5–16% greater than that of sieved mortar. These differences are 1 to 3 times greater than the single operator precision for acceptable range of test results, and are thus significant in the context of C403. The authors propose that this difference is associated with the reduction in paste content in the mortar that accompanies the sieving operation, having observed a 3 to 8% paste volume reduction in sieved mortar. The authors suggest a general correlation between changes in setting time as a function of changes in paste content.

Chapter 6 augments the work on setting from the Chapters 4 and 5 by synthesizing the experimentally observed penetration resistance of cement pastes, mortars, and concrete. That it is reasonable to expect such a synthesis is supported by the overall objective of the research program, i.e., that the hydration of Portland cement is a single growth mechanism that drives the fluid-to-solid transition that is measured by multiple means. Having proposed this hypothesis, it is therefore necessary to show how the independently evaluated penetration resistance of paste, mortar, and concrete relate to each other, given that they all share the same Portland cement paste and are thus driven by the same hydration mechanism. To accomplish this it was necessary to examine the setting

behavior of two concrete mixtures by means of standard laboratory setting tests, a proposed modified C403 test, and several non-standard, yet common variations on indicators used in the field to monitor stiffening of a concrete surface over time. Behavior of the concrete mixtures is shown against the background of the time-dependent penetration behavior as measured by ASTM C191("Time of Setting of Hydraulic Cement by Vicat Needle"), as well as by ASTM C403 tests on mortar. Further, the ability to consolidate the same concrete, deform the concrete surface, create impressions in the surface, and to restore deformations and surface defects with a hand-float is plotted against the background of the standard setting time tests. The paper derived from this chapter integrates prior studies, suggests complicating factors for correlating standard setting tests and field observations, and proposes a useful framework for establishing mixture- and application-specific correlations.

CHAPTER 2

CONCRETE MATURITY METHOD WITH GENERALIZED BERTALANFFY GROWTH MODEL

2.1 Introduction

Jones and Chapman [6] reported that the growth of biological materials is determined by genetic factors that have inherited from previous generations and environmental effects such as nutrient supplies. Similarly, the property development (or growth) of concrete is influenced not only by mixture proportions equivalent with the genetic factor in biological growth but also by temperature and relative humidity of environmental effects. On the other hand, the growth of living species is limited if at least one of contributing sources to the growth reaches to its maximum as stated by Liebig's law of the minimum[7]. Likewise, as reported by Bullard et al. [8], either water or cement for a given concrete mixture has been locally or entirely depleted by the hydration, subsequently the concrete strength reaches to the potential maximum value. Therefore, it is possible to adopt the similarities of fundamental characteristics of biological growth to model the concrete property development, although details of growth mechanisms are different.

Bertalanffy [9] proposed the mathematical model to represent the growth of living organisms via metabolism. The model is based on the assumptions that the growth rate is determined by the net rates between anabolism and catabolism. The anabolic metabolism depends on its characteristics of metabolism (isometric or allometric) according to species, and the catabolism term is assumed to be linearly proportional to the mass with time. Sub-

sequently, the model has been applied to the growth of various species in biology.[10, 11, 12] For example, Vaidya[13] examined several growth functions to model tumor growths in human and mouse and reported that the Bertalanffy model showed higher goodness-of-fit with the data of mouse tumor (sarcoma) than exponential, Gompertz, and logistics models. Also, Zullinger et al. [14] investigated applicability of Bertalanffy, Gompertz, and logistics models to mammalian growths and stated that Bertalanffy model caused the lowest mean square error in large number of data sets.

Richards [15] showed the mathematical flexibility of Bertalanffy model by explaining that monomolecular, logistics, and Gompertz models can be represented by the Bertalanffy model with varying exponent values, also Tjørve and Tjørve [16] reported the Bertalanffy model could unify several sigmoid growth curves via re-parameterization of the functions. Such flexibility of the model enables the Bertalanffy model to extend its application to other fields. Pienaar and Turnbull [10] applied the examined the Richards curve (or the generalized Bertalanffy model) with the unknown exponent n to model the basal area of even-aged coniferous monocultures and reported that the exponent which induce the best-fit is smaller than $2/3$. Also, Marinakis [17] applied Richards curve to represent the technological diffusion from the data source. In concrete technology, Bernhardt [18] also empirically proposed the function for the strength development considering temperature effects. For a given concrete temperature T, the rate of strength development is expressed by

$$\frac{dP}{dt} = P_u \cdot k(T) \left(1 - \frac{P}{P_u}\right)^m \tag{2.1}$$

where P is temperature at time t, T is temperature, and m is a model constant. If $m = 1$ in Eq.(2.1), the model is identical to the generalized Bertalanffy model with unity of the exponent, although it is not mentioned by the author. It is

noted that the solution of Eq.(2.1) with $m = 2$ is adopted by ASTM C 1074 [19] to compute the rate constant for the strength development, $k(T)$. Therefore, it is possible that the Bertalanffy model can be a replacement of the hyperbolic function if the temperature dependency of the Bertalanffy model's parameters can be explicitly correlated with the specified functions such as Arrhenius equation.

By Freiesleben Hansen and Pederson (FHP) method [20], the rate constant $k(T)$ is assumed to follow Arrhenius equation [21]; that is, there is a linear relation between log-transformed rate constant ($\ln k$) and reciprocal temperature ($1/T$). From the estimated linear relation, a constant activation energy can be estimated to represent the temperature sensitivity of rate constant of a given mixture of concrete for its strength development. However, temperature and degree of hydration (or time) dependent activation energy have been reported by several research [22, 23, 24], especially temperature dependent activation energy indicates the nonlinear relation between $\ln k$ and $1/T$ on Arrhenius plot. Such a nonlinearity of Arrhenius plot was also reported in chemistry field of study if complex reactions occur with multiple steps, chains, and slow speeds [25] and in the biological process[26], also several research have been performed to regard such a nonlinearity of Arrhenius plot in the fields of study [27, 28, 29]. However, it is noted that Arrhenius equation is empirically proposed on the basis of the reaction of ideal gas [30], especially, Galwey and Brown [31] criticized application of Arrhenius equation to solid state kinetics. Also, nonlinear pattern of microbial growth rate on Arrhenius plot is observed by Huang et al. [32]. Subsequently, it would be true that there is no rigorous rule to keep the linear relation on Arrhenius plot for rate constants representing complex rate mechanisms, particularly rate constants for concrete strength developments.

In addition, the higher concrete temperature, the greater is maturity at any time computed from the given temperature-time profile with a constant activation energy as well as the relatively higher strength is predicted. In contrast, the strength degradation at later age, called cross-over effects, occurs due to higher concrete temperature at early age, and its mechanisms has been studied by several researchers. [33, 34, 35, 36] Therefore, because of such a conflict, the maturity method cannot explicitly consider the strength degradation by neither FHP nor Nurse-Saul [37, 38] (NS) maturity methods [39].

Therefore, the new framework of maturity method is proposed to predict the strength by using the Bertalanffy model to compute the temperature-dependent parameters (i.e. rate constants), and several of Arrhenius-type functions are investigated to represent the temperature sensitivity of parameters. Also, the proposed framework is validated by using three data sets independently obtained at different time periods and by being compared the predictions to those by ASTM C 1074. This framework would give more choices in the maturity method to predict the concrete strengths and other properties considering temperature-time effects.

2.2 Modeling of Strength Development

2.2.1 Introduction to the Bertalanffy Model

The original growth model proposed by Bertalanffy [9] is expressed by

$$\frac{dP}{dt} = aP^n - bP \tag{2.2}$$

with the assumptions of allometric by the arbitrary exponent n and of isometric by $n = 2/3$, respectively. If the model is used to represent the property development with the limiting value, the exponent n musts not be equal to unity ($n \neq 1$). From the given equation, both model parameters a and b are positive where $0 \leq n < 1$. Also $P(t)$ is denoted by the property or strength of concretes hereafter in the paper. The limiting property P_u (called asymptotic value or equilibrium solution) is calculated by letting the property development rate be equal to zero ($dP(t)/dt = 0$) where $P > 0$.

$$P(t = \infty) = P_u = \left(\frac{a}{b}\right)^{\frac{1}{1-n}} \tag{2.3}$$

Eq.(2.2) is re-formulated to two forms by using Eq.(2.3).

$$\frac{dP(t)}{dt} = aP(t)^n \left\{1 - \left(\frac{P(t)}{P_u}\right)^{1-n}\right\} \tag{2.4}$$

$$\frac{d}{dt}\left(\frac{P(t)}{P_u}\right) = b\left(\frac{P(t)}{P_u}\right)^n \left\{1 - \left(\frac{P(t)}{P_u}\right)^{1-n}\right\} \tag{2.5}$$

Letting $\chi = P(t)/P_u$, the Bertalanffy model can be also expressed by

$$\frac{d\chi(t)}{dt} = b\left(\chi(t)^n - \chi(t)\right) \tag{2.6}$$

where $0 \leq \chi(t) \leq 1$.

Since the Bertalanffy model is a special case of Bernoulli equation, the solution can be derived by the method proposed by Leibniz. Subsequently, the solution of the Bertalanffy model is computed from Eq.(2.4) where P_0 denotes P at $t = t_0$.

$$\left(\frac{P}{P_u}\right)^{1-n} = 1 - \left\{1 - \left(\frac{P_0}{P_u}\right)^{1-n}\right\} \exp\left[-\frac{a\,(1-n)\,(t-t_0)}{P_u^{1-n}}\right] \tag{2.7}$$

$$= 1 - \exp\left[-\frac{a\,(1-n)\,(t-t_0)}{P_u^{1-n}}\right] \quad \text{if } P(t_0) = 0 \tag{2.8}$$

$$= 1 - \exp\left[-b\,(1-n)\,t\right] \quad \text{if } P(0) = 0 \tag{2.9}$$

If $t_0 = 0$ with a fixed n, 2 unknown parameters (a and P_u) must be estimated, while 3 unknowns parameters (a, t_0 or P_0, and P_u) must be computed if $t_0 \neq 0$ or $P_0 \neq 0$ with a fixed n. The model parameters will be estimated on the basis of three data sets, and the goodness of fit of the models according to varying n is investigated. Figure 2.1 presents the solutions of Bertalanffy model with varying n. It is noted that a is a function of P_u and b, as shown in Eq.(2.3). Therefore, for fixed P_u and b, a decreases with the n increasing, and it caused the response of P against t to shift to the right in Figure 2.1 (a). On the other hand, the effect of varying b with n for a fixed a and P_u is shown in Figure 2.1 (b). It is noted that the black solid lines on both plots are identical.

In addition, the P at inflexion is found by

$$P_{ip} = \left(\frac{na}{b}\right)^{\frac{1}{1-n}} = \left(nP_u^{1-n}\right)^{\frac{1}{1-n}} \tag{2.10}$$

and the property at the maximum rate (or inflection point) is a function of the limiting value and the exponent n. Also, the maximum rate is calculated at t_{ip} of inflexion.

$$t_{ip} = -\frac{P_u^{1-n}}{a\,(1-n)} \ln\left(\frac{1-n}{1-\left(P_0/P_u\right)^{1-n}}\right) \tag{2.11}$$

$$= -\frac{P_u^{1-n}}{a\,(1-n)} \ln\left(1-n\right) \quad \text{if } P_0 = 0 \tag{2.12}$$

2.2.2 Modeling of Strength Development

The Bertalanffy model is adopted to model the concrete strength development in the research. As similar with metabolism of biological organism, the strength development rate is also assumed to be determined by the net rate of the accel-

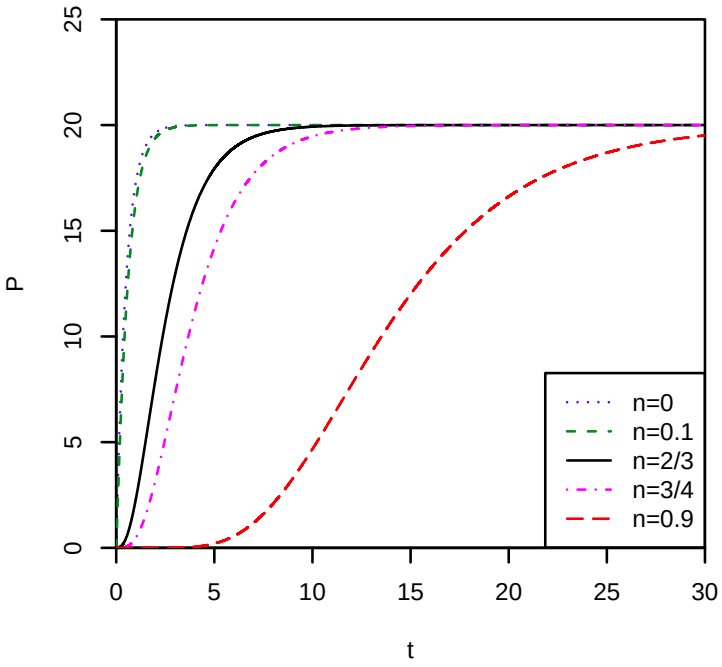

(a) $b = 2$ with varying a and n

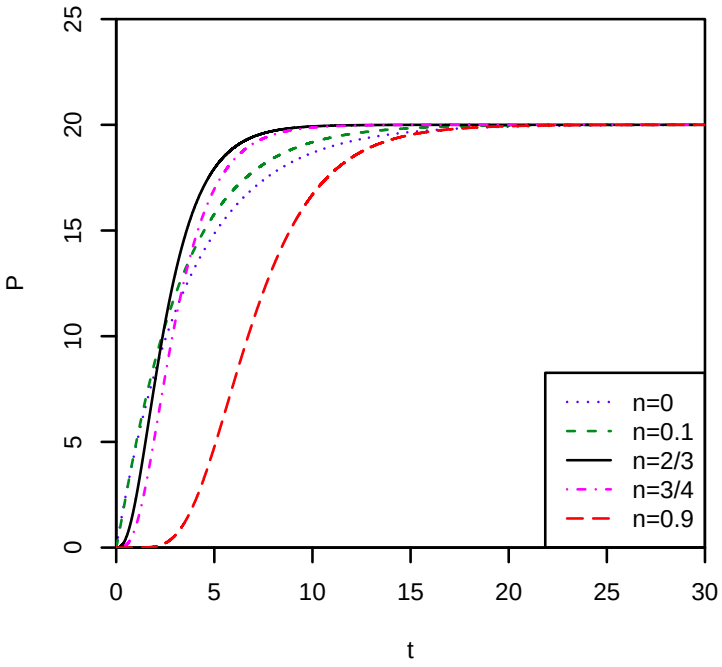

(b) $a = 5.4$ with varying b and n

Figure 2.1: The solutions of Bertalanffy model with $P_u = 20$

eration and the deceleration mechanisms, as formulated by the following.

$$\frac{dP(t)}{dt} = \left(\frac{dP(t)}{dt}\right)_{accel} - \left(\frac{dP(t)}{dt}\right)_{decel} \tag{2.13}$$

The hydration in concretes includes numerous chemical reactions, and several research have been reported on the complexity of the hydration. Therefore, as considering rate law for the hydration that contributes to the strength development, the reaction order could not be explicitly determined. Niven [40] introduced the mathematical frameworks to consider such complex chemical reactions by introducing an arbitrary reaction order, as shown in Eq.(2.14).

$$\left(\frac{dP(t)}{dt}\right)_{acc} = k_a P(t)^n \tag{2.14}$$

In cement chemistry, Bullard et al.[8] stated that the rate of degree of hydration ($d\alpha/dt$) by the nucleation and growth of C_3S and alite is proportional to α^n where $2/3 < n < 1$ in accelerating hydration period, also it was reported that the acceleration rate is determined by the growth of the surface of hydrating product. Therefore, since the strength of concrete P is linearly and/or nonlinearly proportional to the degree of hydration, Eq.(2.14) can represent the accelerating rate of strength development.

On the other hand, the limited amounts of water primarily decelerate the hydration rate[8], and such lacks of water and/or space limitation change the determining step of hydration from nucleation-growth to the diffusion-controlled reaction [41, 42, 43, 44]. Also, reduction of available surface area and pore space for un-hydrated cement to occur nucleation and growth also decelerate the hydration [45, 46]. Therefore, the decelerating rate of strength development is assumed to be proportional to the strength at time t, and the linear relation of

the rate for the degree of diffusion-controlled hydration was discussed in [47].

$$\left(\frac{dP(t)}{dt}\right)_{decel} = k_d P(t) \tag{2.15}$$

Eventually, the strength development for concrete can be formulated by the following.

$$\frac{dP(t)}{dt} = k_a P(t)^n - k_d P(t) \tag{2.16}$$

Also, Figure 2.2 presents two separate terms of strength development rate. The inflexion can be regarded as the point changing the dominant mechanism from accelerating rate to the decelerating mechanism.

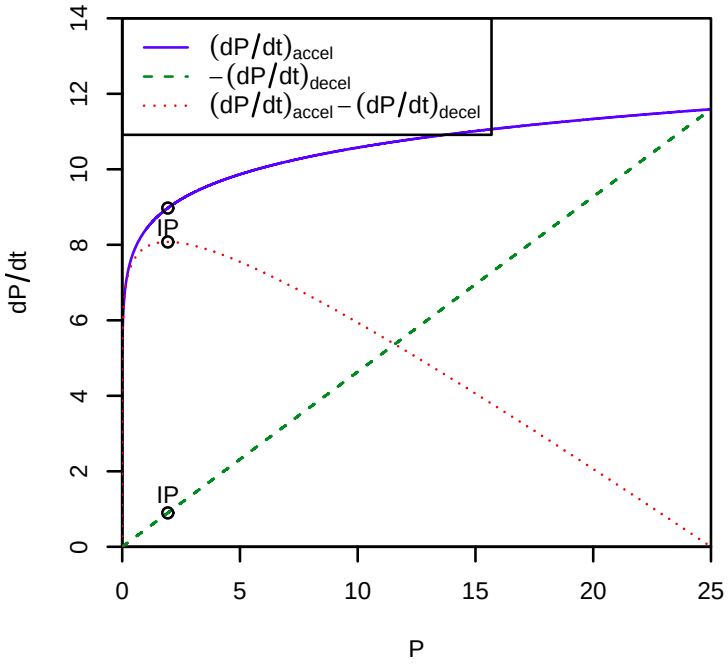

Figure 2.2: The rate of strength development ($P_u = 25$, $n = 0.1$, $k_a = 8.4$)

However, it is noted that the Bertalanffy model extensively considers the strength development, although the primary mechanisms for both accelerating and decelerating rates are based on the hydration. In addition to the hydration, the strength development is affect by the contents and particle size

of aggregates[48], also temperature dependent porosity with degree of hydration [49, 50] is one of factors implicitly embedded in modeling of the strength development in the research. Also, in applying the maturity method, the associated parameters are estimated on the basis of the strength-time data sets. Therefore, this framework does not explicitly consider the hydration since the concrete strength data are implemented.

In the research, the two initial conditions $P(t_0) = 0$ and $P(0) = 0$ are regarded. For the case of $P(t_0) = 0$, 3 unknown parameters must be determined, while two model parameters must be determined by the regression for $P(0) = 0$.

2.3 Experimental Data

The model parameters of the Bertalanffy model are estimated on the basis of strength-time data sets obtained under several constant curing temperature conditions. The proposed method is validated by using four data sets. The first and second data sets were obtained by Klieger[51] (denoted hereafter by KC (Klieger cold series) and KH (Klieger hot series)) and both data sets have been referred by literature[52, 53] to explain the temperature effects on the compressive and tensile strength developments. Since Klieger controlled a consistent slump across the specimens cured under various constant temperatures, the mixture proportions are slightly varied for KC and KH. Thus, two data sets are regarded as independent data sets. Also, Lautz[1] performed the similar experiment with Klieger's on the basis of a single batch mix of concrete and it is used for the third data set, and the data set is named LZ hereafter. However, both data sets include the strength measurements at 4 different test ages within

28 days. Therefore, the fourth data set is currently obtained for five test ages in this research, and data set is denoted by LH in the paper. Mixture proportions of data sets are summarized in Table 5.1.

Table 2.1: Mixture proportions for data sets (Quantities per m^3 concrete)

Data	T ($^\circ C$)	C (kg)	W (kg)	Coarse (kg)	Fine (kg)	Air (%)
KC	-3	307	131	1249	680	4.7
	5	307	130	1247	679	4.9
	13	307	131	1254	683	4.4
	23	307	131	1252	682	4.5
KH	23	307	139	1235	673	4.6
	32	307	139	1238	674	4.5
	41	307	139	1235	673	4.7
	49	307	139	1240	675	4.4
Lautz	-2/14/21/43	522	196	884	813	-
Lee	-1/11/23/42	338	153	1071	735	-

2.4 Development of Maturity Method Framework

2.4.1 Model Parameter Estimation

From Eq.(2.8), the solution of the Bertalanffy model can be expressed by

$$P(t) = P_u \left\{ 1 - \exp\left[-\frac{k_a (1-n)(t-t_0)}{P_u^{1-n}} \right] \right\}^{\frac{1}{1-n}} \tag{2.17}$$

and all data sets measured under constant temperatures are fitted with the equation. In addition, the hyperbolic function

$$P = P_u \frac{k(t-t_0)}{1 + k(t-t_0)} \tag{2.18}$$

is also fitted with the data sets to compare the resulting predictions from both methodologies. It is noted that the hyperbolic function is the solution of Eq.(2.1) with $m = 2$ and is adopted by ASTM C 1074 [19]. The regression in the analysis is performed with functions with 2 parameters and 3 parameters with $t_0 = 0$ or un-determined nonzero t_0. As a result, Figure 2.3 to 2.6 show the strength-time measurements and the fitted curves by the Bertalanffy model with 2 parameters ($n = 0.1$) and by the hyperbolic function with $t_0 = 0$ to compare equivalent results from the two models with the same degree of freedom. The strength degradation effects are observed for all data sets, although its extent is varied depending on data sets. It is noted that the reference temperatures are selected by either $23°C$ or $21°C$ according to data sets, and the corresponding data set is used to predict the strength.

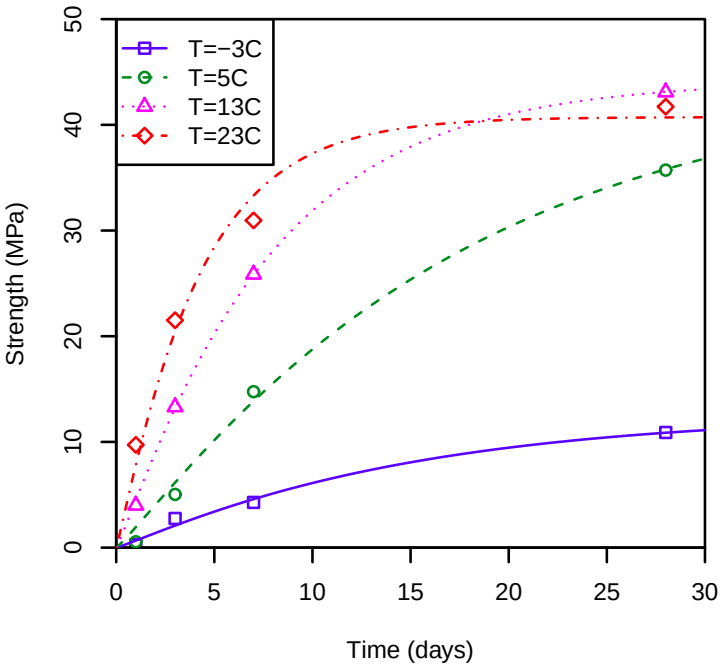

(a) Bertalanffy Model

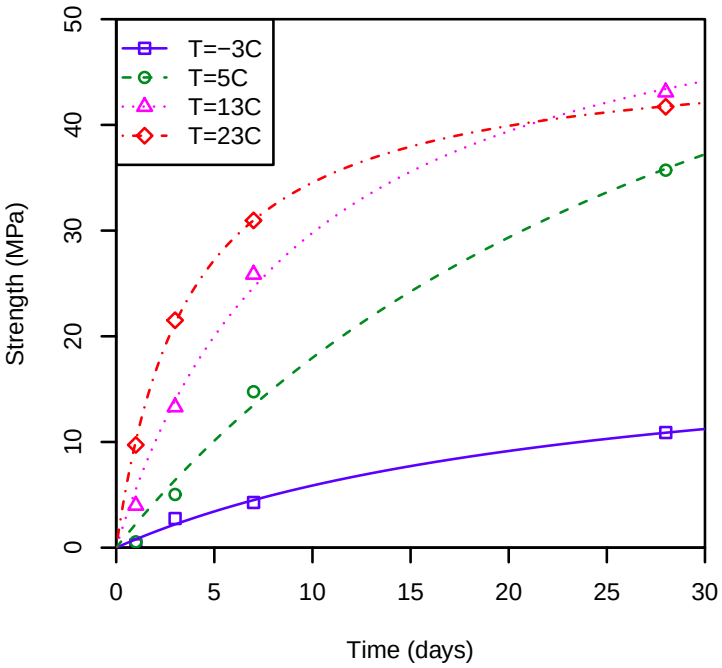

(b) Hyperbolic function

Figure 2.3: Strength-Time Measurements with Curve Fittings of Bertalanffy Model with $n = 0.1$ and Hyperbolic Function (2 Parameters): Klieger's Cold Series

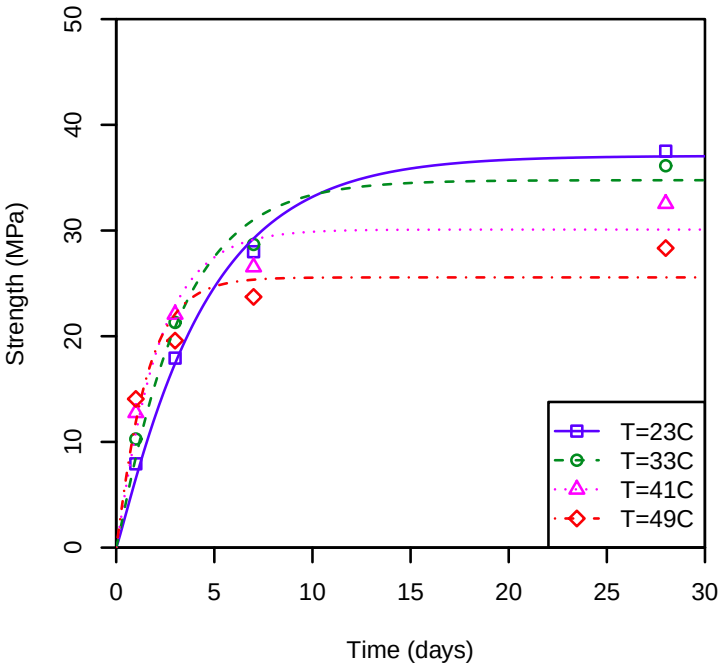

(a) Bertalanffy Model

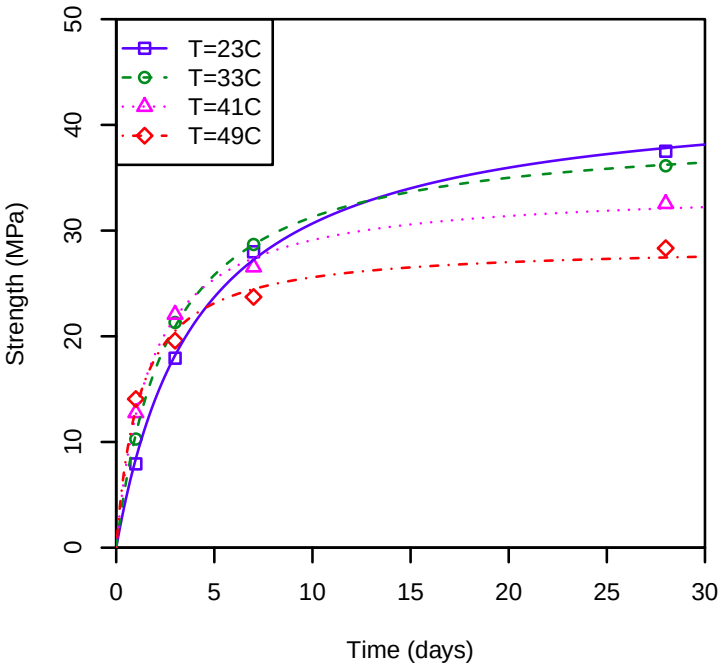

(b) Hyperbolic function

Figure 2.4: Strength-Time Measurements with Fitting Curves of Bertalanffy Model with $n = 0.1$ and Hyperbolic Function (2 Parameters): Klieger's Hot Series

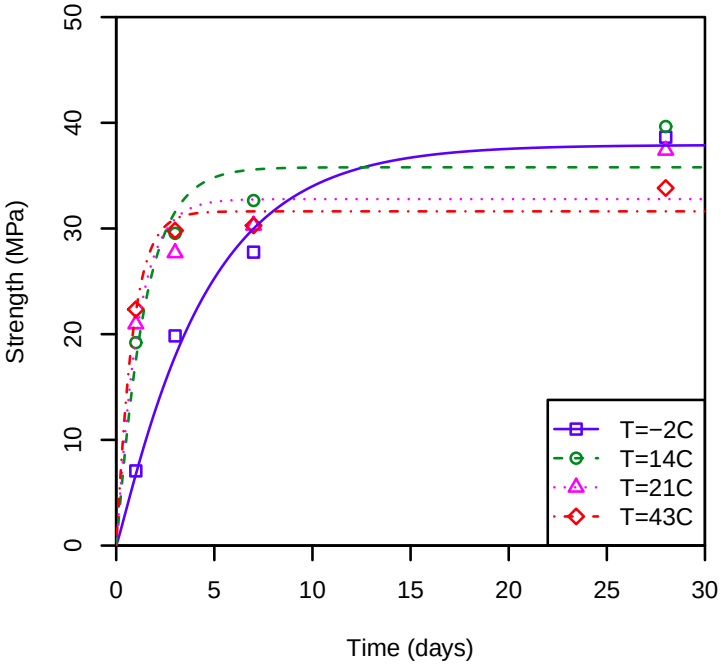

(a) Bertalanffy Model

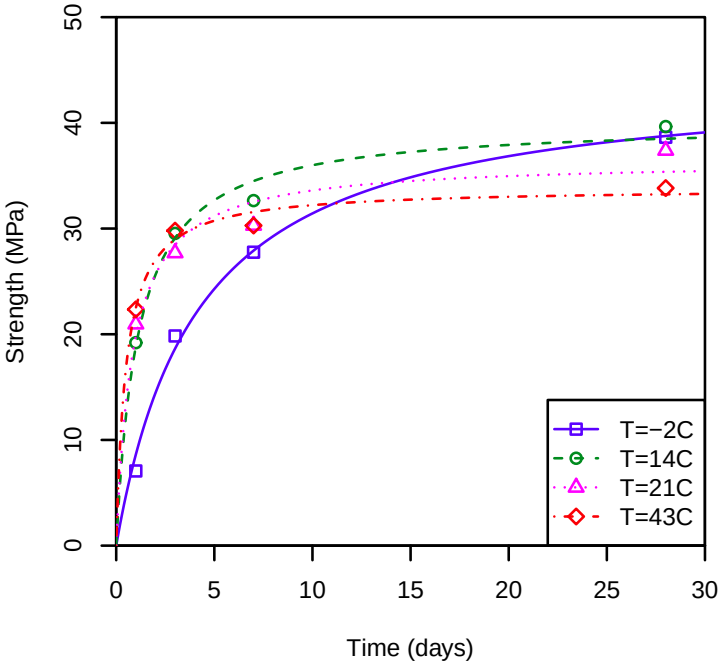

(b) Hyperbolic function

Figure 2.5: Strength-Time Measurements with Fitting Curves of Bertalanffy Model with $n = 0.1$ and Hyperbolic Function (2 Parameters): Lautz's Data

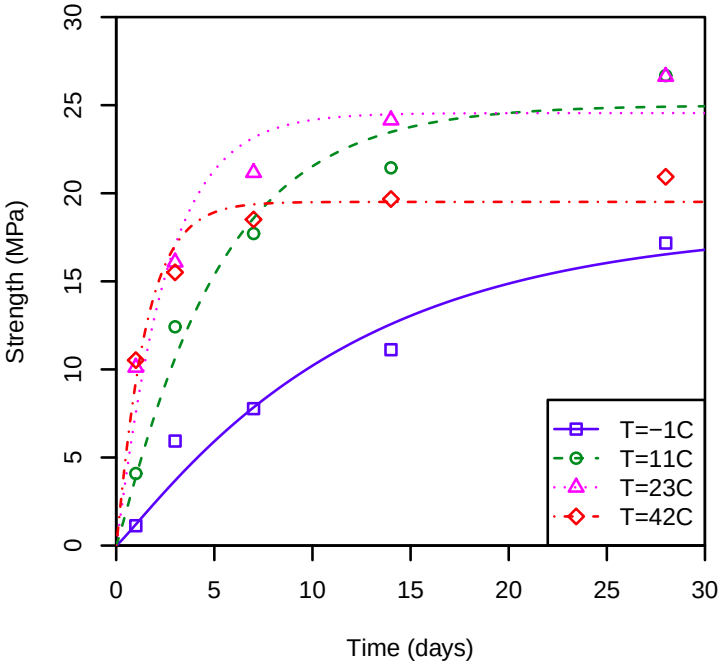

(a) Bertalanffy Model

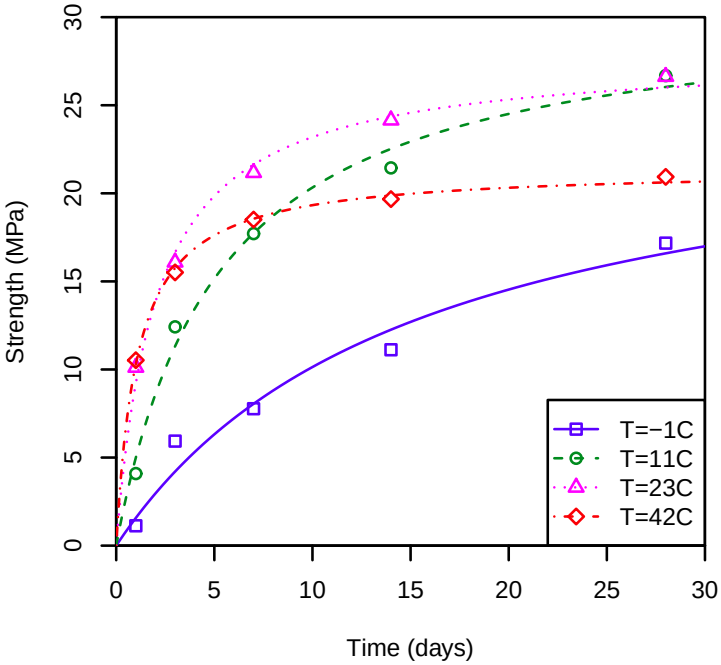

(b) Hyperbolic function

Figure 2.6: Strength-Time Measurements with Fitting Curves of Bertalanffy Model with $n = 0.1$ and Hyperbolic Function (2 Parameters): Lee's Data

2.4.2 Temperature Sensitivity of Model Parameters

The model parameters k_a and k_d are both assumed to be temperature dependent in the research. Several functions representing the temperature sensitivity of model parameters are investigated to consider nonlinearity of Arrhenius plot. Although it is possible to consider such a nonlinearity of Arrhenius plot by using multiple linear lines as reported by Duggleby [54], the investigated five functions are introduced and examined to represent the temperature dependency of the model parameters for wide temperature ranges with the closed form functions.

(1) Arrhenius equation: FHP method implements the activation energy of Arrhenius [21] equation to describe the temperature dependency of rate constants for the strength development. Carino [55] proposed a method to compute the activation energy from the rate constants estimated by the hyperbolic function, and details are provided by ASTM C 1074 [19].

$$k(T) = A_1 \exp\left[-\frac{E_1}{RT}\right] \tag{2.19}$$

(2) Eyring equation: It is an alternative of Arrhenius equation, and the model is theoretically described on the basis of the activation complex (or transition state)[56, 57]. However, Petrou [58] reported that there is negligible difference between Arrhenius and Eyring equations.

$$k(T) = A_2 T \exp\left[-\frac{E_2}{RT}\right] \tag{2.20}$$

(3) Modified Arrhenius equation: To consider the nonlinearity of rate constants on Arrhenius plot, the modified Arrhenius, termed in [59], is one

of possible functions that have been used in the chemical kinetics as described in [60]. It is noted that the equation is identical to the Arrhenius equation if $\alpha_3 = 0$ and Eyring equation if $\alpha_3 = 1$ and $T_r = 1$, respectively.

$$k(T) = A_3 \left(\frac{T}{T_r}\right)^{\alpha_3} \exp\left[-\frac{E_3}{RT}\right] \tag{2.21}$$

(4) Kohlrausch type equation: It is one of functions to consider the nonlinearity of Arrhenius plot. Fang [61] reported that kinetics of some liquids and amorphous materials follow Kohlrausch function. Also, the fluid viscosity is known as thermally activated process, and Ojovan et al. [62] applied the equation to represent "temperature-dependent" activation energy for the viscosity. It is noted that Kohlrausch equation converges to Arrhenius equation if $\gamma_4 = 1$.

$$k(T) = A_4 \exp\left[-\left(\frac{E_4}{RT}\right)^{\gamma_4}\right] \tag{2.22}$$

(5) Modified Arrhenius-Eyring-Polanyi (AEP) equation: It is a mixed equation of Kohlrausch and Eyring equations that can consider the nonlinearity of Arrhenius plot. The equation is applied to represent the temperature dependency of the rate for the microbial growth by Huang et al. [32]. It is noted that the equation converges to Eyring equation as $\gamma_5 = 1$.

$$k(T) = A_5 T \exp\left[-\left(\frac{E_5}{RT}\right)^{\gamma_5}\right] \tag{2.23}$$

2.4.3 Maturity Calculation

From the activation energies and the associated parameters from the section 2.4.2, the maturity of concrete is computed for the given concrete temperature profile with time. The FHP and NS methods implement the equivalent [20]

age and temperature-time factor for the measure of maturity, respectively [37, 38]. This research introduces the unitless maturity computed by integrating rate constant with time, and it is similar method to construct the "universal growth curve" for various species proposed by West et al. [63].

The solution Eq.(2.7) is re-parameterized to achieve a unique relation between the proposed maturity τ and the relative strength r.

$$r = \left(\frac{P}{P_u}\right)^{1-n} \tag{2.24}$$

$$\begin{aligned}\tau &= \frac{k_a\,(1-n)\,(t-t_0)}{P_u^{1-n}} - \ln\left[1-\left(\frac{P_0}{P_u}\right)^{1-n}\right] \\ &= k_m\,(t-t_0) - \beta_0\end{aligned} \tag{2.25}$$

where

$$k_m = \frac{k_a(1-n)}{P_u^{1-n}} \tag{2.26}$$

$$\beta_0 = \ln\left[1-\left(\frac{P_0}{P_u}\right)^{1-n}\right] \tag{2.27}$$

thus, the solution is expressed by the following.

$$r = 1 - \exp\left(-\tau\right) = 1 - \exp\left[-k_m\,(t-t_0) + \beta_0\right] \tag{2.28}$$

If $P(t_0) = P_0 = 0$ set as a special case for this research, $\beta_0 = 0$. It is noted that $k_m = k_d\,(1-n)$ from Eq.(2.3) and (2.26), thus k_m is linearly proportional to the decelerating rate constant k_d for a given exponent n. Also, it is equivalent with that the determining step [25] of reaction mechanism in the strength development is controlled by k_m. Eventually, Eq.(2.28) with $\beta_0 = 0$ is same formula with the solution of Mitscherlich growth model [64]. In other words, the relative strength-unitless maturity is the solution of $dr/dt = k_m\,(1-r)$ with $r(0) = 0$. Also, it is noted that the unique relation of strength-maturity can be achieved

regardless of the concrete mixture proportions because the proposed model implements the normalized limiting strength represented by r in Eq.(2.28).

Since several functions are investigated in the research, the unitless maturity τ for a given concrete temperature profile at any time t can be computed. By the definition, the proposed unitless maturity τ is computed by

$$\begin{aligned}\tau &= \int_{t_0}^{t} k_m \, dt \\ &= k_m(T_r) \int_{t_0}^{t} \frac{k_m(T)}{k_m(T_r)} \, dt \qquad (2.29) \\ &= k_m(T_r) \sum_{i=1}^{n} \frac{k_m(T_i)}{k_m(T_r)} \triangle t_i \qquad (2.30)\end{aligned}$$

where $k_m(T_r)$ is the net rate constant at the pre-determined reference temperature. As similar with the procedure to get the strength-maturity relation by ASTM C 1074, the k_m at the reference temperature is given by the experiment for the reference temperature. The age conversion factor concept is partly adopted because it enables one to reduce the number of required parameters related to the temperature dependency of model parameters. For example of implementing Arrhenius equation, both E_1 and A_1 of Eq.(3.2) must be known unless the age conversion factor concept is used. Since the concrete temperature is measured at discretized time steps, Eq.(2.30) is more preferred than Eq.(2.29) in general applications. The variations of unitless maturity calculation according to the different Arrhenius-type are derived as follows. It is noted that all parameters related to temperature sensitivity must be estimated from the set of k_m against temperature.

(1) Arrhenius equation: E_{k1} is required to be determined or estimated.

$$\tau = k_m(T_r) \sum_{i=1}^{n} \exp\left[-\frac{E_{k1}}{R}\left(\frac{1}{T_i} - \frac{1}{T_r}\right)\right] \triangle t_i \qquad (2.31)$$

(2) Eyring equation: E_{k2} is required to be determined or estimated.

$$\tau = k_m(T_r)\sum_{i=1}^{n}\left(\frac{T_i}{T_r}\right)\exp\left[-\frac{E_{k2}}{R}\left(\frac{1}{T_i}-\frac{1}{T_r}\right)\right]\triangle t_i \tag{2.32}$$

(3) Modified Arrhenius equation: E_{k3} and α_{k3} are required to be determined or estimated.

$$\tau = k_m(T_r)\sum_{i=1}^{n}\left(\frac{T_i}{T_r}\right)^{\alpha_{k3}}\exp\left[-\frac{E_{k3}}{R}\left(\frac{1}{T_i}-\frac{1}{T_r}\right)\right]\triangle t_i \tag{2.33}$$

(4) Kohlrausch equation: E_{k4} and γ_{k4} are required to be determined or estimated.

$$\tau = k_m(T_r)\sum_{i=1}^{n}\exp\left[-\left(\frac{E_{k4}}{R}\right)^{\gamma_{k4}}\left(\frac{1}{T_i^{\gamma_{k4}}}-\frac{1}{T_r^{\gamma_{k4}}}\right)\right]\triangle t_i \tag{2.34}$$

(5) Modified Arrhenius-Eyring-Polanyi equation: E_{k5} and γ_{k5} are required to be determined or estimated.

$$\tau = k_m(T_r)\sum_{i=1}^{n}\left(\frac{T_i}{T_r}\right)\exp\left[-\left(\frac{E_{k5}}{R}\right)^{\gamma_{k5}}\left(\frac{1}{T_i^{\gamma_{k5}}}-\frac{1}{T_r^{\gamma_{k5}}}\right)\right]\triangle t_i \tag{2.35}$$

2.4.4 Temperature Dependent Limiting Strength

The distinguished advantage of the proposed maturity method is to derive a closed form function to express the temperature dependence of the limiting strengths. As mentioned before, both k_a and k_d of the Bertalanffy model are assumed to be temperature dependent, thus they can be represented by the functions as presented in the section 2.4.2. From Eq.(2.26), the function of temperature dependent limiting strength derived by using the following parameterization.

$$P_u(T)^{1-n} = \frac{k_a(T)\,(1-n)}{k_m(T)}$$

Therefore, variations of the equivalent limiting strength are varied according to different Arrhenius type equations. Since $P_u(T_r)$ is generally known in the application of maturity with ASTM C 1074, limiting strength functions for the relative strength can be derived as follows. The relative strength is implemented since it can reduce the number of required parameters, as similar with the derivation of the unitless maturity.

(1) Arrhenius equation: If $E_{a1} > E_{k1}$, P_u increases with concrete temperature increasing linearly on Arrhenius plot. On the other hand, P_u decreases with concrete temperature increasing if $E_{a1} < E_{k1}$, and it can represent the cross-over effects.

$$\left(\frac{P_u(T)}{P_u(T_r)}\right)^{1-n} = \exp\left[-\frac{(E_{a1}-E_{k1})}{R}\left(\frac{1}{T}-\frac{1}{T_r}\right)\right] \tag{2.36}$$

(2) Eyring equation: The expression on the basis of Eyring equation is identical to the relative limiting strength function derived from Arrhenius equation. However, it is noted that the activation energies for k_a and k_m are different from those by Arrhenius equations.

$$\left(\frac{P_u(T)}{P_u(T_r)}\right)^{1-n} = \exp\left[-\frac{(E_{a2}-E_{k2})}{R}\left(\frac{1}{T}-\frac{1}{T_r}\right)\right] \tag{2.37}$$

(3) Modified Arrhenius equation: In addition to the relation between E_{a3} and E_{k3}, α_{a3} and α_{k3} also affect the profile of temperature dependent limiting strength.

$$\left(\frac{P_u(T)}{P_u(T_r)}\right)^{1-n} = \left(\frac{T}{T_r}\right)^{\alpha_{a3}-\alpha_{k3}} \cdot \exp\left[-\frac{(E_{a3}-E_{k3})}{R}\left(\frac{1}{T}-\frac{1}{T_r}\right)\right] \tag{2.38}$$

(4) Kohlrausch equation: Nonlinearity of Arrhenius plot can be considered by using the power inside of exponential function.

$$\left(\frac{P_u(T)}{P_u(T_r)}\right)^{1-n} = \exp\left[-\left(\frac{E_{a4}}{R}\right)^{\gamma_{a4}}\left(\frac{1}{T^{\gamma_{a4}}}-\frac{1}{T_r^{\gamma_{a4}}}\right)+\left(\frac{E_{k4}}{R}\right)^{\gamma_{k4}}\left(\frac{1}{T^{\gamma_{k4}}}-\frac{1}{T_r^{\gamma_{k4}}}\right)\right] \tag{2.39}$$

(5) Modified Arrhenius-Eyring-Polanyi equation: The relative limiting strength by the modified Arrhenius-Eyring-Polanyi equation is identical to that derived on the basis of Kohrlausch function.

$$\left(\frac{P_u(T)}{P_u(T_r)}\right)^{1-n} = \exp\left[-\left(\frac{E_{a5}}{R}\right)^{\gamma_{a5}}\left(\frac{1}{T^{\gamma_{a5}}} - \frac{1}{T_r^{\gamma_{a5}}}\right) + \left(\frac{E_{k5}}{R}\right)^{\gamma_{k5}}\left(\frac{1}{T^{\gamma_{k5}}} - \frac{1}{T_r^{\gamma_{k5}}}\right)\right] \tag{2.40}$$

2.4.5 Strength Prediction

The relative ratio of strength to the limiting strength at any time t for a given temperature profile can be first computed by Eq.(2.28) form the computed maturity by Eq.(2.31) to (2.35). Also, $P_u(T)$ is calculated by functions provided by previous section 2.4.4. Then, the strength is subsequently calculated by Eq.(2.24).

2.5 Application of Proposed Maturity to Strength Prediction

2.5.1 Nonlinear Regression Results

The nonlinear regression to fit the data sets with the Bertalanffy model is executed by R-package [65], a statistical analysis package. The goodness of fit for the examined functions (Bertalanffy models and the hyperbolic functions) are compared by using Akaike information criterion (AIC) [66], a statistical measure indicating relative goodness of fit across the tested functions, and the residual standard error (RSE). The nonlinear regression with the Bertalanffy model by setting n to be a variable caused the bounded value of $n = 0$ for parts of data,

although the Bertalanffy model must be in the range of $0 \leq n < 1$ to hold the positive model parameters k_a and k_d. It is noted that the minimzation of variance is not fully achieved if a regression coefficient is bounded. Therefore, the exponent n of the Bertalanffy model for the research is controlled by fixed values of $n = 0$, $n = 0.1$, $n = 2/3$, $n = 3/4$, and $n = 0.9$ to reduce the bias that could be induced by the cases of bounded values. Subsequently, the effects of n is investigated by the comparisons of resulting AICs and RSEs of models. In addition, the regression results between the Bertalanffy and the hyperbolic function are compared, although the accuracy of regression would be one of components to determine the accuracy of the strength prediction by the maturity method. The effect of exponent n of the Bertlanffy model on the goodness of fit is investigated by estimating the residual standard errors (RSE) according to varying n. Figure 2.7 shows the 95% box-plots of RSE from the nonlinear regressions with 2- and 3-parameters Bertalanffy models with varying n (denoted by BXX in Figure 2.7) and hyperbolic function (denoted by AX in Figure 2.7). The following statistical model is postulated to examine the effect of n of the Bertalanffy model.

$$RSE_{ijkl} = \beta_1 n_i + \beta_2(\text{Data})_j + \beta_3(\text{Temperature})_k + \epsilon_{ijkl} \tag{2.41}$$

The results are summarized in Table 2.2. For a given n, the Bertlanffy model with 3 parameters fit better with the data sets than that with 2 parameters. Also, the temperature effects are not statistically significant even at 90% confidence level. Thus, the goodness of fits of the Bertalanffy model represented by RSE is strongly dependent on n more than the temperature. For the effects of data sets, no statistically significant difference is observed in RSE from KC and LH. However, RSE from KH and LZ are critically greater than that from KC. However, since all experimental data sets are obtained independently, it could give the extent of goodness of fit according to data sets, yet it does not affect determin-

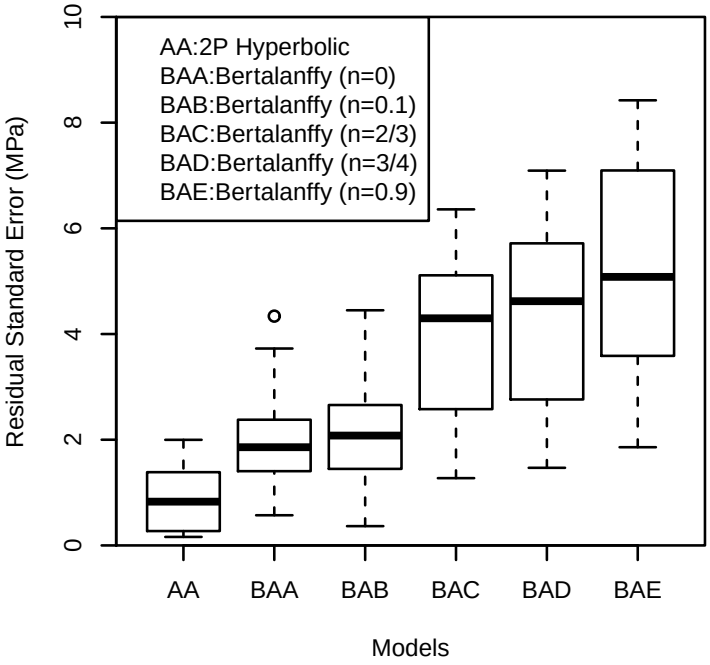

(a) Models with 2 Parameters

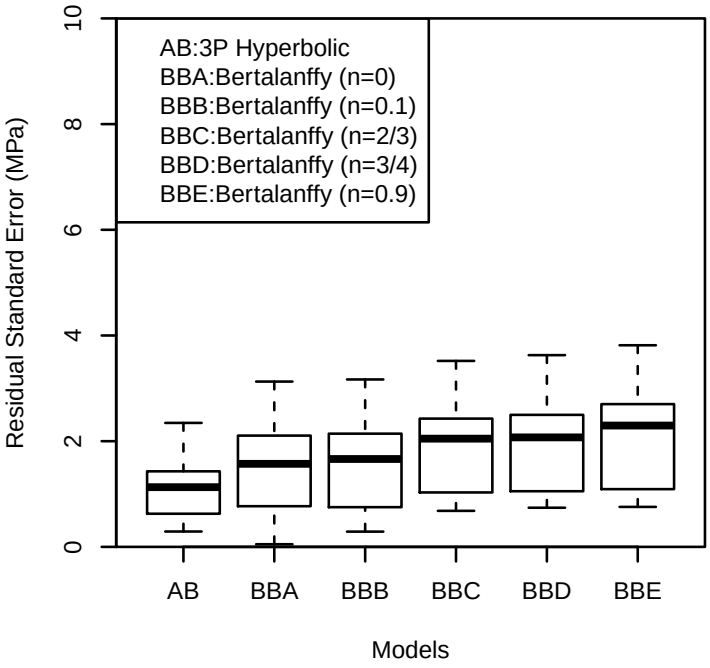

(b) Models with 3 Parameters

Figure 2.7: Comparison of Residual Standard Errors with Bertalanffy Model with varying n and Hyperbolic function

Table 2.2: Effects of n, data, temperature, and models on Residual Standard Error in the nonlinear regression (Adjusted $R^2 = 0.8681$)

	Estimate	Std. Error	t value	Pr(>|t|)
B with 2P ($n = 0$)	1.5879	0.3348	4.74	0.0000
B with 2P ($n = 0.1$)	1.7406	0.3348	5.20	0.0000
B with 2P ($n = 2/3$)	3.5254	0.3348	10.53	0.0000
B with 2P ($n = 3/4$)	3.9000	0.3348	11.65	0.0000
B with 2P ($n = 0.9$)	4.7188	0.3348	14.10	0.0000
B with 3P ($n = 0$)	1.0523	0.3348	3.14	0.0020
B with 3P ($n = 0.1$)	1.1062	0.3348	3.30	0.0012
B with 3P ($n = 2/3$)	1.4905	0.3348	4.45	0.0000
B with 3P ($n = 3/4$)	1.5472	0.3348	4.62	0.0000
B with 3P ($n = 0.9$)	1.6938	0.3348	5.06	0.0000
KH	1.0526	0.3172	3.32	0.0011
LZ	1.3608	0.2660	5.12	0.0000
LH	0.1065	0.2654	0.40	0.6887
Temperature	-0.0103	0.0068	-1.50	0.1348

ing the exponent n of the Bertalanffy model. In addition, RSE decreases with n decreasing for both models. The best goodness of fit is achieved by $n = 0$, although minor significant difference is observed between the case of $n = 0$ and $n = 0.1$; about 0.15 MPa and 0.05 MPa for 2P and 3P models, respectively. However, it is noted that both $n = 0$ and $n = 0.1$ are different from the range of exponent ($2/3 < n < 1$) mentioned by Bullard et al. [8]. Also, the resulting solution of the Bertalanffy model with $n = 0$ is identical to Avrami (or JMAK)

equation [41] with unity of its exponent ($\xi = 1$), as shown by

$$X(t) = 1 - \exp\left[-(kt)^{\xi}\right] \tag{2.42}$$

where $X(t)$ is the volume fraction that has transformed at time t, k is rate constant for nucleation, and ξ is a unknown exponent to be determined. Several research [67, 47, 68] reported that the experimental results induced the exponent of the Avrami model is close to the unity, although it conflicts with the theoretical range described by literature [41]. Therefore, it is noted that the statistical analysis shown in this research is agreement with the aforementioned results. Nevertheless, the strength prediction is made by using $n = 0.1$ despite that the minimum goodness of fit is achieved by the model with $n = 0$ because its discrepancy of RSE is negligible (about 0.2 MPa) and the Bertalanffy model distinguished from Mitscherlich model [64] is intended in the research.

The performances of the Bertalanffy model and the hyperbolic function are compared by using Akaike Information Criterion. AIC is generally used to compare different models than to measure the goodness of fit of the model, and the lower AIC indicates the better model [66]. In addition, Akaike weights shown in Table 2.3 indicate the probability that the model is the best for the data sets. As a result, any of Bertalanffy model does not show higher probability than the hyperbolic function to be the best model for the models having the same number of parameters (2P or 3P). Among the Bertalanffy series, it is observed that the larger numbers of model parameters for a fixed number of data points result in lower AICs. In addition, the higher AIC weight is resulted as n decreases. However, it is noted that the higher goodness of fit for the nonlinear regression does not always lead more accurate strength prediction in the maturity method since the maturity method consists of multiple steps in entire process of the strength prediction.

Table 2.3: Effects of n, data, temperature, and models on Akaike information criterion in the nonlinear regression (Adjusted $R^2 = 0.952$)

	Estimate	t value	Pr(>|t|)	Akaike weight
2P Hyperbolic	8.0332	6.11	0.0000	0.6953
3P Hyperbolic	11.3508	8.63	0.0000	0.1324
B with 2P ($n = 0$)	16.9658	12.90	0.0000	0.0080
B with 2P ($n = 0.1$)	17.3609	13.20	0.0000	0.0066
B with 2P ($n = 2/3$)	22.9084	17.41	0.0000	0.0004
B with 2P ($n = 3/4$)	23.7279	18.04	0.0000	0.0003
B with 2P ($n = 0.9$)	25.1563	19.12	0.0000	0.0001
B with 3P ($n = 0$)	12.4243	9.44	0.0000	0.0774
B with 3P ($n = 0.1$)	13.4380	10.21	0.0000	0.0466
B with 3P ($n = 2/3$)	15.9512	12.12	0.0000	0.0133
B with 3P ($n = 3/4$)	16.2462	12.35	0.0000	0.0114
B with 3P ($n = 0.0$)	16.8905	12.84	0.0000	0.0083
KH	4.9131	4.22	0.0000	NA
LH	6.5259	6.70	0.0000	NA
LZ	7.1559	7.33	0.0000	NA
Temperature	-0.0705	-2.81	0.0055	NA

2.5.2 Temperature Dependency of Model Parameters

One of primary purposes of this research is to investigate five Arrhenius-type functions representing temperature dependency of model parameters k_a and k_m. The investigated functions (Eyring, Modified Arrhenius, Kohrlausch, and Modified Arrhenius Eyring Polanyi equations) except Arrhenius equation have

ability to represent the nonlinearity of Arrhenius plot, although the extent of nonliearity consideration would be different according to functions. It is noted that the nonlinearity of Arrhenius plot in the research is expressed by the additional degree of freedoms provided by variables of the individual functions with a constant activation energy, and it is different from the concept of the temperature and/or degree of hydration dependent activation energy as proposed by other literature [22, 23, 69, 70]. Also, the associated conditions for the negative slope and concavity can be computed by the first and second derivatives of the log-transformed rate constant with $1/T$. Figure 2.9 to 2.16 present Arrhenius plots including the estimated parameters with fitted functions. Especially, Figure 2.9 to 2.12 present the results associated with the Bertalanffy model with 2 parameters and Figure 2.9 to 2.12 show the results led by 3-parameter Bertalanffy model.

For the practical concrete temperature ranges given by the data set ($-1°C \leq T \leq 42°C$), the difference of Arrhenius and Eyring equations are not clearly differentiated from the analysis, and such a negligible difference is observed in both k_a and k_m for all data sets as similarly reported by Petrou [58] on geochemical process. It is noted that its difference due to nonlinearity of Eyring equation increases as functions are extended to higher temperature. However, such nonlinearity is because of additional temperature term T (the reciprocal of $1/T$) in an expression of the first derivative of $\ln k$ with respect to $1/T$. Also, the activation energy (E_1) of Arrhenius equation is greater than that of Eyring equation (E_2) by about maximum $2.5\ kJ/mol$ considering all data sets of k_a and k_m.

The nonlinearity shape of the MAE on Arrhenius plot is different depending on combinations of E_3 and α_3, as shown in Figure 2.8. The sign of α_3 determines

concavity of the curvature of the function on Arrhenius plot; that is concave-down shape is caused when $\alpha < 0$, while the concave-up shape is resulted by $\alpha > 0$. Also, if the sign of activation energy E_3 is different from α_3, parabolic curvature is given, while the same sign of E_3 as α_3 cause monotonically decrease or increase with temperature increasing. The negative slope of Arrhenius plot from MAE function is given under the condition of $E_{k3} > -\alpha_{k_3} RT$. The modified Ar-

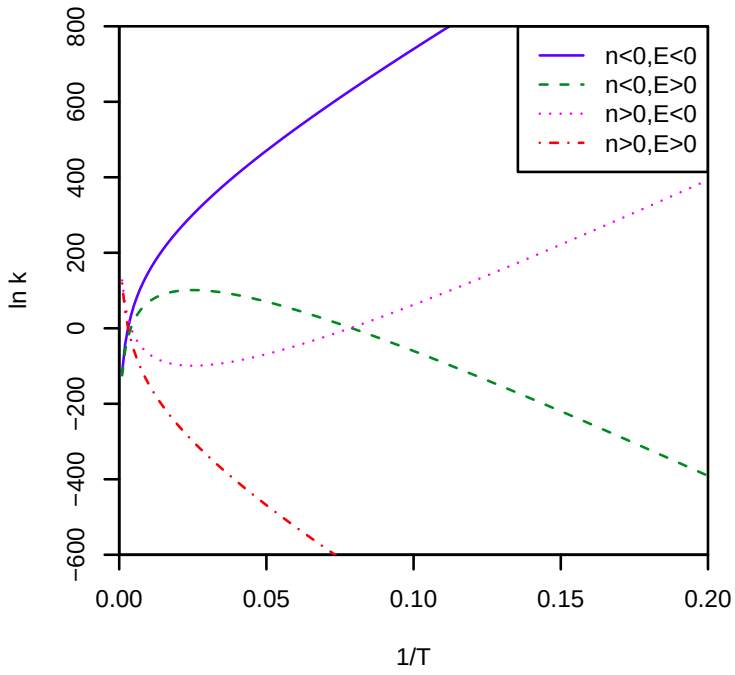

Figure 2.8: Profile of Modified Arrhenius equation on Arrhenius plot with 4 combinations of E_{k3} and α_{k3} conditions

rhenius equation can represent relatively high nonlinearity of model parameters on Arrhenius plot as compared to other functions. The magenta-colored lines in Figure 2.9 to 2.16 indicate profiles fitted by MAE function. The parameters for k_a and k_m of KC data sets are $E_{a3} = 588.1\ kJ/mol$ with $\alpha_{a3} = -226$ and $E_{a3} = -853.2\ kJ/mol$ with $\alpha_{a3} = 378$, respectively. Although any of resulting α_{a3} and α_{k3} is different from 0 (Arrhenius equation), 1/2(classical collision

theory), and 1 (Eyring equation) for all data sets, the estimated activation energies and associated exponents are still applicable in practical applications as reported by literature [71, 72]. However, it is noted that the negative activation energy in the modified Arrhenius equation cannot be clearly explained by kinetics of strength development of concretes except improvement of goodness of fit in curve fittings.

Kohlrausch function is identical to the Arrhenius equation if $\gamma_4 = 1$. Also, if $E_4 > 0$, the concavity of Kohlrausch function on Arrhenius plot is dependent on the range of γ_4. For $0 < \gamma_4 < 1$, the concave-up curvature on Arrhenius plot is resulted, and concave-down curvature is calculated otherwise. Also, the rate constant increases with the temperature increasing only when resulting $\gamma_4 > 0$ as represented by the negative slope on Arrhenius plot. The model parameters given by the Bertalanffy model with 2 parameters caused $E_4 > 0$ with $\gamma_4 > 1$, which indicates the variable negative slope in Arrhenius plot with concave-down curvature, for all data sets as shown in Figure 2.9 to 2.12. However, the estimated model parameters of the Bertalanffy model with the model of 3 parameters estimated from KH data set irregularly resulted in $E_4 > 0$ with $\gamma_4 < 0$ and $E_4 > 0$ with $0 < \gamma_4 < 1$ for k_a and k_m, respectively, as shown in Figure 2.14. Also, the latter pattern is observed in the analysis of k_m estimated by the Bertalanffy model with 3 parameters from LZ data set as presented in Figure 2.15, although its pattern is not clearly visible.

AEP function is identical to Eyring equation if $\gamma_5 = 1$. The mathematical characteristics of AEP function is similar with that of Kohlrausch function. However, the conditions determining concavity and the sign of slope are more complex than Kohrlausch function because of T term in front of the exponent in

Eq.(2.23). Therefore, the negative slope on Arrhenius plot (the higher temperature, the higher rate constant) is achieved under the condition as the following.

$$1 + \gamma_5 \left(\frac{E_5}{RT} \right)^{\gamma_5} > 0 \tag{2.43}$$

Also, the concavity of the curvature of AEP function on Arrhenius plot is a function of T, γ_5, and E_5, and the concave-down profile can be given by the following condition.

$$\gamma_5 \left(\gamma_5 - 1 \right) \left(\frac{E_5}{RT} \right)^{\gamma_5} > 1 \tag{2.44}$$

Based on the analysis, the E_5 and γ_5 from the model parameters estimated by the Bertalanffy model with 2 parameters caused varying negative slope and concave down curvature of Arrhenius plot for given temperature ranges, as shown in Figure 2.9 to 2.12. Exceptionally, for the analysis for k_a and k_m from the Bertalanffy model with 3 parameters with AEP function, the variable negative slope with concave up shape profile is observed in KH and LZ data sets.

2.5.3 Relative Strength-Maturity Relation

Figure 2.17 includes the relative strength $(P(t)/P_u)^{1-n}$ against the unitless maturity τ by Eq.(2.28) according to two different Bertalanffy models (with 2 and 3 parameters). The resulting relations with the Bertalanffy model with 3 parameters showed relatively less variance to Eq.(2.28) than those from the model with 2 parameters. It is noted that all resulting relations can be plotted together since the relative strengths are also scaled by P_u. On the other hand, since ASTM implements the strength-maturity relation obtained from the pre-determined reference temperature, each data set has own relation to use in the strength predictions.

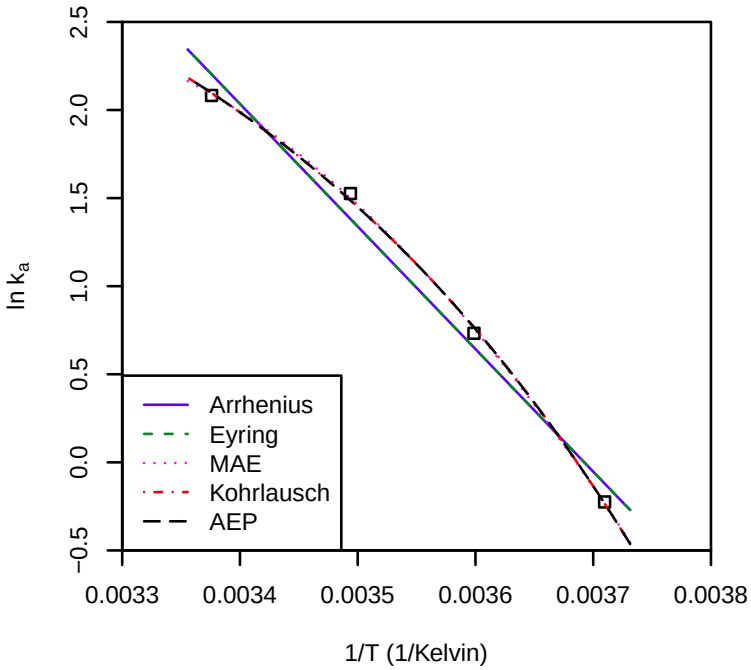

(a) k_a

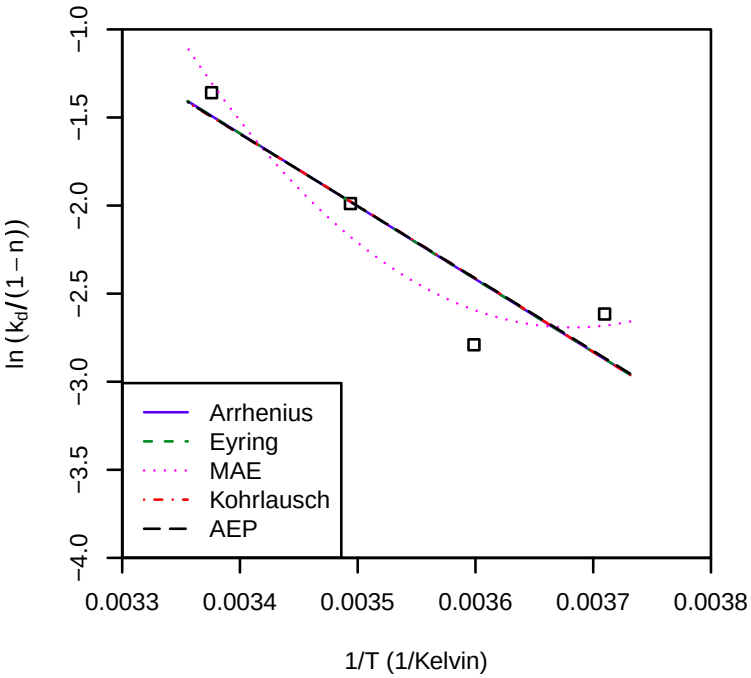

(b) k_m

Figure 2.9: Arrhenius plot of k_a and k_m with the Bertalanffy model of 2 parameters ($n = 0.1$): KC

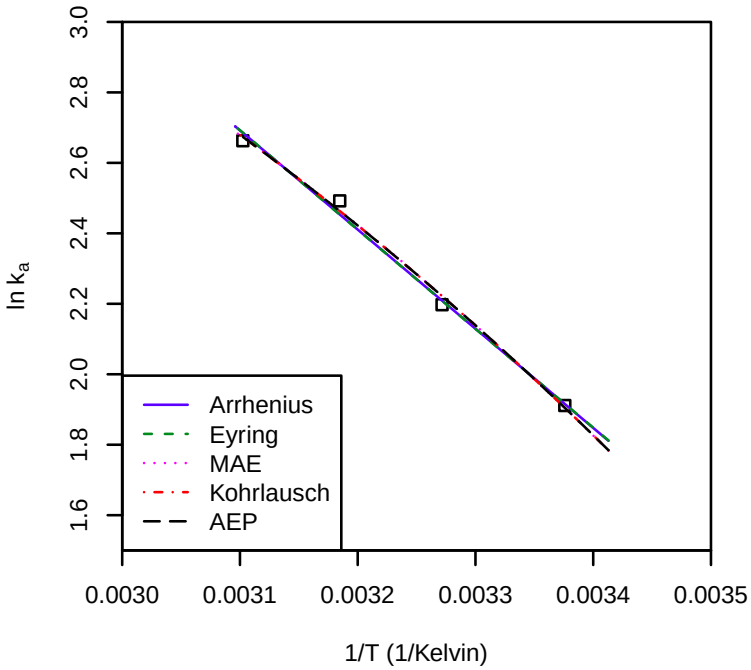

(a) k_a

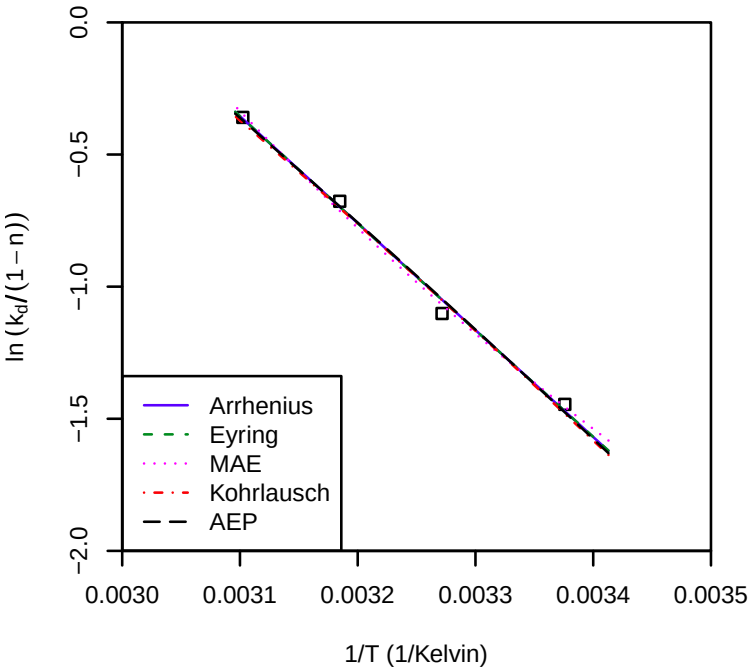

(b) k_m

Figure 2.10: Arrhenius plot of k_a and k_m with the Bertalanffy model of 2 parameters ($n = 0.1$): KH

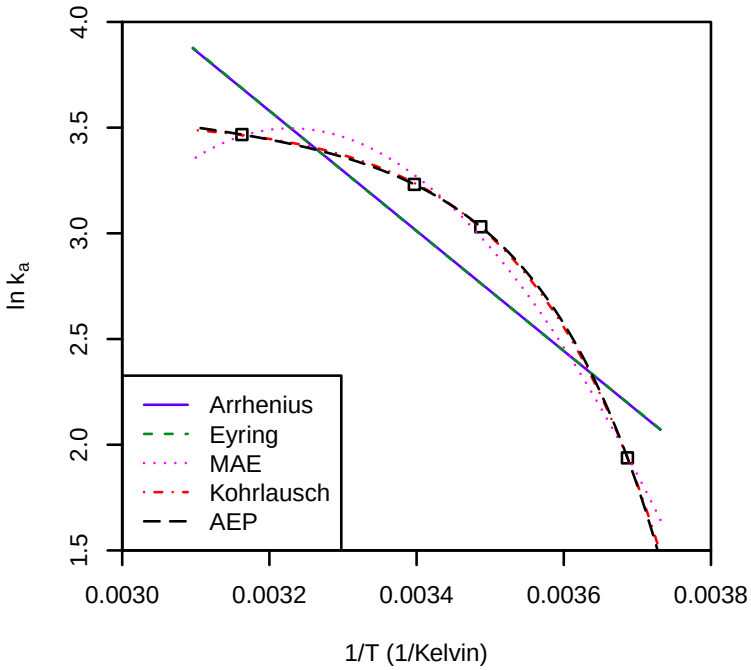

(a) k_a

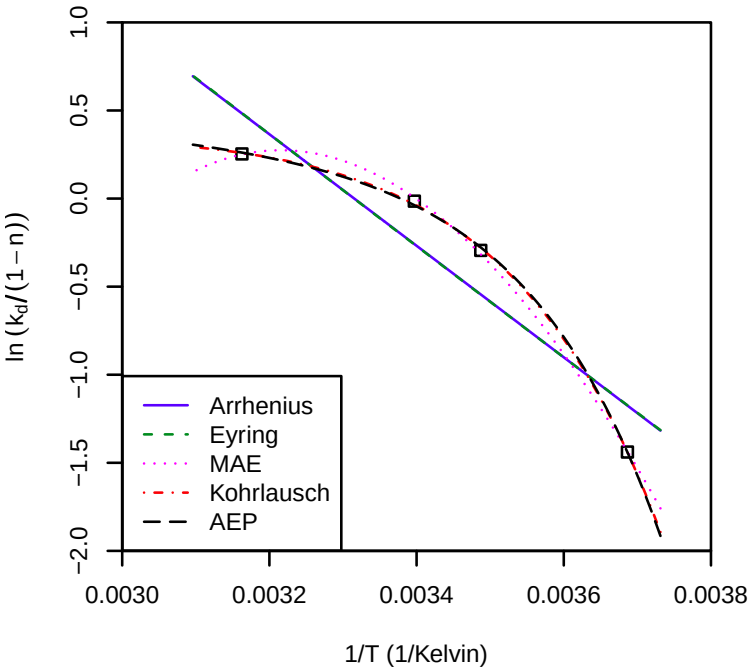

(b) k_m

Figure 2.11: Arrhenius plot of k_a and k_m with the Bertalanffy model of 2 parameters ($n = 0.1$): LZ

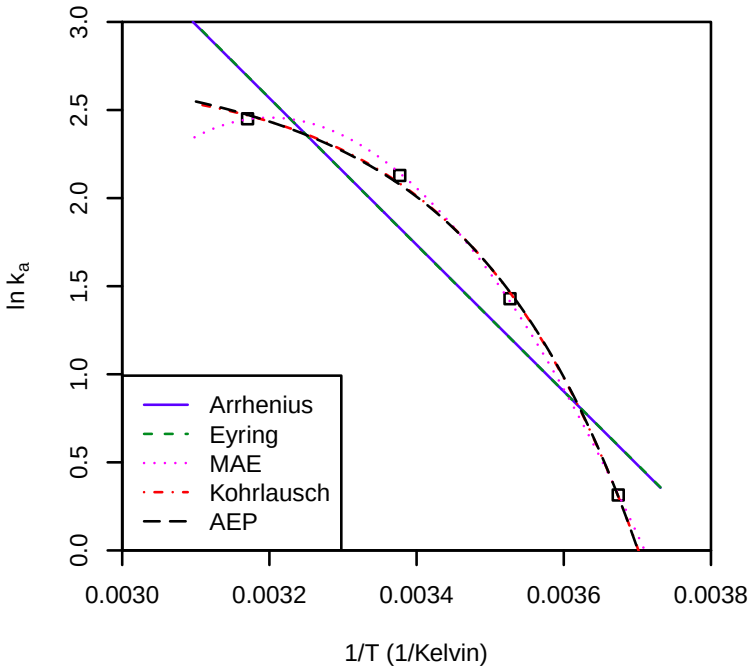

(a) k_a

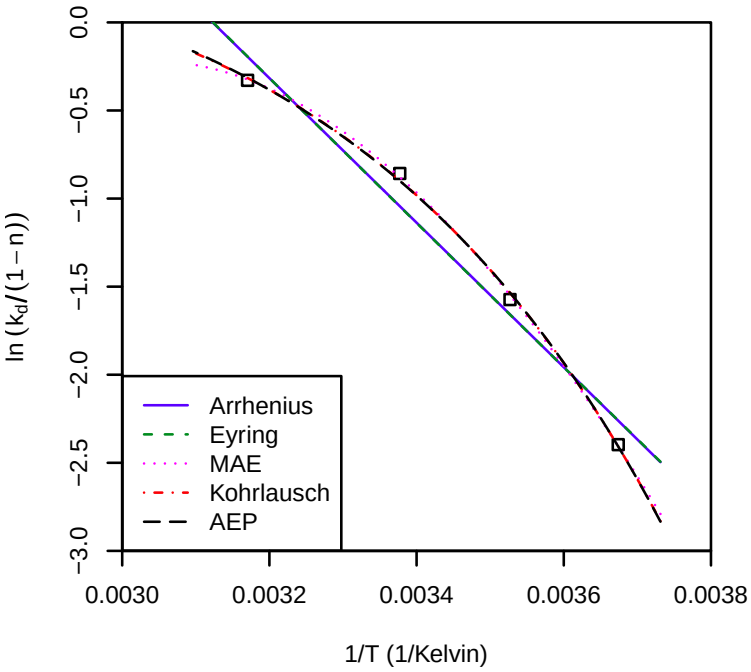

(b) k_m

Figure 2.12: Arrhenius plot of k_a and k_m with the Bertalanffy model of 2 parameters ($n = 0.1$): LH

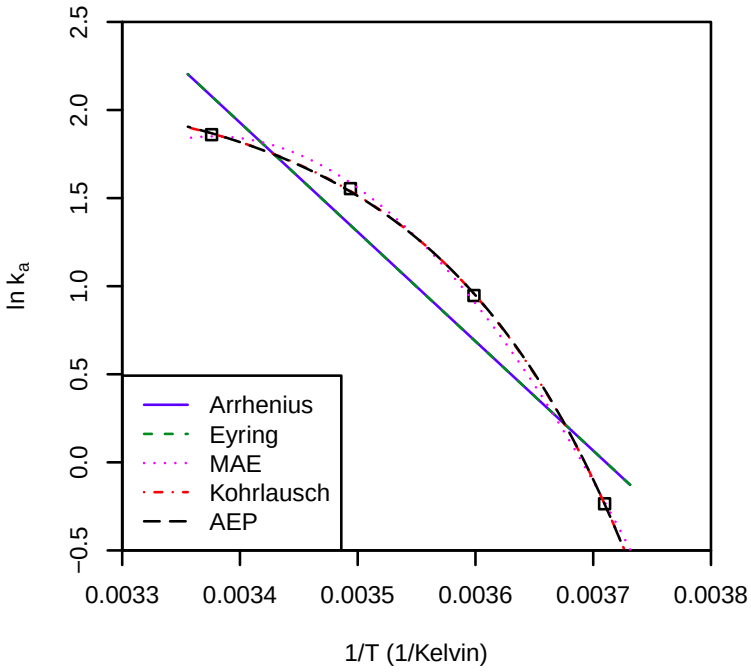

(a) k_a

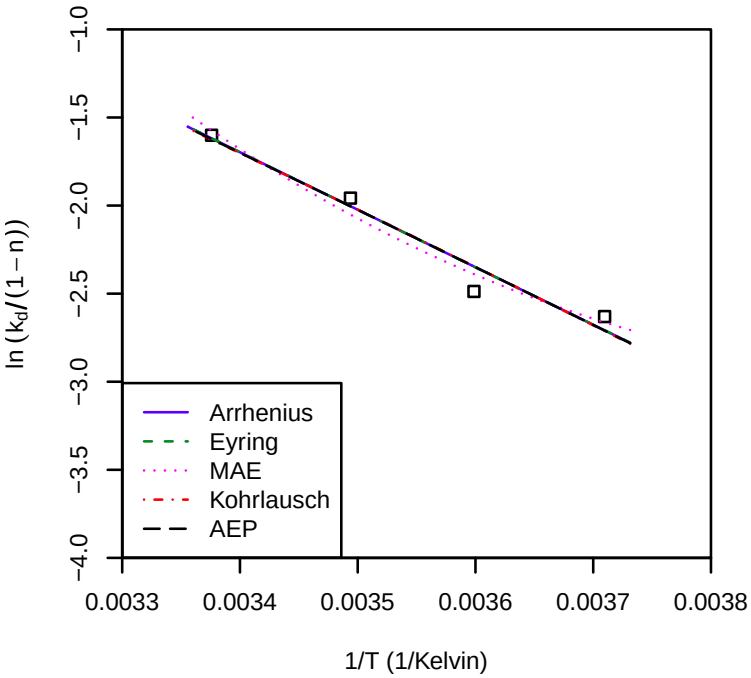

(b) k_m

Figure 2.13: Arrhenius plot of k_a and k_m with the Bertalanffy model of 3 parameters ($n = 0.1$): KC

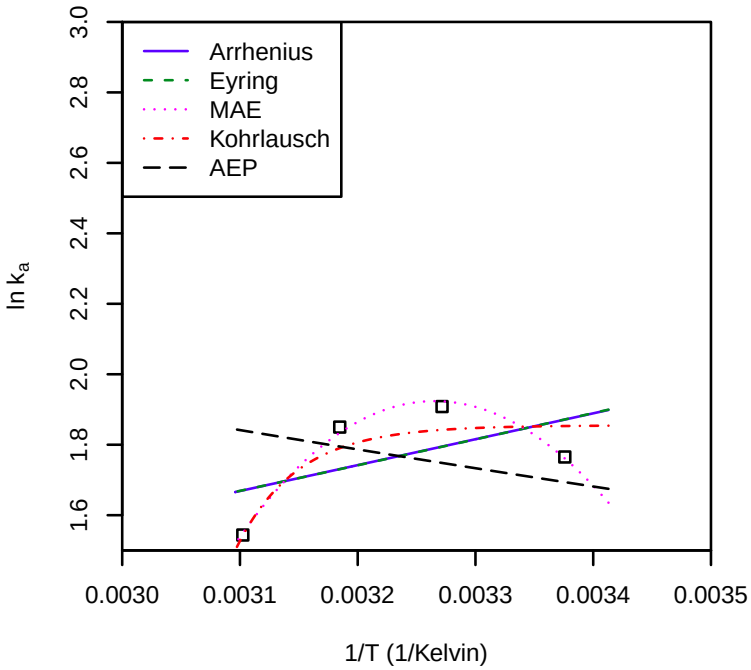

(a) k_a

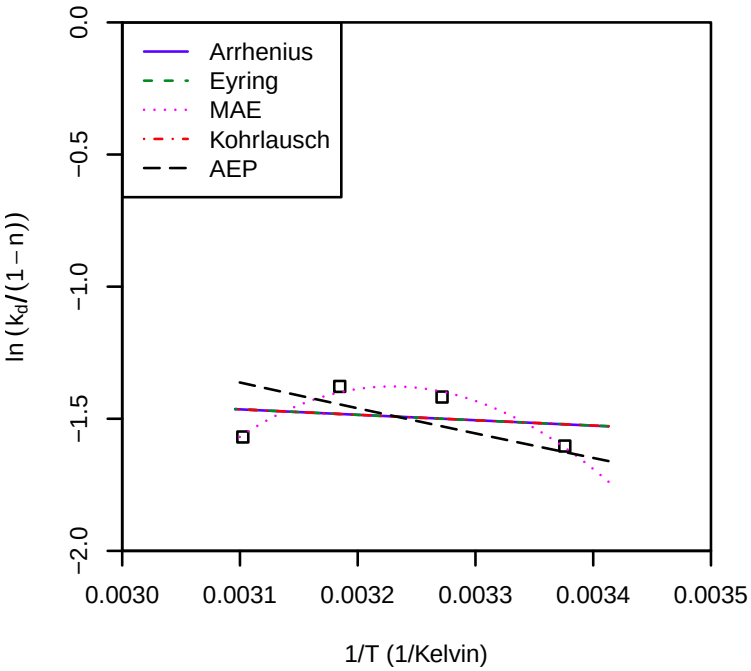

(b) k_m

Figure 2.14: Arrhenius plot of k_a and k_m with the Bertalanffy model of 3 parameters ($n = 0.1$): KH

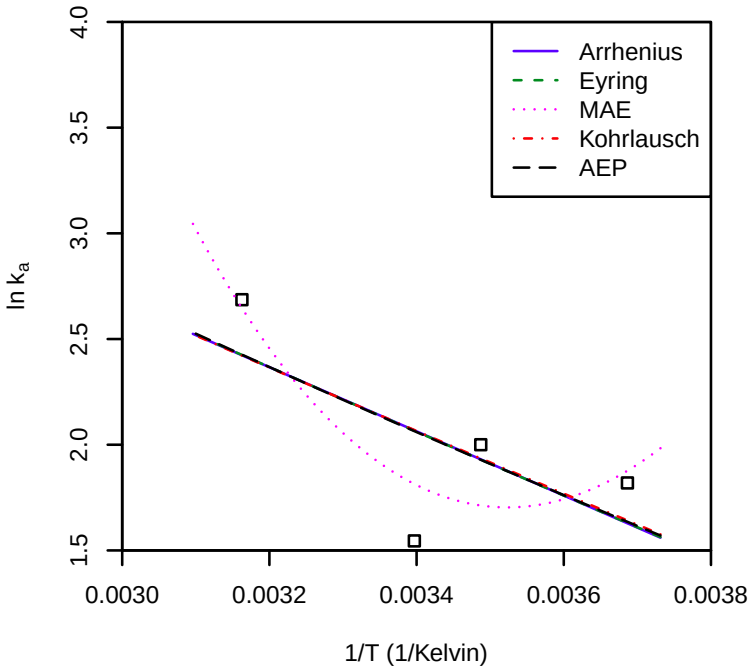

(a) k_a

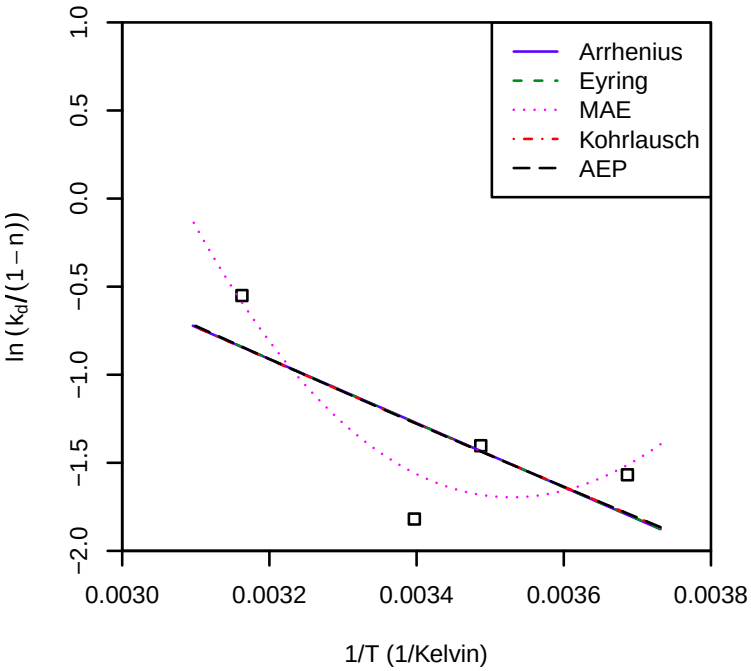

(b) k_m

Figure 2.15: Arrhenius plot of k_a and k_m with the Bertalanffy model of 3 parameters ($n = 0.1$): LZ

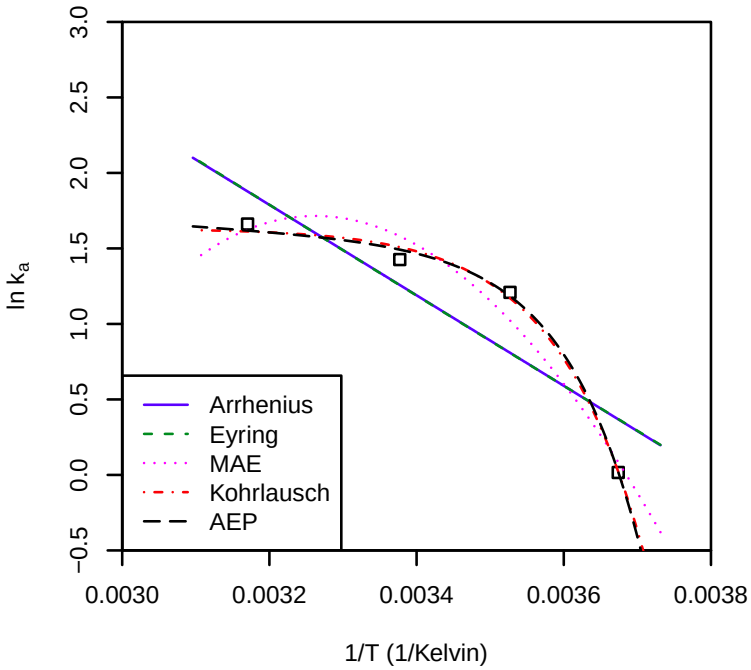

(a) k_a

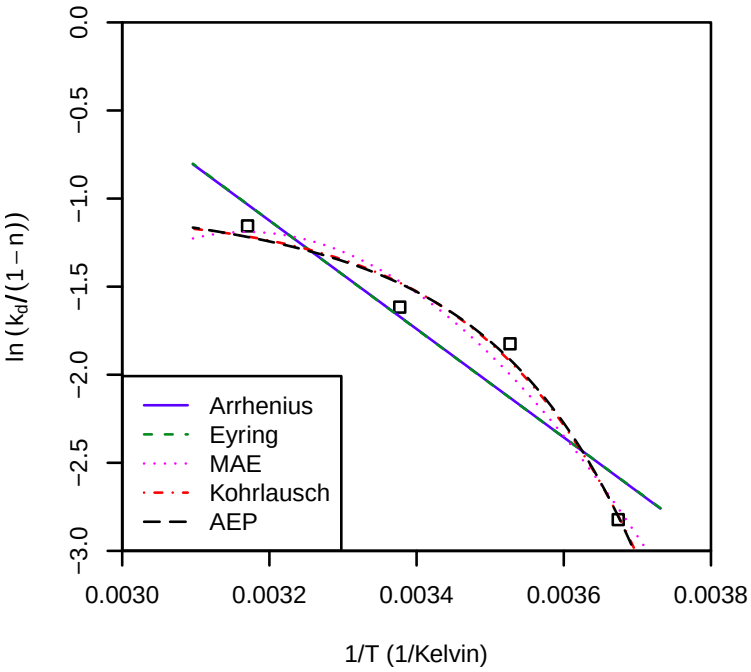

(b) k_m

Figure 2.16: Arrhenius plot of k_a and k_m with the Bertalanffy model of 3 parameters ($n = 0.1$): LH

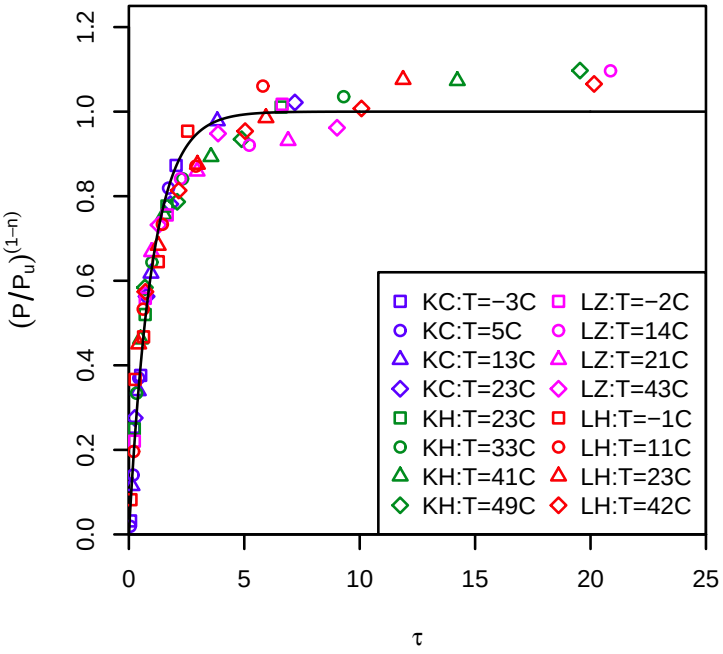

(a) Model with 2 Parameters

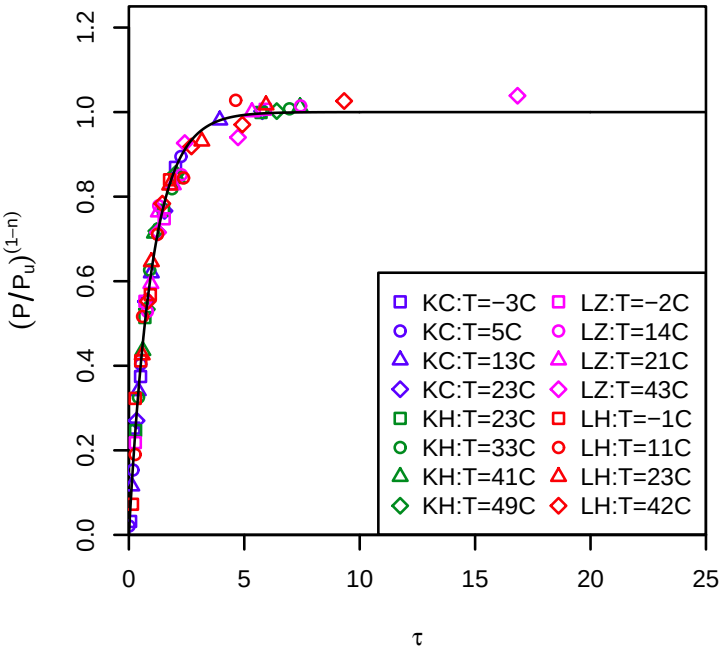

(b) Model with 3 Parameters

Figure 2.17: Relative strength-maturity relation from the Bertalanffy model with 2 and 3 parameters ($n = 0.1$)

2.5.4 Temperature Dependency of Limiting Strengths

In ASTM C 1074 [19], the rate constant k and P_u in Eq.(2.18) are estimated from the data set as regarding them as independent of each other in the regression. Subsequently, the maturity is computed on the basis of rate constant k for strength development, while P_u estimated by the data sets from various constant temperatures are not explicitly taken into account in strength prediction. As mentioned before, one of primary benefits from the proposed method is to derive the closed form function of the limiting strength by adopting several Arrhenius type functions representing the temperature dependency of both k_a and k_m, as introduced in the section 2.4.4. In the proposed method, k_a, k_d, k_m and P_u are correlated in terms of Eq.(2.45).

$$P_u^{1-n} = \frac{k_a}{k_d} = \frac{k_a\,(1-n)}{k_m} \tag{2.45}$$

Eq.(2.45) indicates that k_m is linearly proportional to k_d for a given n. Subsequently, if k_a and k_m can be represented by the function, P_u can be formulated according to various functions as listed in the section 2.4.4.

Figure 2.18 to 2.21 presents the resulting P_u according to data sets and the Bertalanffy model of analysis. The figures are organized according to analysis results from the Bertalanffy model with 2 parameters (B2P) and that with 3 parameters (B3P). Depending on the combinations of function for the limiting strength and the data sets, the derived profile are varied. In other words, the profile of limiting strength with temperature depends on the given mixture proportions and the corresponding concrete temperature ranges. For example, the limiting strength profile from KC and LH data sets showed the parabolic shape, and the maximum limiting strength would be given at around $T = 10°C \sim 15°C$. However, the limiting strength of KH and LZ decreases with

the increasing temperature, although the rate of decrease is also dependent on the temperature. Therefore, it would be interesting the capability of five Arrhenius type functions introduced in the research to represent the temperature dependency of the limiting strengths.

The functions of limiting strength derived by Arrhenius and Eyring equation are identical when the relative limiting strength is formulated. The negative slope is resulted under the conditions $E_{a1} < E_{k1}$ and $0 \leq n < 1$. Therefore, if k_m is more sensitive than k_a to the concrete temperature, the strength degradation at the later age because of high concrete temperature (cross-over effect) is caused. In addition, the concavity of the profile can be identified by the second derivatives, and the concave-up profile is achieved under $E_{a1} - E_{k1} > 2R(1-n)T$ or $E_{a1} - E_{k1} < 0$, while the concave-down profile is given by $0 < E_{a1} - E_{k1} < 2R(1-n)T$. Such concavity depends on the data sets. The limiting strength functions on the basis of Arrhenius and Eyring equations fit relatively well in the results from KH and LZ data sets with B2P since the estimated limiting strengths decrease with the temperature, while larger discrepancies are observed in KC and LH since the estimated P_u are parabolic. Therefore, the functions based on Arrhenius and Eyring equations are not appropriate when the estimated limiting strengths monotonically decrease or increase with temperature.

For the limiting strength function by MAE, the negative slope against temperature (the cross-over effect) is achieved only when

$$\alpha_{a3} + \frac{E_{a3}}{RT} < \alpha_{k3} + \frac{E_{k3}}{RT} \tag{2.46}$$

where $0 \leq n < 1$ in the Bertalanffy model. It is similar pattern with the function from Arrhenius or Eryring equation except considering the power α_{a3} and α_{k3} additionally. However, it is noted that the slope is dependent on the tem-

perature and it is changed at $T = -\left(E_{a3} - E_{k3}\right) / \left(R\left(\alpha_{a_3} - \alpha_{k3}\right)\right)$. However, the limiting strength function by MAE is parabolic, the concavity is also critical to represent the limiting strength in wide ranges of temperatures. Subsequently, the concave-down pattern is observed where

$$\left[\frac{RT\left(\alpha_{a3} - \alpha_{k3}\right) + \left(E_{a3} - E_{k3}\right)}{RT(1-n)}\right]^2 - \frac{RT + 2\left(E_{a3} - E_{k3}\right)}{RT(1-n)} < 0 \tag{2.47}$$

and the concave-up pattern is caused otherwise. As mentioned above the function by MAE relatively fit well for all data sets, especially for the parabolic profile of limiting strength from KC and LH data sets.

The relative limiting strength derived from Kohlrausch and AEP equations also have the same mathematical characteristics, although coefficients in the functions are altered with individual equations. The negative slope is given by

$$\gamma_{a5}\left(\frac{E_{a5}}{RT}\right)^{\gamma_{a5}} < \gamma_{k5}\left(\frac{E_{k5}}{RT}\right)^{\gamma_{k5}} \tag{2.48}$$

for $E_{a5} > 0$ and $E_{k5} > 0$ where $0 \leq n < 1$. Also, the concave-down profile of the function is given by

$$\begin{aligned} &\left(\gamma_{a5}\left(\frac{E_{a5}}{RT}\right)^{\gamma_{a5}} - \gamma_{k5}\left(\frac{E_{k5}}{RT}\right)^{\gamma_{k5}}\right)^2 \\ -\gamma_{a5}\left(\gamma_{a5}+1\right)(1-n)&\left(\frac{E_{a5}}{RT}\right)^{\gamma_{a5}} + \gamma_{k5}\left(\gamma_{k5}+1\right)(1-n)\left(\frac{E_{k5}}{RT}\right)^{\gamma_{k5}} < 0 \end{aligned} \tag{2.49}$$

for $0 \leq n < 1$. As regarding the analysis with parameters from B2P, The limiting strengths derived by both Kohlrausch and AEP equations represent the nonlinearity of limiting strength with wider ranges of temperature in all data sets. On the other hand, from the results with B3P, both functions describe nonlinearity of the limiting strengths for KC and LH data sets, while relatively larger deviations are observed for LZ data set. For KH data set with the analysis of

B3P, the function from Kohlrausch showed the best fit with the estimated limiting strengths, yet that with AEP function represents the limiting strengths with larger variance.

2.6 Statistical Analysis of Predicted Strengths

The strengths are predicted on the basis of the computed unitless maturity and the limiting strengths, as described in the previous sections. The strengths predicted by the proposed maturity method is compared to those by ASTM C 1074.

Considering the data structure of this analysis, the computation of correlation can be performed according to several levels (or categories). In the research, the analysis associated with the predicted strength is performed according to two levels as follows.

- Level I: The associated analysis is performed according to combinations of individual data sets and methods (e.g. variations of functions). In other words, within a given method and data set, the analysis is performed including all temperatures and test ages.
- Level II: The analysis is executed for the predicted strengths of all data sets according to variations of functions.

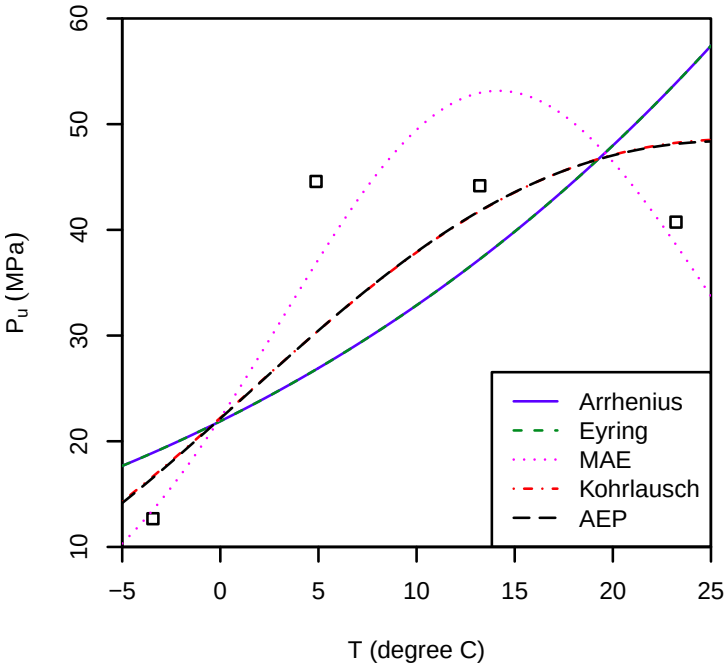

(a) Model with 2 Parameters

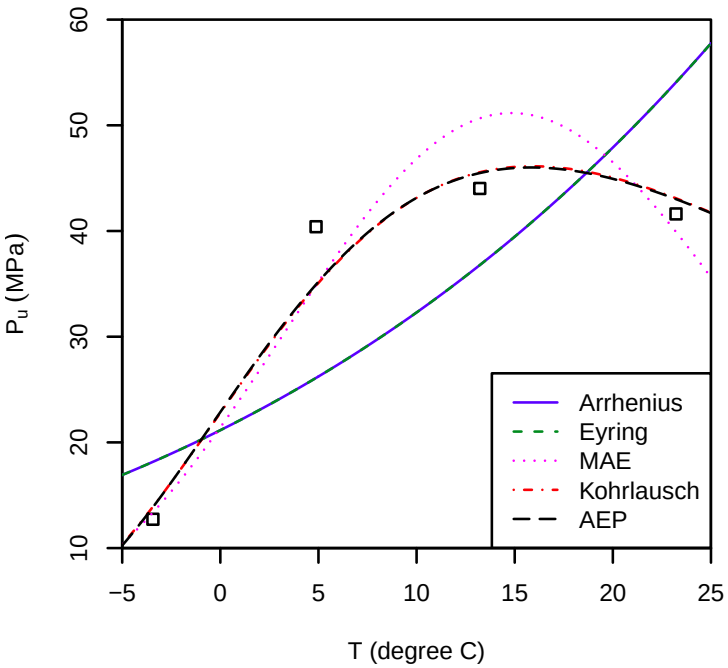

(b) Model with 3 Parameters

Figure 2.18: The limiting Strength P_u ($n = 0.1$): KC

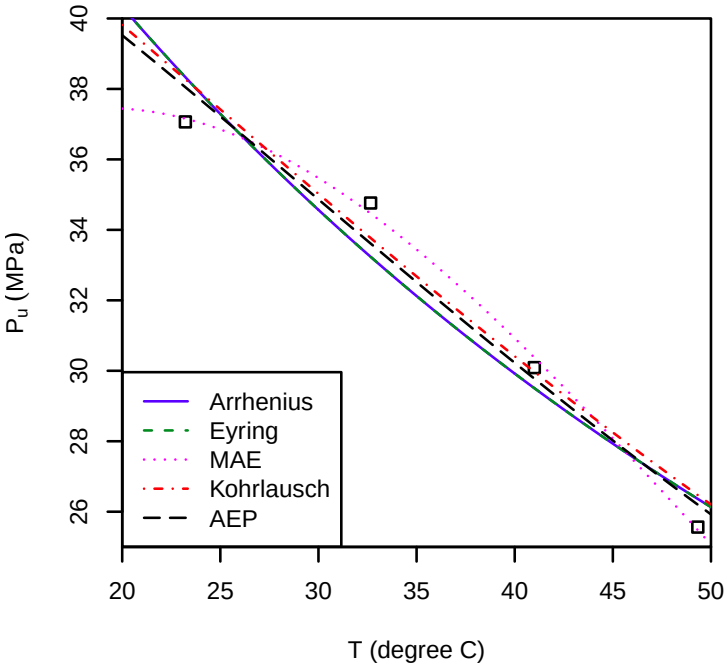

(a) Model with 2 Parameters

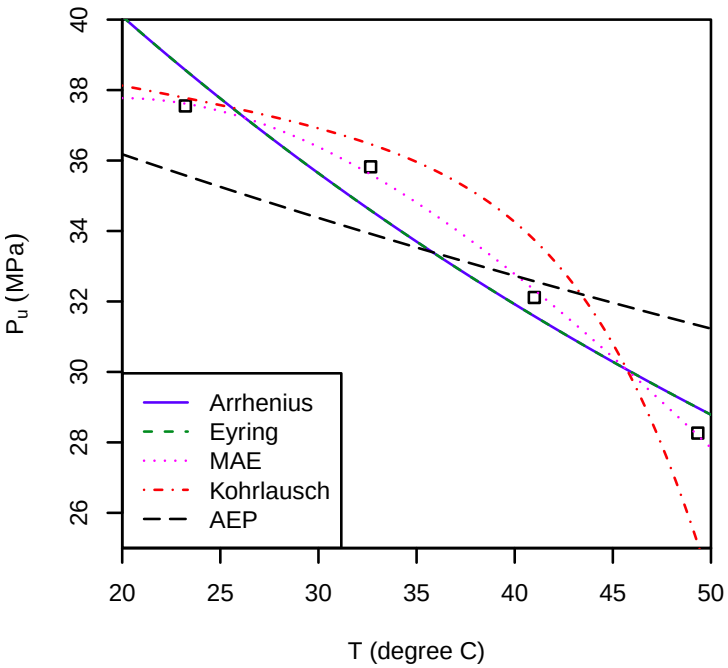

(b) Model with 3 Parameters

Figure 2.19: The limiting Strength P_u ($n = 0.1$): KH

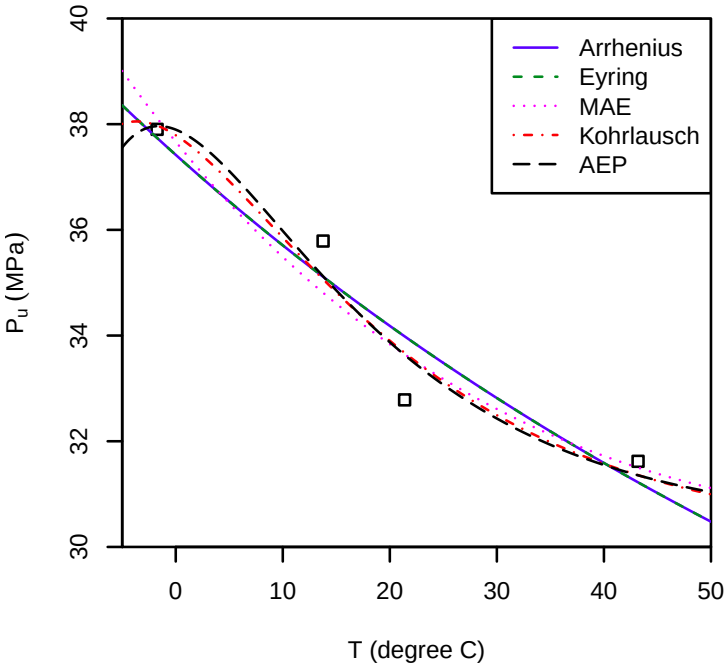

(a) Model with 2 Parameters

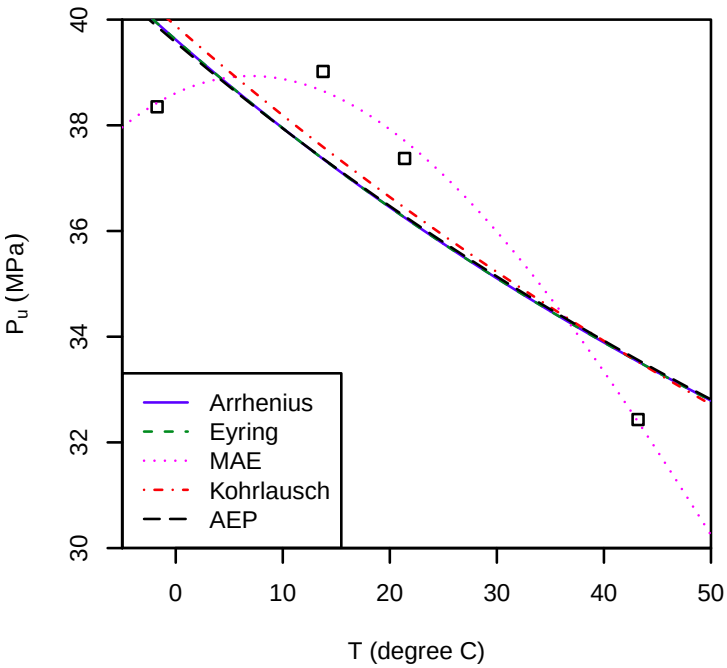

(b) Model with 3 Parameters

Figure 2.20: The limiting Strength P_u ($n = 0.1$): LZ

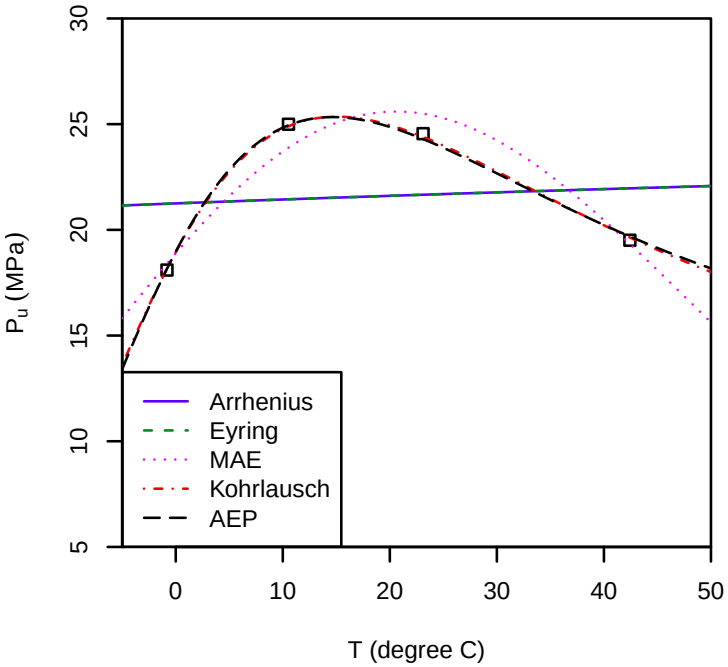

(a) Model with 2 Parameters

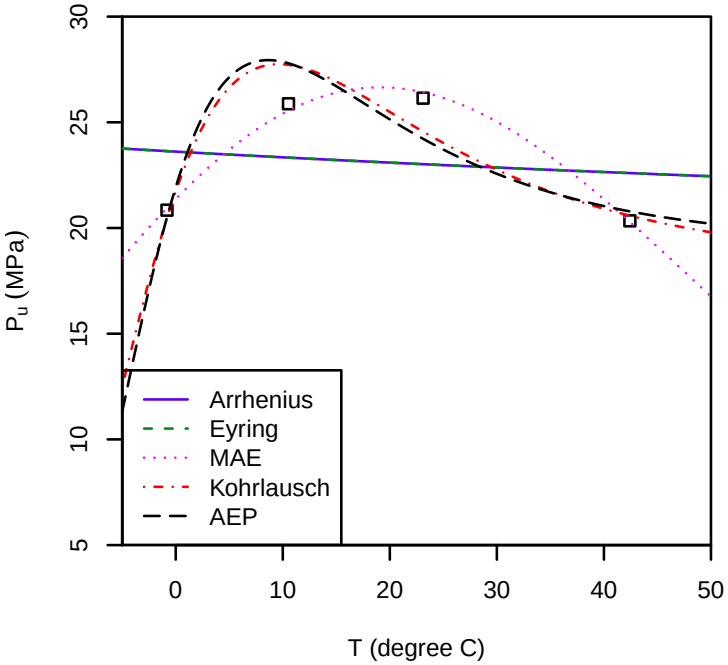

(b) Model with 3 Parameters

Figure 2.21: The limiting Strength P_u ($n = 0.1$): LH

2.6.1 Correlation between Predictions and Measurements

The first statistical analysis for predicted strengths is to compute the correlation ρ between the predictions and measurements by

$$\rho = \frac{\sum_{i=1}^{N} \left(P_i - \bar{P}\right) \left(M_i - \bar{M}\right)}{(N-1)\,\sigma_P \sigma_M} \tag{2.50}$$

where P_i and M_i are predicted and measured strengths, respectively, also $\bar{P}$ and $\bar{M}$ are their mean values. σ_P and σ_M are standard deviation of prediction of measurements, respectively. The correlation is a measure to examine the extent of linearity between variables. Therefore, if ρ is closer to 1, the predicted strengths are linearly proportional to the measurements with less variance. On the other hand, the lower correlation factor is induced by the nonlinearity and/or larger variances. Unfortunately, the correlation itself cannot explicitly evaluate whether a particular method cause accurate predictions. However, it would explain that how much variations in the strength prediction are generated by a specific method. Also, it provides certainties to perform the multi-linear regression analysis to examine the details of methodologies; that is, the higher correlations regardless of the methods enable one to perform the multi-linear regression analysis to examine the factors affecting the predictions such as methods, data sets, temperature, and times.

Figure 2.22 shows the comparison of predicted against measured strengths by ASTM C 1074 and by the proposed methods, and it shows that the proposed method predicts the strength with less variation than ASTM C 1074. The resulting correlations for the level I data structure are summarized in Table 2.4 and 2.5 according to the number of parameters in the Bertalanffy model. In three data sets except the case of KC data sets, the highest correlations are achieved when MAE, Kohlrausch, and AEP equations are implemented, then

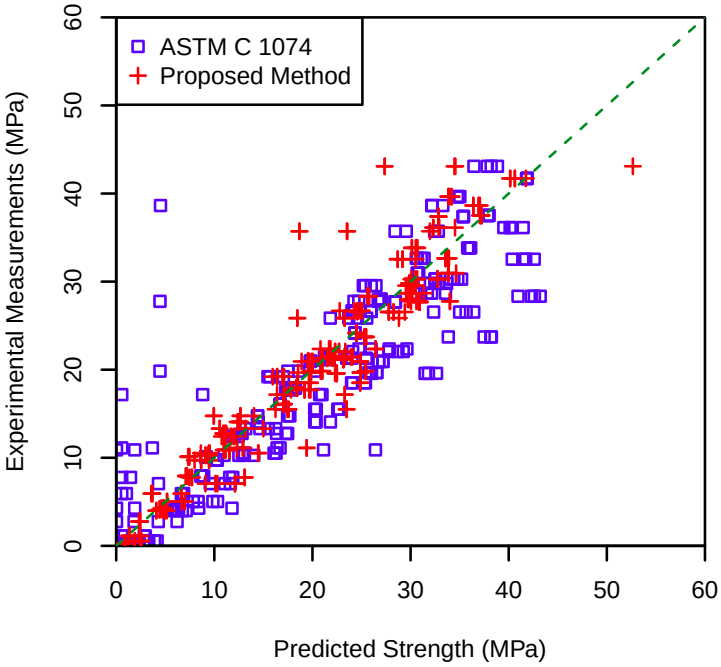

(a) 2 Parameters

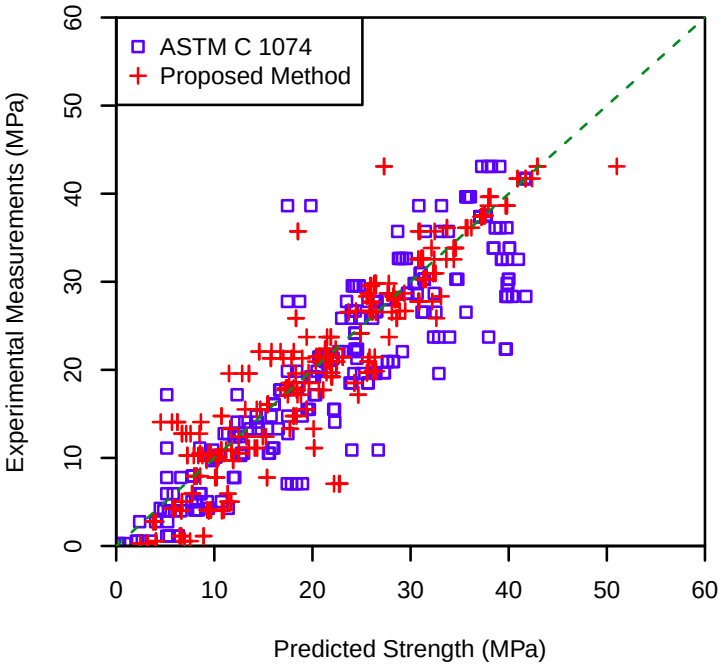

(b) 3 Parameters

Figure 2.22: Comparison of Measured Strengths with the Predictions

Table 2.4: Correlation between predictions and measurements by 2 parameter models: Level I

Data	KC	KH	LZ	LH
FHP	0.9597	0.8869	0.9007	0.9120
NS	0.9672	0.9044	0.6538	0.8639
B-Arrhenius	0.9239	0.9754	0.9020	0.9030
B-Eyring	0.9238	0.9754	0.9015	0.9026
B-Modified Arr.	0.9851	0.9797	0.9520	0.9783
B-Kohrlausch	0.9702	0.9768	0.9508	0.9788
B-Eyring Polanyi	0.9705	0.9770	0.9503	0.9785

Table 2.5: Correlation between predictions and measurements by 3 parameter models: Level I

Data	KC	KH	LZ	LH
FHP	0.9560	0.9025	0.6485	0.8970
NS	0.9698	0.9417	0.6422	0.8775
B-Arrhenius	0.9174	0.9673	0.8509	0.8971
B-Eyring	0.9174	0.9673	0.8509	0.8968
B-Modified Arr.	0.9714	0.9675	0.8664	0.9689
B-Kohrlausch	0.9842	0.9626	0.8482	0.9588
B-Eyring Polanyi	0.9845	0.9705	0.8519	0.9563

the Bertalanffy model with Arrhenius and Eyring equations gave the second highest correlations. In both cases, the LZ data set caused relatively lower correlation regardless of the methods. Such data set-wise results are also reflected

Table 2.6: Correlation between predictions and measurements: Level II

Method	2P	3P
FHP	0.9175	0.9014
NS	0.8716	0.9084
B-Arrhenius	0.9224	0.8924
B-Eyring	0.9222	0.8922
B-Modified Arr.	0.9791	0.9439
B-Kohrlausch	0.9727	0.9423
B-Eyring Polanyi	0.9726	0.9560

in computation of correlation for level II, as shown in Table 2.6. The highest correlation is resulted for the case that MAE, Kohrlausch, and AEP are used in the predictions regardless of cases of B2P and B3P. For the predictions based on Arrhenius and Eyring equations, the resulting correlation is higher than both of ASTM methods in the prediction with B2P, while slightly lower correlation by about 0.01 is caused in prediction with B3P.

Therefore, the proposed method gave less variation in the predicted strengths than ASTM C 1074.

2.6.2 The factors affecting the strength prediction

The relative accuracy in the strength prediction between the proposed method and ASTM C 1074 cannot be shown by using the computation of correlation, while the extent of uncertainty can be measured. In other words, the correlation

analysis cannot evaluate whether the given method over or underestimates the strengths. Therefore, the multi-linear regression analysis is performed to investigate the extent of accuracy in the strength prediction either by the proposed method with variations of Arrhenius type functions or ASTM C 1074.

The associated statistical model is postulated by

$$E_{ijk} = \beta_1 P_i + \beta_2 \left(\text{Method}\right)_j + \epsilon_{ijk} \tag{2.51}$$

to investigate the effect of method variations (NS and FHP) within ASTM C 1074 or the proposed method. Also, since the individual data sets used the different mixture proportions, particularity of data set in terms of strength predictions would be varied. Therefore, an additional model is implemented to examine the effects of data sets by introducing dummy variables.

$$E_{ijk\ell} = \gamma_1 P_i + \gamma_2 \left(\text{Method}\right)_j + \gamma_3 \left(\text{Data}\right)_k + \epsilon_{ijk\ell} \tag{2.52}$$

In the analysis results, if the predictions are close to the experimental measurements, the resulting slope of β_1 and γ_1 are close to unity. Also, if β_1 or γ_1 are less than 1, it indicates the given method overestimates the strength, while it underestimates the strength if β_1 or γ_1 are greater than 1. In addition, β_2, γ_2, and γ_3 change the intercept with 0 or 1 of the associated dummy variable.

Table 2.7 and 2.8 summarizes the results on the basis of Eq.(2.51). The slope of prediction β_1 from ASTM C 1074 is less than 1, thus it generally overestimates the strengths. On the other hand, the slope of proposed method is closer to 1 and slightly greater than 1. From Table 2.7, the slope of NS method is statistically significant at 5% level, and it indicates NS method predicts higher strength than FHP method. However, there is no significant difference within the basis-functions of the proposed method is observed, as presented in Table 2.8. Also,

Table 2.7: Analysis results for predictions by the ASTM C 1074 with Eq.(2.52)

ASTM C 1074 with 2 Parameters (Adjusted $R^2 = 0.9527$)				
	Estimate	Std. Error	$t-$value	$Pr(>\|t\|)$
P	0.8506	0.0264	32.18	0.0000
FHP	1.1472	0.7384	1.55	0.1215
NS	2.9125	0.6947	4.19	0.0000
ASTM C 1074 with 3 Parameters (Adjusted $R^2 = 0.9585$)				
P	0.8998	0.0258	34.86	0.0000
FHP	-0.2557	0.7181	-0.36	0.7221
NS	1.6731	0.6732	2.49	0.0136

results associated with the effects of data sets are shown in Table 2.9 and 2.10. Similar values of the slope γ_1 are caused, and the effects of data sets are varied according to the ASTM C 1074 and the proposed method.

Therefore, the predicted strengths by the proposed method predicts the strength relatively closer to the measurements with less uncertainties by ASTM C 1074.

Table 2.8: Analysis results for predictions by the proposed method with Eq.(2.52)

ASTM C 1074 with 2 Parameters (Adjusted $R^2 = 0.9792$)				
	Estimate	Std. Error	$t-$value	$Pr(>\|t\|)$
P	1.0049	0.0173	58.02	0.0000
B-Arrhenius	-0.1822	0.5393	-0.34	0.7356
B-Eyring	-0.1846	0.5393	-0.34	0.7323
B-Kohlrausch	0.2720	0.5341	0.51	0.6110
B-MAE	-0.0671	0.5380	-0.12	0.9008
B-AEP	0.2337	0.5346	0.44	0.6623
ASTM C 1074 with 3 Parameters (Adjusted $R^2 = 0.9670$)				
P	1.0081	0.0225	44.71	0.0000
B-Arrhenius	-0.3077	0.6901	-0.45	0.6559
B-Eyring	-0.3098	0.6901	-0.45	0.6538
B-Kohlrausch	-0.7570	0.6968	-1.09	0.2781
B-MAE	-0.8563	0.6984	-1.23	0.2210
B-AEP	-1.3586	0.7061	-1.92	0.0552

2.7 Discussion

2.7.1 Advantages of the Proposed Method

The Bertlanaffy model consists of two separate part to regard the two mechanisms, accelerating and decelerating mechanisms. The proposed method is

Table 2.9: Analysis results for predictions by ATSM C 1074 with Eq.(2.51)

ASTM C 1074 with 2 Parameters (Adjusted $R^2 = 0.9613$)				
	Estimate	Std. Error	$t-$value	Pr(>|t|)
P	0.8514	0.0270	31.51	0.0000
FHP	1.3337	0.7966	1.67	0.0953
NS	3.1007	0.7639	4.06	0.0001
KH	-3.1601	0.8623	-3.66	0.0003
LZ	3.1592	0.8482	3.72	0.0002
LH	-0.6934	0.7655	-0.91	0.3659
ASTM C 1074 with 3 Parameters (Adjusted $R^2 = 0.9607$)				
P	0.8863	0.0284	31.19	0.0000
FHP	0.6005	0.8180	0.73	0.4635
NS	2.5004	0.7814	3.20	0.0015
KH	-1.9470	0.8564	-2.27	0.0238
LZ	1.2426	0.8760	1.42	0.1572
LH	-1.2961	0.7715	-1.68	0.0941

to effectively consider the temperature dependency of the limiting strength from the measured temperature-time data. Since ASTM C 1074 cannot regard such strength degradation due to early high concrete temperature, the proposed method potentially includes the advantage to consider such strength reduction for concretes exposed to the high temperature. Based on the given sets of data, the strength reduction mainly occurs above $10°C$. However, it is noted that the strength reduction under cold temperature near freezing point $0°C$ would

Table 2.10: Analysis results for predictions by the proposed method with Eq.(2.51)

ASTM C 1074 with 2 Parameters (Adjusted $R^2 = 0.9802$)				
	Estimate	Std. Error	$t-$value	$Pr(>\|t\|)$
P	1.0103	0.0193	52.43	0.0000
B-Arrhenius	0.9692	0.5884	1.65	0.1005
B-Eyring	0.9668	0.5885	1.64	0.1013
B-MAE	1.0849	0.5873	1.85	0.0656
B-Kohlrausch	1.4258	0.5841	2.44	0.0152
B-AEP	1.3874	0.5845	2.37	0.0182
KH	-1.1625	0.5357	-2.17	0.0307
LZ	-1.4155	0.5708	-2.48	0.0136
LH	-2.2323	0.4898	-4.56	0.0000
ASTM C 1074 with 3 Parameters (Adjusted $R^2 = 0.9718$)				
P	1.0079	0.0236	42.75	0.0000
B-Arrhenius	-0.3496	0.7240	-0.48	0.6295
B-Eyring	-0.3516	0.7240	-0.49	0.6275
B-Kohlrausch	-0.7987	0.7297	-1.09	0.2745
B-MAE	-0.8981	0.7310	-1.23	0.2201
B-AEP	-1.4002	0.7376	-1.90	0.0585
KH	2.8271	0.6218	4.55	0.0000
LZ	-0.7002	0.6780	-1.03	0.3024
LH	-1.5454	0.5845	-2.64	0.0086

be different from the cross-over effects since it would be due to lower level of degree of hydration in lieu of the change of smaller-scale structure. Therefore, more fundamental studies on the concretes under cold temperature are required.

2.7.2 Explanation of Cross-Over Effects by the proposed method

The cross-over effect have been explained by different hydrated products with temperatures [33] and the lower density of the micro-structure [51], and it can be also explained by the mechanisms of the strength development in the research. When considering the function of limiting strength on the basis of Arrhenius equation, the cross over effect occurs when the determining rate constant is more sensitive to the temperature, $E_{a1} < E_{k1}$. If the concrete temperature rises, both rate constants representing accelerating and decelerating mechanisms increase. However, if the decelerating mechanism is much highly sensitive to the temperature than the accelerating mechanisms, the cross-over effect is observed. When explaining with other Arrhenius-type equations, the results can be similarly explained by the individually associated parameters.

2.7.3 Difference of the Proposed Method from ASTM C 1074

The proposed method provides the alternative function to compute the rate constants of strength development. For ASTM C 1074, the effect of limiting strength is regarded in performing the nonlinear regression by using the hyperbolic func-

tion. However, its temperature dependency is not regarded in the strength prediction. Therefore, ASTM C 1074 method is impossible to consider the crossover effects. The proposed method manipulates two temperature dependent rate constants, and the flexibility of the Bertalanffy model makes it possible to represent the limiting strength as a function of concrete temperature with the closed form. Although the cause of strength reduction at cold concrete temperature (near freezing point) is different from that at high concrete temperature, several functions to consider the nonlinearity of Arrhenius plot for model parameters could explicitly consider the temperature dependent limiting strength.

2.7.4 Strength-based Degree of Hydration

The strength development is based on the hydration. However, the maturity method implements the strength data to estimate the temperature sensitivity of model parameters, subsequently combinational mechanisms with the hydration such as bond of pastes with aggregates are also reflected in the parameters without clarifying the correlation of mechanisms. Also, the exponent to minimize the variance in the nonlinear regression is much less than 2/3, limit value of isometric assumption, and it does not match with the characteristic of hydration that would induce greater exponent value than 2/3. Even if the relative strength-maturity relation ranges from 0 to unity, more researches to recognize the temperature dependent mechanism that contribute to the strength development is required. However, if the property of interest is much highly sensitive to the chemical reaction such as the setting time of paste, the exponent value would be greater than the limit value.

2.8 Conclusion

The research proposed the framework of maturity method by adopting the Bertalanffy model to estimate the accelerating and decelerating rate constants for strength development, and five Arrhenius type functions are tested to represent the temperature dependency of model parameters. Subsequently, the strengths of concretes are predicted on the basis of relation between relative limiting strength and unitless maturity. The proposed method is applied to 4 independently obtained data sets, and the results in the application processes are compared to those by ASTM C 1074. Eventually the following conclusions are drawn.

- The predicted strengths by the proposed method are closer to the experimental measurements than those by ASTM C 1074. One of reason is because the proposed method actively considers the temperature dependency of limiting strengths.
- The closed form functions to represent temperature dependency of the limiting strengths are derived on the basis of five Arrhenius types of equations by using the temperature dependent model parameters of the Bertalanffy model.
- The relation of temperature sensitivity of accelerating and decelerating mechanisms will determine if the cross-over effect is observed. If decelerating rate constant is more sensitive to the temperature, the cross-over is estimated from the proposed method. However, its extent is dependent on the Arrhenius-type equations.
- The predicted strengths on the basis of MAE, Kohlrausch, and AEP equa-

tions caused higher correlation with the measurement since they can consider higher nonlinearity of model parameters on Arrhenius plots.

More researches are required to investigate the ranges of activation energies for Arrhenius type equations. Also, it will be necessary to investigate the applicability of the proposed method to various properties other than the compressive strength.

CHAPTER 3

THE RELATIONSHIP BETWEEN THE NURSE-SAUL DATUM TEMPERATURE AND THE FHP ACTIVATION ENERGY FOR CONCRETE MATURITY

3.1 Brief summary of Carino's work

Carino[55] reviewed the fundamental background of the maturity method in general, with emphasis on both the linear Nurse-Saul (NS) method and the non-linear, Arrhenius equation-based, Freiesleben-Hansen-Pederson (FHP) method for computing maturity of concrete as a function of both time and temperature. He reviewed the role of the NS Datum Temperature (T_d) and the FHP activation energy (E_a) as variables that can be used to tune the procedures to the temperature sensitivity of the particular concrete mixture in question. On the basis of the applied principles of chemical kinetics that underlie the maturity method, Carino showed that while E_a can characterize the influence of temperature on the rate of strength-gain of a given mixture at any temperature, the corresponding value of T_d for the same mixture depends also on the temperature or temperature range of interest. He demonstrated a means of computing a value of T_d compatible with a given value of E_a, for a given range of concrete temperature. His method is based on a best-linear-fit to the FHP and ASTM C1074 nonlinear "age-conversion factor" curve, over the temperature range of interest. Therefore, the best-linear-fit of age conversion factor over the given concrete temperature range by Carino's approach has a single degree of freedom since a point $(T_r, 1)$ is already fixed. An example of the application of Carino's method is shown in Figure 3.1, in which the solid curve is the ASTM C1074 age conver-

sion factor for a reference temperature (T_r) of $20°C$, and an activation energy (E_a) of $42.7\ kJ/mol$. Two best-fit linear approximations are shown for temperature, $0°C \leq T \leq 20°C$ and $20°C \leq T \leq 40°C$. The X-axis (temperature axis) intercepts of $-4.4°C$ and $9.0°C$, respectively are the corresponding values of T_d that would approximate the relative maturity (or "equivalent age") obtained by the nonlinear (FHP) approach for the given E_a and T_r. The resulting datum temperatures from best-linear-fits are at each temperature range. However, the

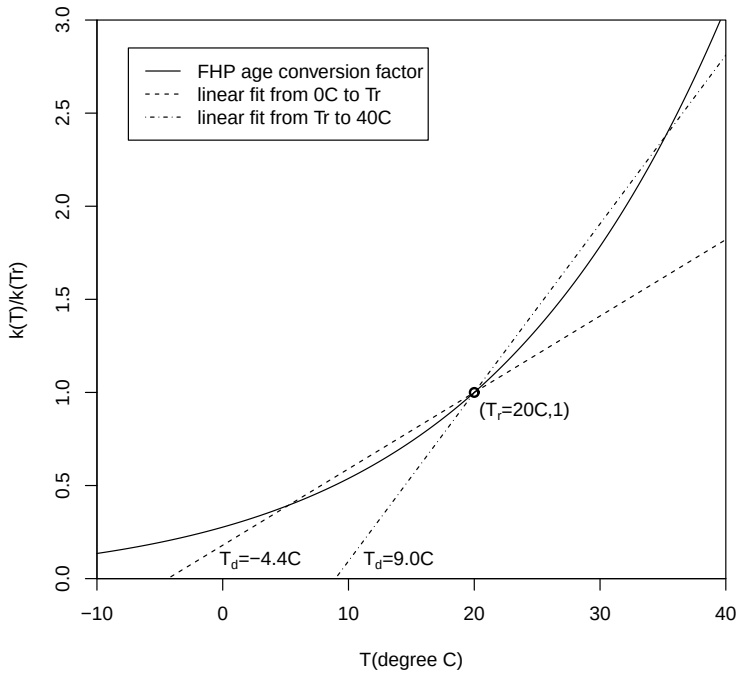

Figure 3.1: Age conversion factor curve for $T_r = 20°C$, showing Carino's method for obtaining compatible datum temperatures for $T = [0°C, 20°C]$ and $T = [20°C, 40°C]$

age conversion factor (or Carino's "affinity ratio"[55]) is the ratio of the rate of strength gain at a given temperature relative to the rate of strength gain at a predetermined "reference temperature." This means that the value of the age

conversion factor must equal 1 at the reference temperature. This fact constrains Carino's method for finding a compatible T_d as foll ows: the temperature range over which the compatible T_d is sought must either begin or end at the reference temperature. Also, Carino's computation of a unique value of T_d that is compatible with a given value of E_a over a given temperature range is actually a special case of the general principle that as the magnitude of the temperature range gets smaller about T_r, there exists a unique value of T_d that is compatible with a given value of E_a at T_r. As presented in this paper, by basing the computation of T_d on the more fundamental "rate constant curve" rather than the age conversion factor, this general principle can be expanded to finding a uniquely compatible T_d at any temperature, regardless of T_r. Further, once a compatible value of T_d can be found for any temperature, a number of ways are presented to expand this to an appropriate value of T_d over an expected temperature range or for a specific time-temperature record (temperature profile). Results can be applied to either the NS maturity concept[19, 37, 38] or to the relative maturity expressed by FHP[20].

3.2 Background: The rate constant and the maturity method

One way to describe the difference between the linear NS and the nonlinear FHP methods for computing maturity is to first consider that the development of microstructure that contributes to development of concrete properties proceeds at a rate that is temperature dependent. As detailed by Carino[73, 55, 74, 39], the influence of temperature on the rate of strength gain is characterized by a so-called "rate constant," $k(T)$, that can be obtained experimentally for any given concrete or mortar mixture at a series of given isothermal temperatures,

using the methods of ASTM C1074 Appendix A[19]. However, the physical meaning of "rate constant" in this context differs somewhat from the classical application in chemical kinetics, in which the "rate constant" is an algebraic term in the "rate law" used to describe masses of products and reactants as a function of time[25]. In the concrete maturity case the "product" of the chemical reaction of cementitious materials is strength or some other measurable and time-dependent property of interest. Thus the so called rate constant at any temperature can be computed from strength versus time data collected at that temperature, as described in ASTM C1074 Appendix A[19]. A mathematically similar approach, known as the Michaelis-Menton method, has been employed in the study of rates of enzyme reactions[25, 75].

Carino[19, 55, 74] offers a clear and complete example of finding the rate constant by first measuring compressive strength versus time at various isothermal temperatures for mortar with W/C=0.43. Values of $k(T)$ were found by fitting these data to the hyperbolic equation, as re-plotted by the authors in Figures 3.2 and 3.3. (also adapted from ASTM C1074)

Figure 3.3 plots values of $k(T)$ as a function of T. The smooth curve is fitted to the data by the Arrhenius Equation[21], and the straight line is the best linear fit over the entire temperature range of the data points. Herein lies the first fundamental difference between the NS and the FHP methods: the NS method implicitly assumes the linear relationship between rate constant, $k(T)$ and temperature shown in Eq.(3.1)[55]. The FHP method is based on the nonlinear Arrhenius equation[21, 55, 20] shown in Eq.(3.2).

$$k(T) = \beta\,(T - T_d) \tag{3.1}$$

$$k(T) = A \exp\left[-\frac{E_a}{RT}\right] \tag{3.2}$$

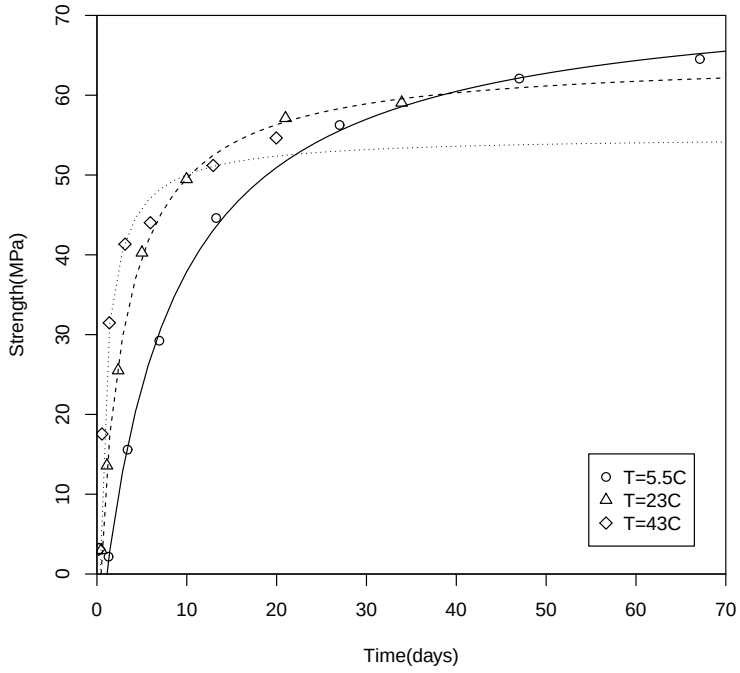

Figure 3.2: Strength-time measurements and fitting with hyperbolic function ($S(t)$ =strength at time t, k =rate constant, t_0 =time to initiate the strength development)

where $k(T)$ is rate constant, β is slope (constant), T_d is datum temperature, A is pre-exponential factor, E_a is the activation energy, R is the ideal gas constant, and T is concrete temperature.

The nonlinear character of the data was well-represented by Eq.(3.2) with calculated activation energy of $42.7\ kJ/mol$ and $A = 1.2 \times 10^7$ with 0.999 adjusted-R^2 and SSE(Sum of Square Error)$= 0.00113$. The best linear fit, described by Carino[73, 55] and as referred to in ASTM C 1074, was obtained by the authors by the least squares method yielding a Datum temperature of $4.6°C$(0.899 adjusted-R^2 and $SSE = 0.041$) It is interesting to note that in Saul's early development of what later came to be the NS method, he fixed T_d at

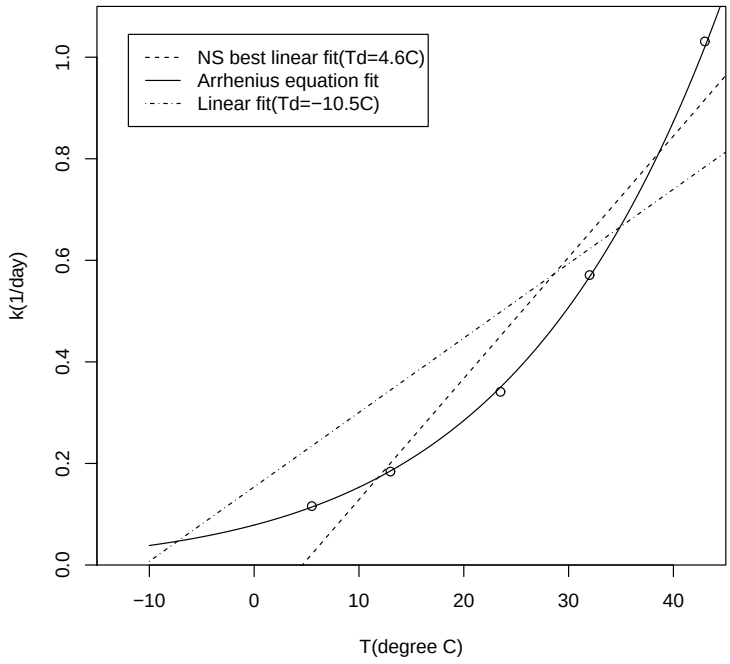

Figure 3.3: Rate constant curve showing NS-type linear approximations to the nonlinear Arrhenius-based fit of Carino's experimental data. Best linear fit over all 5 data points provides $T_d = 4.6°C$. Best fit also shown for line constrained to cross Saul's fixed datum temperature of $-10.5°C$.

$-10.5°C$. In this specific example, when all data points are fitted by a linear model that is forced to pass through Saul's $-10.5°C$, the adjusted-R^2 decreases to $0.765(SSE = 0.128)$. It may also be observed, however, that while a single value of activation energy pertains over the entire range of temperature studied, the best-fit value of Datum Temperature will vary depending on the range of temperature of interest. Thus, as can be seen in Figure 3.4, the best-fit Datum Temperature for mortar in the temperature range of $5.5°C$ to $23°C$ would be about $-2.9°C$, increasing to $14.7°C$ for the temperature range of $23°C$ to $43°C$. It is also interesting to note that a physically valid datum temperature, at which

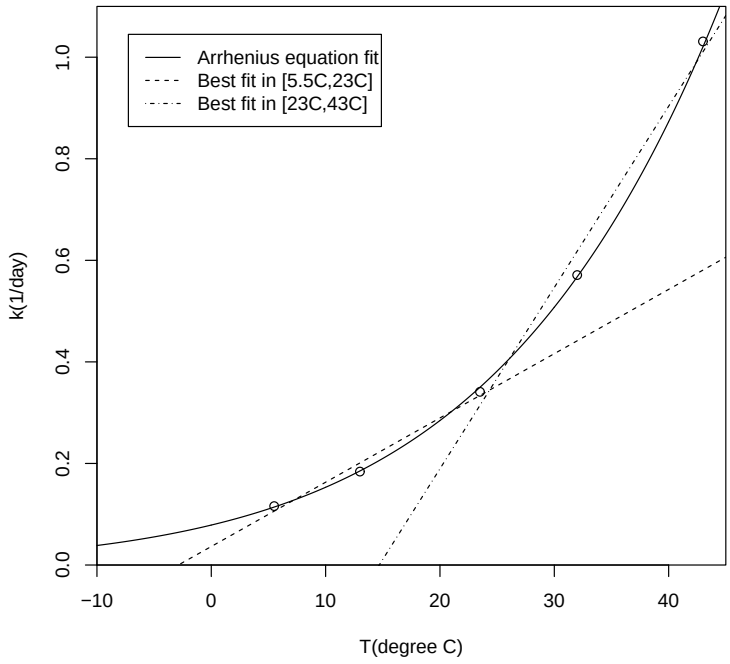

Figure 3.4: Rate constant curve showing best linear fit for partitioning of Carino's data set according to temperature range

no measurable strength gain can occur, would be where the y-value of the exponential curve is negligible, which appears here to be well colder than $-10°C$. At the same time, the best fit value of Datum Temperature for computational purposes is considerably warmer than even Saul's $-10.5°C$ as indicated by a higher value of adjusted-R^2.

3.3 Derivation of datum temperature compatible with a given activation energy and at any given temperature

Referring to Figure 3.4, as an example, as the temperature range of interest becomes infinitesimally small ($\max(T) - \min(T) \to 0$), one can represent the rate constant as a function of temperature by NS-linear model or FHP-Arrhenius equation with equal accuracy. Mathematically, the linear model becomes the tangent to the Arrhenius Curve at a given temperature. Consequently, if the activation energy and a particular temperature of interest are given, a compatible Datum Temperature and tangent slope can be found for that particular temperature that will produce the identical value of $k(T)$, using the equations derived below.

Recall the Arrhenius equation expressed in Eq.(3.2). The slope of the tangent at any arbitrary point (T_i, k_i) on Arrhenius equation is calculated using the first derivative of Eq.(3.2) at temperature T_i.

$$\frac{dk(T_i)}{dT} = \frac{E_a A}{RT_i^2} \exp\left[-\frac{E_a}{RT_i}\right] \tag{3.3}$$

Thus, the equation of the line that relates temperature to rate constant and is tangent to the Arrhenius Curve at T_i is given by

$$k_t(T) = \frac{E_a A}{RT_i^2} \exp\left[-\frac{E_a}{RT_i}\right] T + \beta_0 \tag{3.4}$$

where β_0 is the intercept on the $k-$axis($T = 0$). Subsequently, β_0 can be computed by using the condition that the linear model passes through point (T_i, k_i).

$$k_t(T_i) = k_i = \frac{E_a A}{RT_i} \exp\left[-\frac{E_a}{RT_i}\right] + \beta_0$$

$$\beta_0 = k_i - \frac{E_a A}{RT_i} \exp\left[-\frac{E_a}{RT_i}\right] = A \exp\left[-\frac{E_a}{RT_i}\right] \left(1 - \frac{E_a}{RT_i}\right) \tag{3.5}$$

$$k_t(T) = \frac{E_a A}{RT_i^2} \exp\left[-\frac{E_a}{RT_i}\right] T + A \exp\left[-\frac{E_a}{RT_i}\right] \left(1 - \frac{E_a}{RT_i}\right) \tag{3.6}$$

Consequently, an equivalent expression for Eq.(3.6) that relates temperature to rate constant and is tangent to the Arrhenius Curve at T_i is given by Eq.(3.7).

$$k_t(T_i) = \frac{E_a A}{RT_i} \exp\left[-\frac{E_a}{RT_i}\right] + A \exp\left[-\frac{E_a}{RT_i}\right] \left(1 - \frac{E_a}{RT_i}\right) \tag{3.7}$$

Therefore, the compatible Datum Temperature for computational purposes, T_d, at a given temperature T_i to make the rate constant from both NS-linear and FHP-Arrhenius models equal, can be derived from Eq.(3.7) for the condition $k_t(T_d) = 0$ as follows:

$$0 = \frac{E_a A}{RT_i^2} \exp\left[-\frac{E_a}{RT_i}\right] T_d + A \exp\left[-\frac{E_a}{RT_i}\right] \left(1 - \frac{E_a}{RT_i}\right) \tag{3.8}$$

$$T_d = T_i - \frac{T_i^2}{E_a/R} \tag{3.9}$$

where the units of T_i and E_a are $^\circ K$ and J/mol, respectively. Specific examples according to varying activation energies are shown in Figure 3.5 and tabulated form is also presented in Table 3.1. Note that while the plots in Figure 5 appear to be linear, this is merely an artifact of the small temperature range (on the absolute Kelvin scale). The relationship itself is a second order polynomial. On the other hand, if the Datum Temperature and concrete temperature of interest are given, the compatible activation energy can be calculated using Eq.(3.10), which is derived from Eq.(3.9).

$$E_a = \frac{RT_i^2}{T_i - T_d} \tag{3.10}$$

It is noted that in applying Eq.(3.10) T_i must be greater than T_d. One could interpret this constraint as Saul did[38] by assuming that when $T_i \leq T_d$, no useful property development can take place. Further, if $T_i < T_d$, the activation energy becomes negative ($E_a < 0$) which although kinetically possible[25], is not meaningful in the present context.

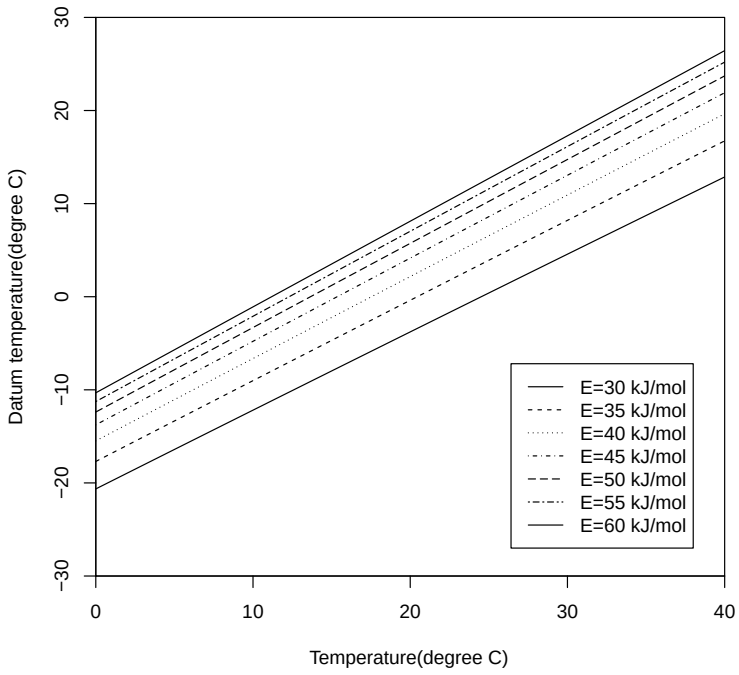

Figure 3.5: Temperature dependent datum temperature expressed in Eq.(3.9)

For Type I cement without additives ASTM C 1074[19] recommends a Datum Temperature of $0°C$ at curing temperature ranging from $0°C \sim 40°C$, and Activation Energy of $E_a = 40 \sim 45\ kJ/mol$, independent of curing temperature. As can be seen in Figure 3.5, a Datum Temperature of $0°C$ produces the identical rate constant as an activation energy of $E_a = 45\ kJ/mol$ at a concrete temperature of $15.4°C$, and produces the identical rate constant as an activation energy of $E_a = 40\ kJ/mol$ at a concrete temperature of $17.5°C$. At the extremes of the ASTM range of curing temperature, a Datum Temperature of $-13.7°C$ would be compatible with $E_a = 45\ kJ/mol$ at $0°C$, and a Datum Temperature of $21.9°C$ would be compatible with $E_a = 45\ kJ/mol$ at $40°C$.

Table 3.1: Tabulated datum temperature ($^{\circ}C$) at a given T_i, per Eq.(3.9)

T_i	$E_a(kJ/mol)$						
$(^{\circ}C)$	30	35	40	45	50	55	60
0	-20.6	-17.7	-15.5	-13.8	-12.4	-11.3	-10.3
5	-16.4	-13.3	-11.1	-9.3	-7.8	-6.7	-5.7
10	-12.2	-9.0	-6.6	-4.8	-3.3	-2.1	-1.1
15	-8.0	-4.7	-2.2	-0.3	1.2	2.5	3.5
20	-3.8	-0.4	2.2	4.1	5.7	7.0	8.1
25	0.4	3.9	6.6	8.6	10.2	11.6	12.7
30	4.6	8.2	10.9	13.0	14.7	16.1	17.3
35	8.7	12.5	15.3	17.5	19.2	20.7	21.9
40	12.9	16.7	19.6	21.9	23.7	25.2	26.4

3.4 Comparison of two approaches

Recall that Carino's method for finding a compatible T_d is based on a linear fit to the age conversion factor curve over the temperature range of interest (such range constrained to begin or end at T_r). Values of T_d expressed by Eq.(3.9) are based on the tangent to the Arrhenius Rate Constant curve. Not only is there the distinction of T_d at a given single temperature versus a temperature range, but the approaches are also distinguished by the difference between the Arrhenius rate constant curve (or simply, an Arrhenius curve) and the age conversion factor curve. One can generate the age conversion factor curve from an Arrhenius curve by plotting as the dependent variable the ratio of the rate constant at T_i to the rate constant at the predetermined T_r. (Although T_r is commonly selected as $20^{\circ}C$[19], it is a variable and its value affects the age conversion factor and

all subsequent calculations.) The impact of these distinctions will be discussed after comparing the results obtained by the two approaches.

Figure 3.6 compares datum temperature computed by both approaches. Solid and dotted lines indicate datum temperature computed by Carino's approach applied to temperature ranges of $0°C \leq T \leq 20°C$ and $20°C \leq T \leq 40°C$, respectively, as a function of varying activation energies. The superimposed curves represent solutions to Eq.(3.9) at concrete temperatures of $0°C$, $10°C$, $20°C$, $30°C$, and $40°C$ from the bottom line.

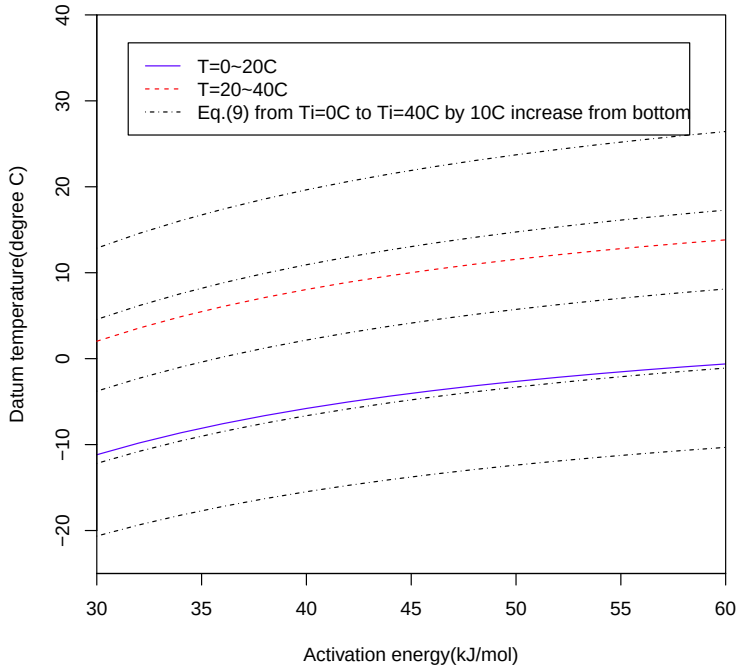

Figure 3.6: Comparison of Carino's method with Eq.(3.9)

The range of datum temperature by Eq.(3.9) at any given activation energy produces a band of values that include results of Carino's approach. Both ap-

proaches show a consistent pattern that computed datum temperature increases with activation energy. In general the T_d produced by Eq.(3.9) at a temperature near the midpoint of Carino's temperature range closely approximates Carino's T_d for $0°C \leq T \leq 20°C$, and is consistently about $3°C$ higher than Carino's T_d for $20°C \leq T \leq 40°C$. There is a systematic difference, however, influenced by activation energy, that can be observed by calculating the average of datum temperatures computed by Eq. (3.9) for given concrete temperature ranges and comparing the result to Carino. This is shown in Figure 3.7. One observes that

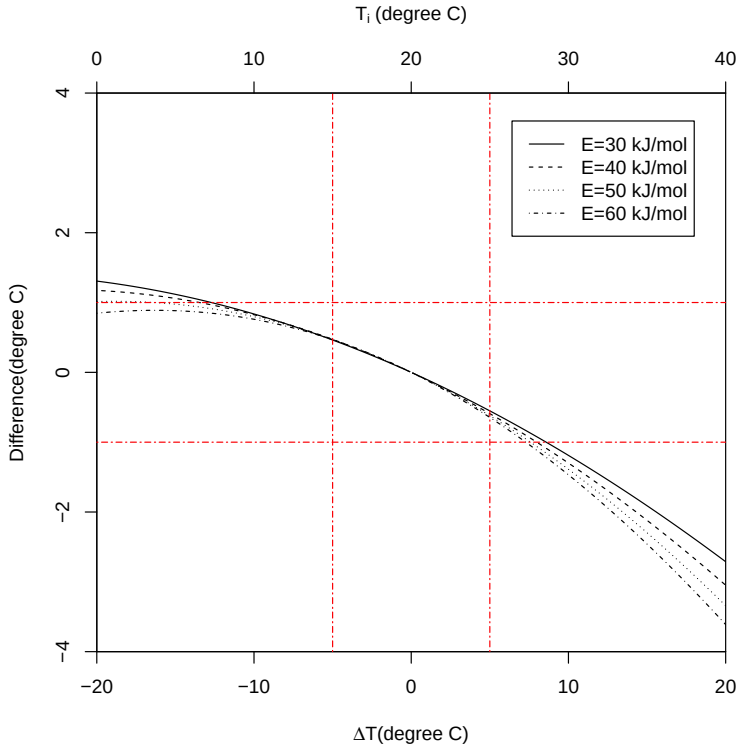

Figure 3.7: Difference between two approaches ($T_{d,carino} - T_{d,Eq(9)}$). Lower horizontal axis shows the difference ($T_i - T_r$), and upper horizontal axis shows T_i assuming $T_r = 20°C$. ($T_{d,carino} - T_{d,Eq(9)}$)

the difference between the two approaches is small (and generally negligible for most applications) between $T_r - 10°C$ and $T_r + 5°C$ (or $10°C \sim 25°C$ for

$T_r = 20°C$). When $T \geq T_r$ Eq.(3.9) provides a higher T_d, and when $T \leq T_r$ Carino's approach provides a higher T_d. The absolute value of the difference increases with E_a when $T \geq Tr$, and decreases with E_a when $T \leq Tr$. E_a makes little difference at all for concrete temperatures within $5°C$ of T_r. Finally, the fact that any difference vanishes at $T_i = T_r$ is a consequence of the fact that the X-intercept of the tangent to the age conversion factor curve at the reference temperature is identical to the X-intercept of the tangent to the Arrhenius rate constant curve at the same temperature. (See Appendix to this paper.)

3.5 Adapting Equation (3.9) to compute T_d for a Range of Concrete Temperatures

Eq.(3.9) transforms a given value of E_a to a compatible value of T_d at a given single value of temperature. While interesting, this is useful only in rare isothermal cases. The power of the maturity method is the ability to predict concrete properties from a record of variable temperature over time, where thermal variability is caused by a combination of heat of hydration and heat transfer with environment. It is therefore necessary to investigate compatibility of E_a and T_d over a range of temperatures of interest. Therefore, multiple approaches are proposed as follows for applying Eq.(3.9) to a given temperature range. For each approach a value of T_d is computed under the assumption that $E_a = 42.7\ kJ/mol$, as determined in Carino's example as illustrated in Figures 3.2 and 3.3. To remain consistent with Carino's development, each approach is first applied to two general temperature regimes: $0°C \leq T \leq 20°C$ and $20°C \leq T \leq 40°C$. In these cases it is assumed that the concrete temperature is distributed uniformly

over these ranges as would be the case for a monotonic temperature increase or decrease from one end of the range to the other. In addition, two actual concrete temperature profiles obtained by Lautz[1] are examined, which fortuitously are also in the approximate ranges of ($0°C \leq T \leq 20°C$-Ithaca winter outdoors) and ($20°C \leq T \leq 40°C$-Ithaca lab with insulated forms). These profiles are shown in Figure 3.8, and indicate a non-uniform distribution of temperature over time.

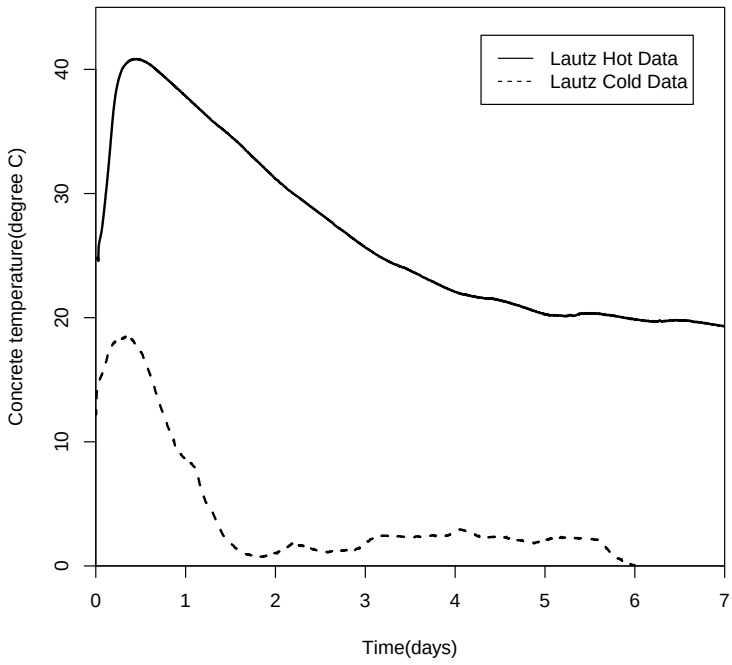

Figure 3.8: Lautz concrete temperature measurements. Hot and cold profiles truncated at 7 and 6 days, respectively, for all analyses in this paper.

Details of the various methods used to obtain values of T_d are described in Table 3.3, and the results are summarized in Table 3.4.

Table 3.2: Minimum, maximum, average, and mid value of concrete temperature measured by Lautz[1]

	Lautz's cold data	Lautz's hot data
Minimum	$0.0°C$	$19.3°C$
Maximum	$18.5°C$	$40.8°C$
Average	$4.3°C$	$26.5°C$
Mid-value	$9.3°C$	$30.1°C$

Table 3.3: Options for assigning values of T_d over a Range of Concrete Temperatures

Method		Description	
A		– ASTM recommendation for Type I cement with no additives at curing temperature from 0C to 40C – Inferred datum temperature from Nurse's[37] work	
B		– Datum temperature proposed by Saul[38], referring "minimum temperature"	
C	1	Datum temperature computed by best-linear-fit to rate constant data in accordance with ASTM C 1074 APPENDIX, based on:	– All avaialble data for rate constant versus temperature
	2		– Selected data considering temperature range of interest
	3		– Numerically generated data set of rate constant versus temperature for desired, temperature range computed by Arrhenius equation

			for a given E_a
D		– Carino's compatible datum temperature computed from Age Conversion Factor curve for the given concrete range. Note: the reference temperature must be the upper or lower bound of the desired concrete range.	
E	1	–Average datum temperature taken as a average of values computed by Eq.(3.9) at maximum and minimum temperature for the given temperature range	
	2	–Datum temperature computed by Eq.(3.9) at the average of maximum and minimum temperature over the range	
F		– Casagrande-type approach[76]. – Datum temperature is computed by Eq.(3.9) at the intersection point of two tangential lines at maximum and minimum) concrete temperatures over the range (See Appendix to this paper.)	
G	1	–Average datum temperature taken as average of datum temperatures calculated by Eq.(3.9) over each time step for given concrete temperature profile	
	2	–Datum temperature computed by Eq.(3.9) at average of the temperatures at each time step for given concrete temperature profile	

Table 3.4: Summary of datum temperatures computed by various methods

Method		Assumed uniform $T = 0°C \sim 20°C$	Assumed uniform $T = 20°C \sim 40°C$	Non-uniform $T = 0°C \sim 18.5°C$	Non-uniform $T = 19.3°C \sim 40.8°C$
A		$0°C$	$0°C$	$\mathbf{0°C}$	$\mathbf{0°C}$
B		$-10.5°C$	$-10.5°C$	$\mathbf{-10.5°C}$	$\mathbf{-10.5°C}$
C	1	$4.6°C$	$4.6°C$	$\mathbf{4.6°C}$	$\mathbf{4.6°C}$
	2	$-2.9°C$	$14.7°C$	$\mathbf{-2.9°C}$	$\mathbf{14.7°C}$
	3	$-6.1°C$	$11.7°C$	$\mathbf{-6.1°C}$	$\mathbf{11.7°C}$
D		$-4.4°C$	$9.0°C$	[a] $\mathbf{-4.4°C}$	[b] $\mathbf{9.2°C}$
E	[c] 1	$-5.6°C$	$12.1°C$	$\mathbf{-6.2°C}$	$\mathbf{12.2°C}$
	2	$-5.6°C$	$12.1°C$	$-6.2°C$	$12.2°C$
F		$-4.1°C$	$13.4°C$	$\mathbf{-5.0°C}$	$\mathbf{13.6°C}$
G	1	$-5.6°C$	$12.1°C$	$\mathbf{-10.7°C}$	$\mathbf{9.0°C}$
	2	$-5.6°C$	$12.1°C$	$-10.7°C$	$9.1°C$

[a] Approximate value since Lautz's cold temperature profile does not include the reference temperature.

[b] The computed datum temperature by Method D for the concrete temperature range from $19.3°C$ to $20°C$ is $3.1°C$ using $T_r = 20°C$ as the upper bound of the range. Tabulated value is for the range $20°C$ to $40.8°C$, using $T_r = 20°C$ as the lower bound of the range.

[c] Note that Method E and G are identical methods for uniform concrete temperature distribution.

Bold values are used to compute maturity in the next section.

3.6 Discussion of results

While the options explored here are not necessarily exhaustive, a wide range of candidate values for Td is nevertheless computed, from a low of -10.7C (G) to a high of $14.7°C$ (C-2), in addition to the $0°C$ suggested by ASTM C1074 and Saul's $-10.5°C$. Any of these values could be proposed for NS maturity computation along side of an FHP analysis using $E_a = 42.7\ kJ/mol$, with an impact on any subsequent comparison between NS and FHP results. It is also noted that when dealing with the uniformly distributed temperature range of $0°C \sim 20°C$, the maximum difference is $10.7°C$, all within the three variants of method C. A similar maximum difference is observed for uniform ($20°C \sim 40°C$), and again within method C. The case originally made by Carino, that the appropriate value of T_d is significantly influenced by temperature range, is well supported by these data, regardless of the computational approach. Method G is the only one to intentionally explore the influence of the actual temperature profile (in lieu of merely the range). Since the average temperature over the time period is lower than the midpoint of the range, T_d for the actual profiles is depressed by about $5°C$ for the colder profile and by about $3°C$ on the warmer profile. A more pragmatic assessment of the impact of these variations in T_d is based on their impact on calculated maturity as presented in the next section.

3.7 Maturity calculation

While it is recognized that an evaluation of the practical impact of the assignment of T_d would necessarily include assessment of the variations in predicted concrete properties such as compressive or flexural strength, this paper will ex-

plore only the impact on cumulative values of maturity as influenced by the various values of T_d computed above. In each case maturity is calculated under the assumption that Lautz's cold and hot temperature profiles pertain[1], representing concrete in the field under cold and hot weather conditions. Figures 3.9 and 3.10 show NS maturity calculated by

$$M(T_i, t) = \sum_{i=1}^{n} (T_i - T_d) \triangle t \tag{3.11}$$

where $\triangle t$ is the length of time step over which T_i was recorded, and $(T_i - T_d) \geq 0$. In the particular case of method C-1 applied to the cold profile, the computed T_d was higher than the coldest concrete temperature. An algebraically literal application of Eq.(3.11) would demand a negative maturity for time steps over which $T_i < T_d$. For this analysis, therefore, a negative maturity increment was not allowed, with a minimum value of $(T_i - T_d) = 0$. One of the general principles evident in Figures 3.9 and 3.10 is that the lower the concrete temperature, the greater the impact of the datum temperature. The maturities computed for the cold concrete differ by almost a factor of 8 for the various values of T_d, while the difference is slightly over a factor of 3 for the hot concrete. Therefore, selection of datum temperature may be of more significance for cold weather concrete than for hot weather concrete.

Recalling that the first fundamental difference between the NS and the FHP methods is the linear (NS) vs nonlinear (Arrhenius) relationship between temperature and rate constant, the second fundamental difference is that NS computes cumulative maturity expressed in units of time $\times$ temperature, while FHP (nonlinear, Arrhenius based) computes relative maturity as a ratio to the maturity that would have accumulated at a fixed, isothermal reference temperature (T_r). The FHP result is expressed in time units of "Equivalent Age." Thus one cannot make a direct comparison between values of maturity computed by the

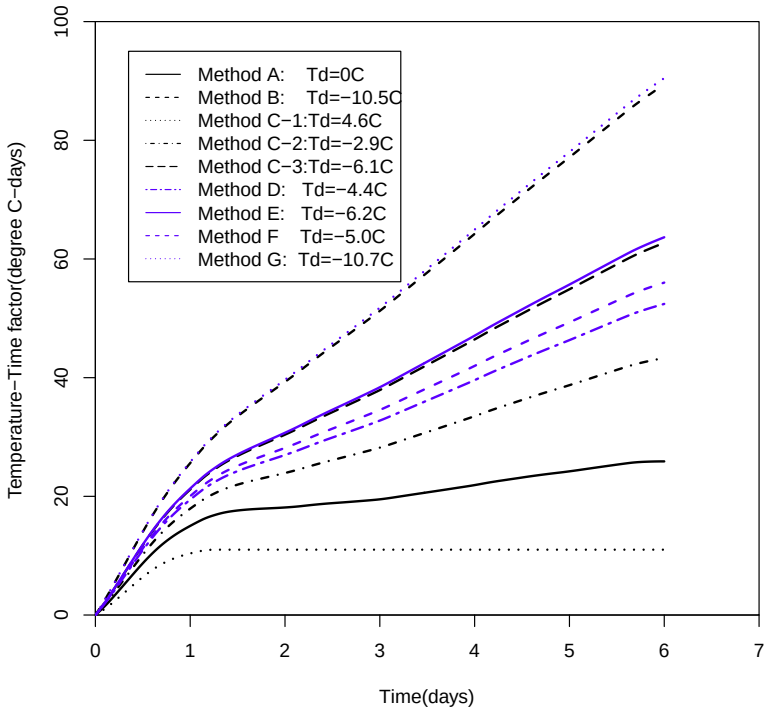

Figure 3.9: NS maturity for Lautz's cold concrete temperature profile

two methods. However, one can readily apply the relative maturity approach to the NS method as suggested by Carino to enable a valid comparison, as described in Eq.(3.12).

$$M(T_i, t) = \sum_{i=1}^{n} \frac{T_i - T_d}{T_r - T_d} \triangle t \tag{3.12}$$

Figure 3.11 and Figure 3.12 present equivalent age from NS-based equivalent ages for cold and hot data sets, using $T_r = 20°C$. When expressed as equivalent age, cold concrete results vary by about a factor of 4, while the hot concrete results vary by less than a factor of 2. It is also intriguing that for the cold concrete temperature profile, the datum temperatures by Method C-3, E, and F, produce results that are very similar to the FHP equivalent age. Results from Methods D and G were the most similar and nearly identical to FHP for the hot

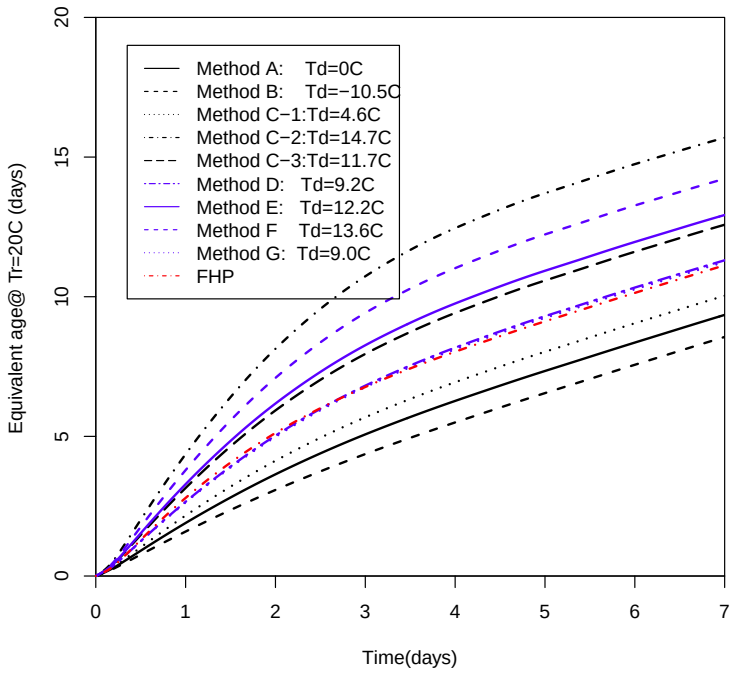

Figure 3.10: NS maturity for Lautz's hot concrete temperature profile

concrete temperature profile. Note that relative NS maturities based on Saul's T_d of $-10.5°C$ and ASTM's $0°C$ are significantly lower than that computed by FHP.

3.8 Discussion

Given that this paper has concentrated on datum temperature, it may be useful to reflect on its development and meaning. Nurse[37] initially computed his "degree C-hours" as without the deliberate notion of a datum temperature, but his development implicitly made $0°C$ the baseline or datum value, (i.e. $(T - T_d)t$ where $T_d = 0°C$. Since his work was initially developed for steam curing, Nurse

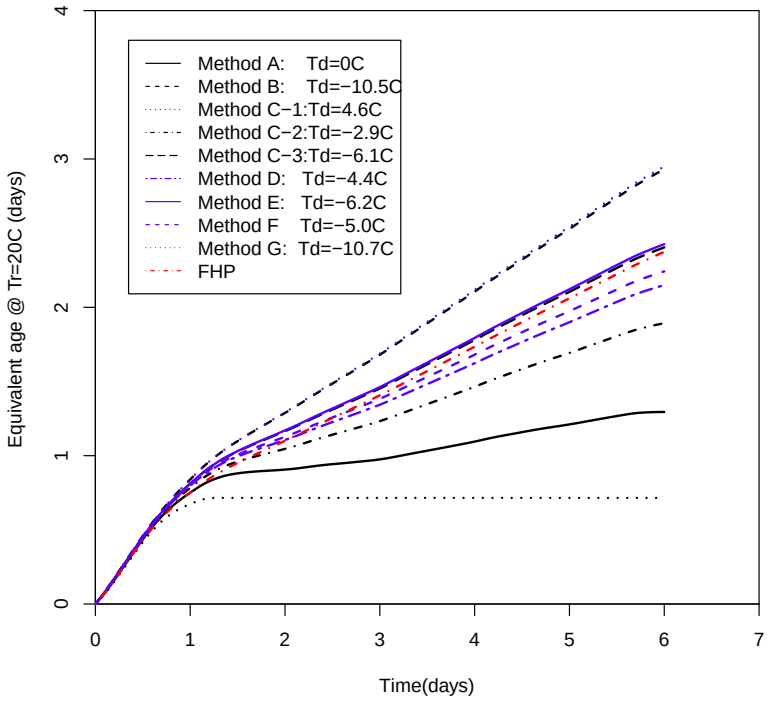

Figure 3.11: Equivalent age for Lautz's cold concrete temperature profile with varying methods

never had to confront $T < 0$, so he always computed the area under the time-temperature curve above the X axis, i.e., above $T = 0°C$. Saul[38] then modified Nurse's contribution by explicitly defining the "Minimum temperature for compressive strength development," and suggested $-10.5°C$ in a footnote to his paper. (Note the subtle but important distinction between "strength development" and hydration.) Plowman[77] used the term "datum temperature," defined as the curing temperature at which the strength of concrete remains constant irrespective of age. He demonstrated experimentally that for his mixtures no strength development occurred after 5 days at a "datum temperature" of $11°F(-12°C)$. Other values were ultimately proposed ranging from $5°C$ to

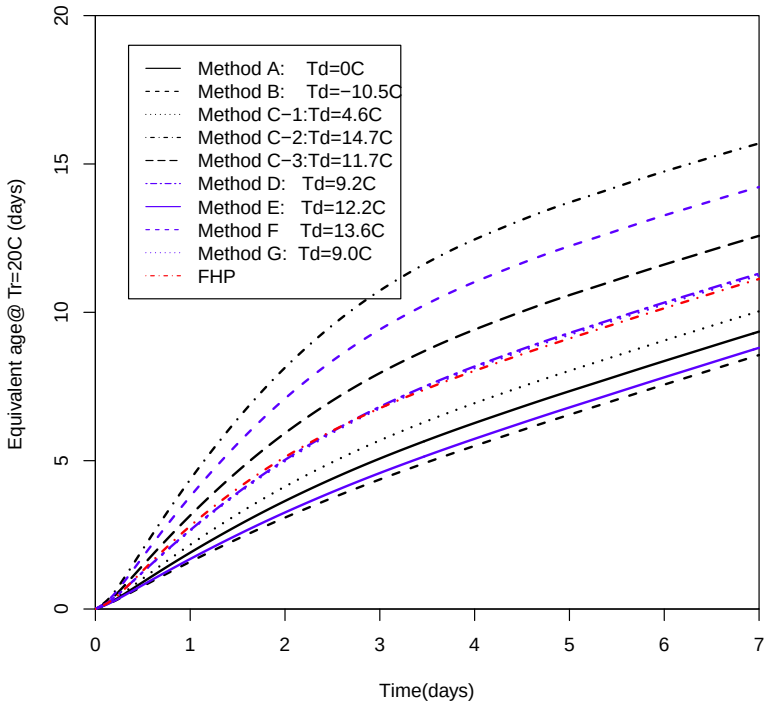

Figure 3.12: Equivalent age for Lautz's hot concrete temperature profile with varying methods

$20°C$[53, 77]. More fundamental research has suggested that T_d may not really be a physical threshold, demonstrating that hydration of Portland cement can proceed, albeit slowly, at temperatures as low as $-40°C$.[78] (Of course bulk water in large capillary pores is subjected to freezing at about $-10°C$ to $-8°C$.[33, 78, 79]) Nevertheless, in regard to maturity calculations and to the topic of this paper in particular, datum temperature continues to have a computational value independent of a literal, physical/chemical interpretation. This is best demonstrated by the rate constant graph in Figure 3.3 in which the non-linear Arrhenius curve trends towards a zero rate constant at a temperature far lower that any conventional assumptions for T_d. Meanwhile the X-intercept

(rate constant $= 0$) for nearly all of the linear approximations discussed herein is well above values such as Saul's $-10.5°C$, yet these linear approximations return useful values for the rate constant. The fundamental goal of this paper has been to continue Carino's exploration of methods for finding values of a computationally useful datum temperature that would enable use of the linear NS method with "accuracy comparable to using the [nonlinear] Arrhenius function," to paraphrase Carino[55]. As pointed out earlier, the most meaningful evaluation of "accuracy" relates to the ability to predict concrete strength (or other property) via the maturity method, which is at least a two part process of transforming time and temperature records, datum temperatures, or activation energies into maturity or equivalent age values, followed by converting these values into concrete strength on the basis of prior correlations. Even though this paper has shown dramatic differences in maturity values resulting from variations in T_d, it must also be recognized that the establishment of strength-maturity relationships based on a selected value of T_d is also to a large extent a self-calibrating operation that reduces the unilateral effect of T_d on the resulting error in strength prediction. As long as the same method and T_d is used to establish maturity values for the strength-maturity curves as is used to compute maturity from field records, the strong effect of T_d is to some extent weakened. Nevertheless, when the goal is to approximate the more physically correct, nonlinear effect of temperature on concrete property development with a simpler linear model, this paper and Carino's earlier work have shown multiple ways to achieve that goal. Figures 3.11 and 3.12 demonstrate the convergence of the NS and FHP methods for the appropriate matching of T_d to E_a.

3.9 Example application

Barnett et al.[5] has proposed the effect of Ground Granulated Blast Furnace Slag(GGBFS) addition on activation energy on the basis of measurements of mortar cube strength with time. For mortars with a water-to-binder ratio in the range of 0.51 to 0.62, Ea is reported as a function of GGBFS addition as shown in Figure 3.13. Compatible values of datum temperature were computed using

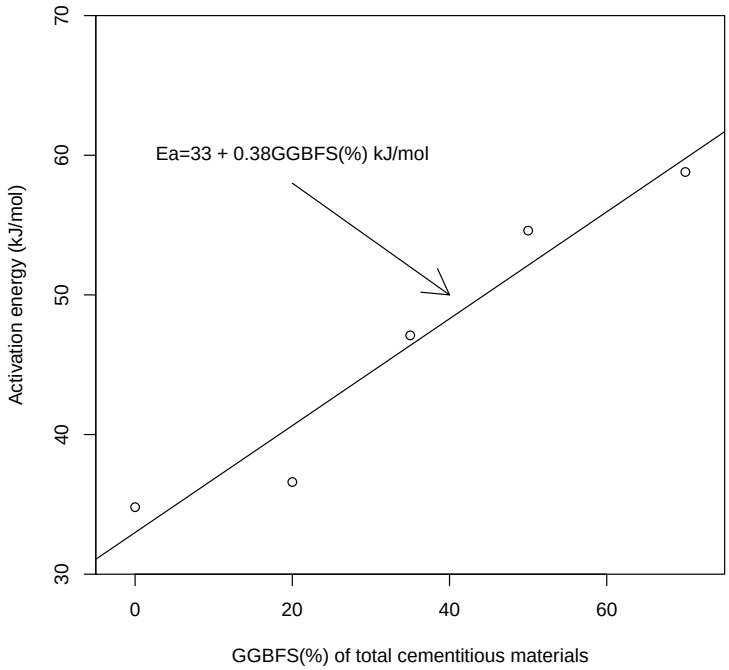

Figure 3.13: Activation energy with varying GGBFS content re-plotted by authors (after Barnett et al.[5])

Equation (9) for $T = 10°C$, $20°C$, $30°C$, and $40°C$, coupled with the fitted line in Figure 3.13. The results are shown in Figure 3.14.

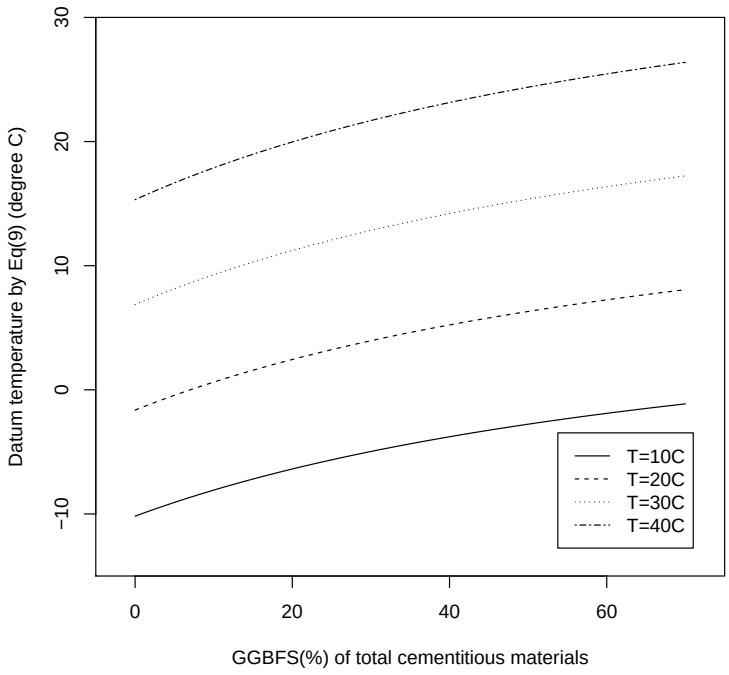

Figure 3.14: Datum temperature by Eq.(3.9) at various concrete temperatures with GGBFS (%) of total cementitious materials

3.10 Conclusion

(1) As pointed out by others[73, 55], a computationally appropriate value of datum temperature depends on the range of concrete temperature over which the maturity method will be applied.

(2) For a given activation energy and concrete temperature, a compatible datum temperature can be estimated, either by Carino's numerical method applied to the age conversion factor graph, or the closed-form solution based on the rate constant graph proposed here as Eq.(3.9). For most applications, the difference between the two results is small. Methods proposed here may be somewhat easier to apply over a range of temperatures

than Carino's numerical method, especially when the temperature range of interest is not bounded above or below by the reference temperature.

(3) Several methods to compute a single datum temperature applicable over a range of concrete temperatures have been shown. Precisely which method leads to the closest convergence with the FHP age conversion factor appears to differ with concrete temperature.

(4) The selection of T_d has a significant impact on the computed maturity, with a proportionately greater impact on cooler concrete. Therefore, appropriate assignment of datum temperature may be of more significance for cold weather concrete than for hot weather concrete.

(5) When comparing the utility of NS versus FHP for a given concrete mixture in any given application, it is appropriate to similarly characterize the temperature sensitivity of the mixture in both methods. Differences in the efficacy between NS and FHP that have been attributed to the mechanics of the methods themselves may be due in large part to assumed (and incompatible) values of T_d and E_a.

(6) If convergence of the results of the NS and FHP methods is desirable, such is more likely to be achieved with a temperature-adjusted value of T_d than with the fixed values proposed by Saul or by ASTM C1074.

(7) When applying a temperature-adjusted T_d to the NS method, it is important that $(T_i - T_d) \geq 0$.

3.11 Appendix

3.11.1 Compatible T_d at the reference temperature by both rate constant and age conversion curves

If Carino's approach is applied to an infinitesimally small concrete temperature range near the reference temperature($T = [T_r, T_i]$ and $Ti \to T_r$ or $T = [T_i, T_r]$ and $T_i \to T_r$), a tangential linear model to the FHP age conversion factor curve can be can be derived in a manner similar to that used to obtain Eq.(3.9). The age conversion factor γ of FHP method at any given temperature T is expressed by

$$\gamma(T) = \frac{k(T)}{k(T_r)} = \exp\left[-\frac{E_a}{R}\left(\frac{1}{T} - \frac{1}{T_r}\right)\right] \tag{3.13}$$

Thus, the first derivative of Eq.(3.13) is expressed in Eq.(3.14).

$$\frac{\gamma(T)}{dT} = \frac{E_a}{RT^2}\exp\left[-\frac{E_a}{R}\left(\frac{1}{T} - \frac{1}{T_r}\right)\right] \tag{3.14}$$

Since the tangential linear model γ_t at concrete temperature T_i crosses the point $(T_i, \gamma(T_i))$, the general form of the tangential linear model to the FHP age conversion factor at T_i can be derived as follows:

$$\gamma_t(T) = \frac{E_a}{RT_i^2}\exp\left[-\frac{E_a}{R}\left(\frac{1}{T} - \frac{1}{T_r}\right)\right]T + \left(1 - \frac{E_a}{RT_i}\right)\exp\left[-\frac{E_a}{R}\left(\frac{1}{T} - \frac{1}{T_r}\right)\right] \tag{3.15}$$

Therefore, the associated datum temperature can be computed by letting $\gamma_t(T) = 0$, such that

$$0 = \frac{E_a}{RT_i^2}\exp\left[-\frac{E_a}{R}\left(\frac{1}{T} - \frac{1}{T_r}\right)\right]T_d + \left(1 - \frac{E_a}{RT_i}\right)\exp\left[-\frac{E_a}{R}\left(\frac{1}{T} - \frac{1}{T_r}\right)\right] \tag{3.16}$$

Consequently, the datum temperature is formulated by

$$T_d = T_i - \frac{T_i}{E_a/R} \tag{3.17}$$

Thus, for the condition, $T_i - T_r \to 0$, the datum temperature is computed by

$$T_d = T_r - \frac{T_r}{E_a/R} \tag{3.18}$$

Therefore, the difference of two approaches at the reference temperature in

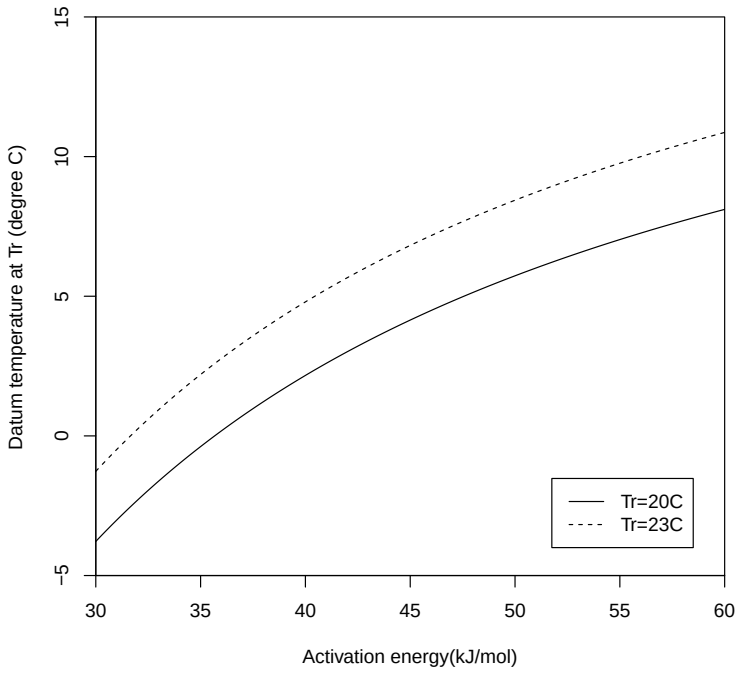

Figure 3.15: Compatible datum temperatures at the reference temperatures for varying activation energies

Figure 3.7 is zero. For a typical reference temperatures, $T_r = 20°C$ and $T_r = 23°C$, the associated datum temperatures as a function of activation energy are presented in Figure 3.15.

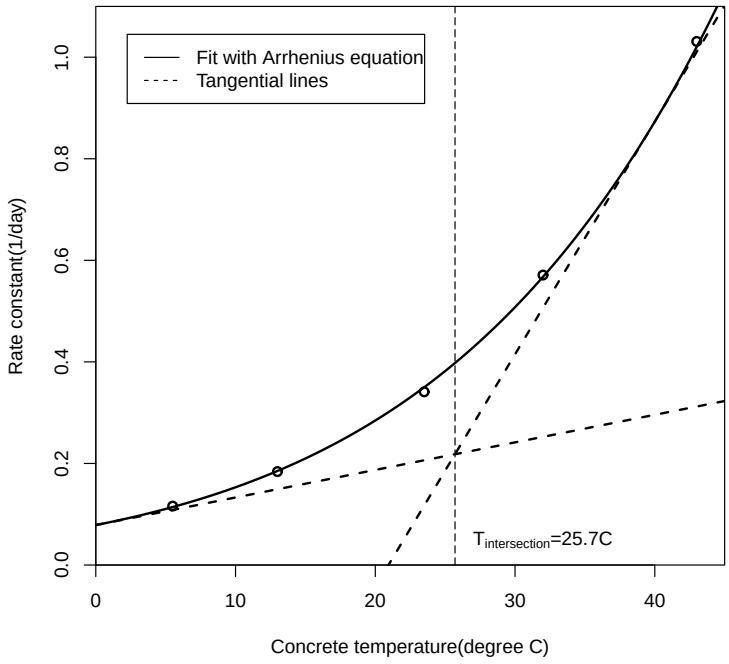

Figure 3.16: Finding a characteristic temperature within a range of temperatures by using Casagrande's tangential linear method

3.11.2 Casagrande-type approach (Method F)

The characteristic concrete temperature is computed by a Casagrande-type approach[76]. That is, datum temperature is computed at the intersection point of two tangential lines at maximum and minimum concrete temperatures. The intersection point of two tangential linear models can be computed by graphically as shown in Figure 3.16 or numerically by Eq.(3.19).

$$T_{intersect} = \frac{\exp\left[-\frac{E_a}{RT_{min}}\right]\left(1-\frac{E_a}{RT_{min}}\right) - \exp\left[-\frac{E_a}{RT_{max}}\right]\left(1-\frac{E_a}{RT_{max}}\right)}{\frac{E_a}{R}\left\{\exp\left[-\frac{E_a}{RT_{max}}\right]/T_{max}^2 - \exp\left[-E_a/\left(RT_{min}\right)\right]/T_{min}^2\right\}} \tag{3.19}$$

In Method F, described in the main paper, the intersection points associated with the given concrete temperature distributions are summarized in Table 3.5.

Table 3.5: Intersection points computed by Eq.(3.19)

Uniform	Uniform	Nonuniform	Nonuniform
$T = 0°C$	$T = 20°C$	$T = 0°C$	$T = 19.3°C$
$\sim 20°C$	$\sim 40°C$	$\sim 18.5°C$	$\sim 40.8°C$
$11.6°C$	$31.4°C$	$10.7°C$	$31.7°C$

Because the Arrhenius equation is an exponential function, the intersection point (or characteristic temperature) is higher than the middle value of maximum and minimum concrete temperatures. As a result, the resulting datum temperature is higher than Method E.

CHAPTER 4

DIFFERENCE IN SETTING BEHAVIOR BETWEEN PREPARED AND SIEVED MORTARS IN THE C403 TIME OF SETTING TEST

4.1 Introduction and Background

As evident from its title, "Time of Setting of Concrete Mixtures by Penetration Resistance," ASTM C403-08 [80] is used to quantify the setting behavior of "concrete", even though the penetration resistance test itself is actually performed on mortar extracted from the concrete by sieving. In developing the C403 procedure, Tuthill and Cordon [81] directly adopted the proctor penetration apparatus from the geotechnical test method for measuring the relationship between moisture content and penetration resistance in fine-grained soils (currently published as ASTM D1558-10 [82]). Since D1558-10 is not intended for use with granular soils, the originators of C403 introduced the intermediate step of passing fresh concrete through an ASTM E11-09 [83] $4.75\ mm$ (#4) sieve to obtain mortar as a surrogate "fine-grained soil." In applying the Proctor penetration method to the sieved mortar, Tuthill and Cordon noted that the "... equipment provides an accurate, rapid, and economical method of determining hardening characteristics of concrete mortar which, though not equal to those of corresponding concrete, are of similar character and reliably indicative of what may be expected of the concrete." The required "Wet-sieving[1]" (sieving, hereafter) is a time-intensive procedure in which the fresh concrete is passed over a sieve

[1]The term "wet sieving" is used in ASTM C403. This term is used in other ASTM test methods (such as C430-08) to imply that a stream of water is used to help wash solid materials through the sieve. In the specific case of ASTM C403 no water is used to assist in the sieving process and the term merely implies that the concrete being sieved has been recently mixed and is in that sense "wet."

accompanied by manual or mechanical vibration as described in ASTM C172-10 [84]. In the experience of the authors and others, with stiff concrete mixtures it can be difficult to sieve a sufficient quantity of mortar by merely vibrating the sieve alone, such that it is expedient to vigorously rub the stiff concrete over the sieve. The extracted (or sieved) mortar is then collected, placed, and consolidated into a container having least dimensions of $152\ mm$ ($6\ in.$) for both width and depth, into which the proctor needles are subsequently intruded. ($A\ 300\ mm \times 600\ mm$ ($6\ in. \times 12\ in.$) cylinder mold cut to 2/3-height is a convenient container for this purpose.)

Over multiple experiments with the C403 test, the authors have observed the phenomenon first identified by Kelly [3]: significant differences between the setting behavior of mortar sieved from a particular fresh concrete mixture, and the setting behavior of mortar prepared without the addition of coarse aggregate to have the identical composition as the mortar fraction of the same concrete. This is shown in Fig. 4.1 in which it is seen that the sieved mortar had the time of initial setting that was 36 minutes or 14% earlier than that of the prepared mortar, and the time of final setting of the mixed mortar was 58 minutes or 16% earlier. Such pattern is as is suggested by the note in Section 5.3 of ASTM C403 [80], "... it has been shown that the initial and final setting times may be increased when using the prepared mortar." While Kelly [3] offered no explanation for the difference in behavior, the significance of his findings can be quantified by comparison with the C403 precision statements, in which Kelly's results clearly show a difference greater than that considered by C403 to be an acceptable difference among samples of the same mortar. In particular, the authors make reference to the three-sample, single-operator precision included in ASTM C403 as of the 2006 version. In 2006 ASTM C403 [80] updated the precision statement

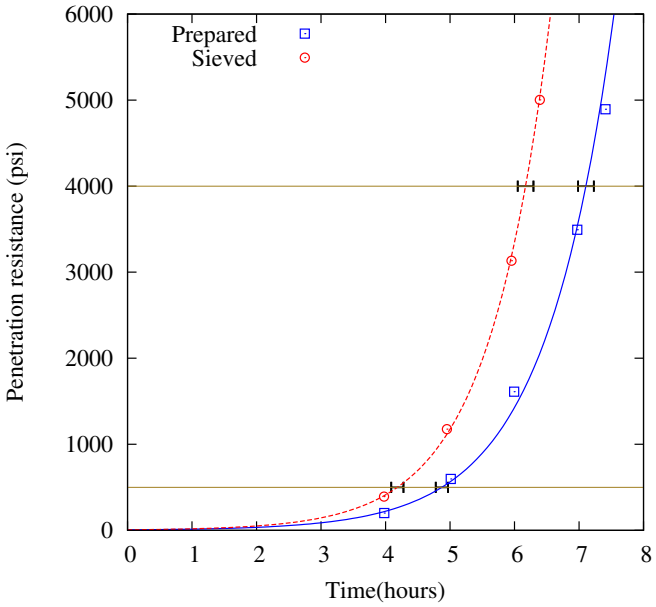

Figure 4.1: Penetration resistance of sieved and mixed mortars measured by Kelly [3] with exponential curve-fits by the authors. (Horizontal line segments in the Figure denote acceptable range of three results for initial and final setting time per C403.)

by replacing previously published values of coefficient of variation (COV) with fixed time intervals obtained from an inter-laboratory study [85]. The largest reported single operator precision (denoted by "acceptable range of three results") is 11.4 minutes (denoted subsequently by A_i) for initial, and 14.6 minutes (denoted subsequently by A_f) for final setting times, respectively.

The purpose of this paper is to further explore and quantify the difference in setting between prepared and sieved mortar. This is useful because although C403 is clear that the setting behavior of concrete is to be quantified on the basis of sieved mortar, in some cases it is convenient to study setting behavior on mortars intentionally-mixed (prepared) to represent the mortar fraction of a given concrete of interest [4, 86]. Although C403 notes a possible difference in the setting behavior between "prepared mortar" (intentionally mixed to rep-

resent the mortar fraction of concrete) and "sieved mortar" (sieved from fresh concrete in accordance with C403), users of the test are not alerted to the likely magnitude or significance of this difference. The paper therefore quantitatively reports differences of setting times between prepared and sieved mortars based on experiments performed by the authors and two data sets from the literature [3, 4].

4.2 Experiment

A series of experiments were performed to investigate the effects of sieving on mortar composition and penetration resistance. Experiment B required mixing concrete, sieving-out the coarse aggregate, and comparing the subsequent penetration resistance results with those obtained from intentionally mixed mortar (no coarse aggregate). This experiment therefore not only provided data on setting behavior of prepared-versus-sieved mortar, but validated the C403-08 precision statements, and served as the pilot for techniques for analyzing changes in mortar composition as a result of sieving. Experiment C also began with mixing concrete followed by sieving, accompanied by detailed before- and after-sieving analysis of paste content and aggregate grading, but did not include penetration resistance tests. Experiment D not only replicated Experiment C, but also examined a prepared mortar and included penetration resistance testing. Experiment E replicated experiments C and D in methodology, but varied the mortar mixture proportions.

4.2.1 Materials

Mixture proportions for all experiments are summarized in Table 5.1. The general targets were to create concrete with 60% mortar volume (experiment B, C, and D) and 55% mortar volume (experiment E), all with 30% paste volume in the concrete. This translates to mortar with a 50% and 55% paste volume-fractions. All pastes were mixed with W/C = 0.45 (giving the paste a 41% cement volume-fraction). The proportions actually realized were slightly different due to the measured air content of about 5 to 7% in the pre-sieved, non-air-entrained mortar. This translates to an air content of 2.5 to 3.8% in the associated non-air-entrained concretes. Details of aggregates and properties are shown in Table 5.2, in which in all cases the term "paste" refers to "air-free paste," while the terms "mortar" and "concrete" include the volume of all ingredients including air.

4.2.2 Experimental Procedure

All mortars and concretes were mixed in accordance with either ASTM C305-13 [91] or C192-07 [92] in an ambient laboratory temperature of $23°C$ ($73°F$). For Experiment B concrete was sieved over an aggregate testing screen in a large frame per ASTM E11 [83] with dimensions $L590\ mm \times W360\ mm \times D60\ mm$(23 $in.$ $\times$ 14 $in.$ $\times$ 2.5 $in.$). For Experiments C, D, and E the mortars were sieved over standard $200\ mm$ $(8\ in.)$ circular brass sieves. Modified $300\ mm \times 600\ mm$ ($6 \times 12\ in.$) cylinder molds were used for mortar containers as noted previously. Penetration resistance tests were performed in an environmental chamber at constant $23°C$ ($73°F$).

Table 4.1: Mixture Proportion for mortars and concrete (per $1\ m^3$ (or 1 cubic yard) of mortar or concrete)

Ingredients	Experiment B[b], C[c], D[d]		Experiment E	
	kg/m^3 (lb/CY)		kg/m^3 (lb/CY)	
	mixed mortar	mixed concrete	mixed mortar	mixed concrete
Cement[a](Type I)	620 (1046)	380 (640)	644(1085)	377(636)
Water	279 (471)	171 (288)	290(488)	170(286)
Fine aggregates	1260 (2123)	770 (1682)	1078(1818)	632(1065)
Coarse aggregates	-	998 (1682)	-	1151(1940)
$V_{paste}/V_{concrete}$[d]	-	29%	-	29%
V_{paste}/V_{mortar}	48%	48%	50%	52%
P/A[e]	1.0	1.0	1.2	1.2

[a] Type I cement from the same manufacturer was used for all experiments, yet the cement for experiments B was from a different production run from that used for experiments C, D, and E.

[b] Concrete was designed and batched; sieved mortar was extracted from the concrete. Mortar was designed and batched with the identical composition of the concrete mortar fraction.

[c] Concrete was designed and batched, and sieved-mortar was extracted.

[d] In all cases the term "paste" indicates cement and water only, air is not included. Air is classified as a separate component of the mixtures.

[e] $P/A = V_{paste}/V_{fine}$.

Table 4.2: Properties of Aggregates

Experiment	Types	Absorption (%)	Specific Gravity	Fineness Modulus
B	Fine	2.8	2.65	2.99
	Coarse	1.2	2.57	7.32
C	Fine	2.2	2.62	2.75
	Coarse	1.5	2.65	7.51
D	Fine	2.2	2.62	2.99
	Coarse	1.5	2.65	7.24
E	Fine	2.2	2.62	2.55
	Coarse	1.5	2.65	7.44

[a] Aggregate properties obtained per ASTM C127-08 [87] and C128-08 [88]

[b] Sieve analyses per ASTM C136-06 [89] for both fine and coarse aggregates before mixing.

[c] Coarse aggregates met grading requirements for ASTM C33 size number 7 [90] with a nominal size of $12.5\ mm$ ($1/2\ in.$).

[d] Aggregates sieved in Experiments B was sampled from the stockpiles. All aggregates used in Experimens C, D, and E were taken directly from the aggregate sieves and remixed into the concrete for greater precision in evaluating the effects of mortar-sieving on aggregate particle size distribution.

4.2.3 Calculation Method of Setting Times

Curve-fits and initial- and final set-time intercepts were determined by both power (Eq.(6.2)) and exponential (Eq.(6.3)) functions. The power function as

proposed by Popovics [9] has been adopted by ASTM C403-08. C403 "Equation (1)" is the power function written in logarithmic format to facilitate graphical determination or linear regression of setting-times, producing a readily interpretable value of R^2 for quantifying goodness-of-fit. C403 "Equation (2)" is the direct algebraic form of the same power function, but its use requires a non-linear regression. ASTM C403 Equation (1) is reproduced as Eq.(6.2) in this paper. Alternatively, the exponential function (shown here as Eq.(6.3)) has been used effectively by other researchers [10,18] for fitting penetration resistance data. For the data reported here, either function can be used to effectively represent the data as shown in Tables 4.3 and 4.4, while neither function consistently produced the superior goodness-of-fit as indicated by R^2.

$$\log PR(t) = a + b \log t \tag{4.1}$$

$$\log PR(t) = c + dt \tag{4.2}$$

4.3 Experimental Results and Analysis

4.3.1 Penetration Resistance

Results of all penetration resistance tests are shown in Tables 4.3 and 4.4, which will be discussed subsequently in more detail. Discussion of the experiments in order, however, begins with Experiment B which examined penetration resistance for each of three containers of prepared mortar and three containers of sieved mortars as shown in Figures 4.2 (a), 4.2 (b), and 4.2 (c). Figure 4.2 (a) shows the results of 3 replicates of penetration testing for the prepared mortar, while Figure 4.2 (b) shows the same for the sieved mortar. Note that for the pre-

pared mortar the experimentally-determined range of values over three replicates for initial- and final-setting-time was 6.6 and 1.9 minutes, as compared to the ASTM ranges of 11.4 and 14.6 minutes. (ASTM ranges are shown as horizontal error bars in the figure.) For sieved mortar, on the other hand, the observed ranges in initial and final set were 11.4 and 7.9 minutes. Thus, differences in setting times within the sieved mortar replicates, and again within the prepared mortar replicates were within the ASTM precision. However, when the pooled results of the sieved mortar are compared with those of prepared mortar, it is observed that the difference in setting times between sieved and prepared mortar is larger than the C403 range of variability. This suggests a significant effect. Figure 4.2 (c) shows only the curves fitted by the power function for the entire prepared-mortar data set vs. that for the sieved-mortar data set.

The results of Experiment D presented in Fig. 4.3 indicate the same general effect of sieving as seen in Experiment B and as observed by Kelly [3]. In this case only single samples, each of prepared and sieved mortars, were tested, but the difference remains larger than the C403 range. It is noted, however, that the magnitude of the differences between sieved and prepared mortar is greater in Experiment D than had been observed in Experiment B which had been prepared with identical proportions. The only known differences in materials between the two experiments are the batch of bagged cement from the same manufacturer, a slight change in grading curve of the coarse aggregate and significantly coarser sand for Experiment B (See Table 5.2). However, as described above, Experiments B and D used different types of sieves.

To maintain a paste content of 30% and the target P/A of 1.2, the concrete mixture for Experiment E incorporated 5% less fine and 5% more coarse aggre-

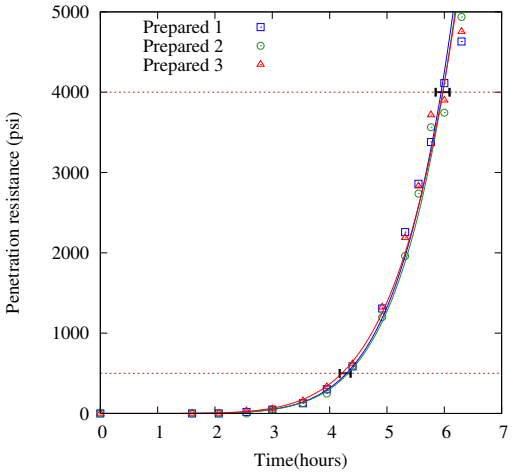

(a) Prepared Mortar

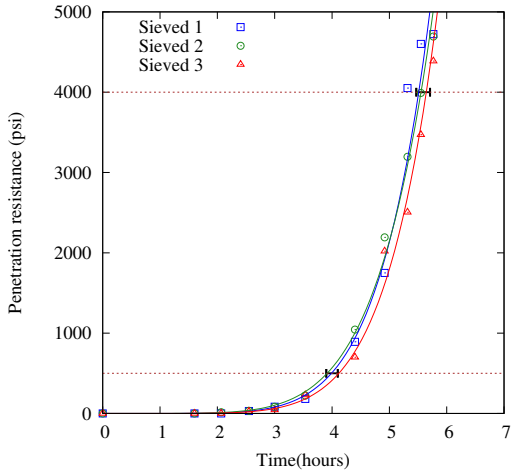

(b) Sieved Mortar

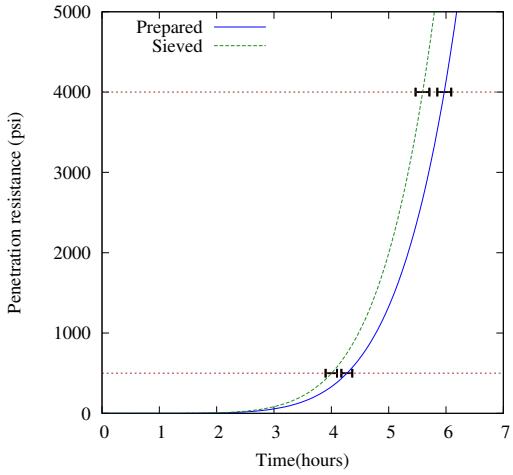

(c) Average penetration resistances of mixed and sieved mortars

Figure 4.2: Penetration resistance with time for each of three samples for prepared and sieved mortars in Experiment B (Lines have been fitted with the power function.)

gate compared with the mixture for experiments B, C, and D. Figure 4.4 presents the comparison of penetration resistance between sieved and prepared mortar. The difference between initial and final setting times in Experiment E varies depending on the curve-fitting function used. The best-fit is obtained with the exponential function with differences between sieved and prepared mortar that

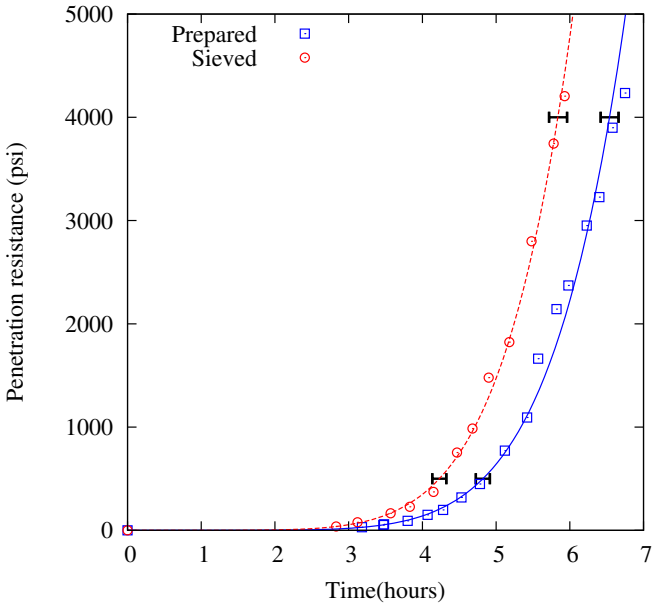

Figure 4.3: Penetration resistance with time for mixed and sieved mortars in experiment D (Lines have been fitted with the power function.)

are greater than the ASTM C403 acceptable range introduced earlier. A somewhat poorer-fit is obtained with the power function required by C403, but with smaller resulting differences between final setting times for sieved and prepared mortar, which in this case is within the ASTM range of single operator precision. Within the database presented here, Experiment E manifested the smallest observed difference of initial and final setting times (with the exception of data from Chung, et al. [4] to be discussed).

Table 4.3 and 4.4 summarize computed setting times from all penetration resistance results conducted in this study and collected from the literature. In these tables setting times in bold font are derived from the function that produced the best-fit to the penetration resistance data. (This is also seen by comparing the values of R^2 across the two tables.)

Table 4.3: Estimated setting times of experiments and literature estimated by the power function ($A_i = 11.4$ min. and $A_i = 14.6$ min.)

Experiments	Initial[a]	Final[b]	R^2	RE%[c] initial	RE%[d] final	K[e] initial	K[f] final	b[g]
B-Prepared	**4.27**	**5.97**	0.998	6.7%	6.7%	1.7	1.7	6.42
B-Sieved	**3.95**	**5.55**	0.987					6.60
D-Prepared	**4.82**	**6.54**	0.997	14.0%	12.0%	3.1	2.9	6.83
D-Sieved	**4.23**	**5.84**	0.997					6.46
E-Prepared	3.85	5.40	0.994	8.7%	3.3%	1.7	0.7	6.17
E-Sieved	3.54	5.22	0.984					5.36
Kelly-Prepared	**4.79**	**7.15**	0.999	14.3%	15.6%	3.2	4.0	5.17
Kelly-Sieved	4.19	6.19	0.998					5.32
Chung-Prepared	3.97	5.86	0.982	1.1%	2.5%	0.2	0.6	5.26
Chung-Sieved (W/C=0.4)	**3.92**	**5.72**	0.971					5.45
Chung-Prepared	**5.10**	**7.64**	0.991	0.2%	-0.3%	0.1	-0.1	5.09
Chung-Sieved (W/C=0.4)	**5.09**	**7.66**	0.998					5.02

[a] Initial setting times estimated by specified functions

[b] Final setting times estimated by specified functions

[c] RE% initial = $|t_{initial\ set,prepared} - t_{initial\ set,sieved}|/t_{initial\ set,sieved} \times 100\%$

[d] RE% final = $|t_{final\ set,prepared} - t_{final\ set,sieved}|/t_{final\ set,sieved} \times 100\%$

[e] K initial=$(t_{initial\ set,prepared} - t_{initial\ set,sieved})/A_i$

[f] K final= $(t_{initial\ set,prepared} - t_{initialset,sieved})/A_f$ (see discussion 4.1)

[g] Estimated b in Eq.(6.2) and d in Eq.(6.3) by curve-fittings.

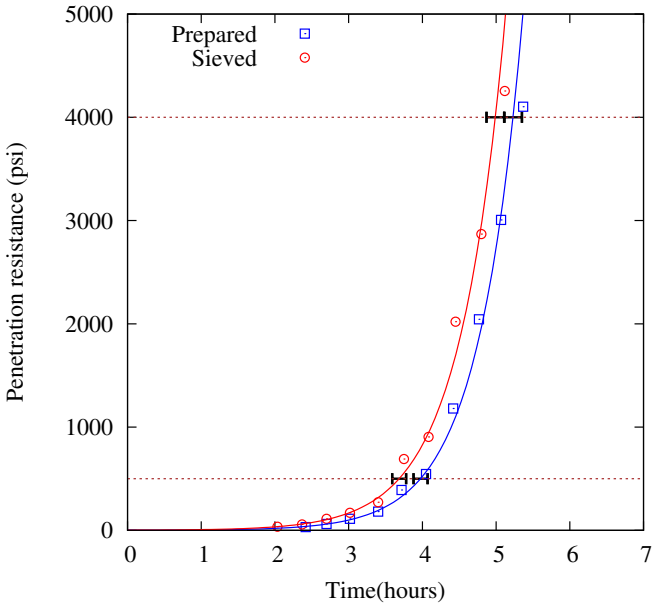

Figure 4.4: Penetration resistance with time for mixed and sieved mortars in experiment E (Lines have been fitted with the exponential function.)

4.4 Discussion

4.4.1 Difference in Setting Times of Prepared and Sieved Mortars

As pointed-out earlier, the note in Section 5.3 of ASTM C403 [80] alerts the operator that "initial and final setting times may be increased when using the prepared mortar." From the results obtained in this study, the difference alluded to in that note can be as much as a 6% to 14% increase in initial setting time, and a 3% to 12% increase in final setting time for prepared mortar in comparison to sieved mortar. These differences varied by experiment and by the function used to fit the data. The magnitude of these differences are indicated in Ta-

Table 4.4: Estimated setting times of experiments and literature estimated by the exponential function ($A_i = 11.4$ min. and $A_i = 14.6$ min.)

Experiments	Initial[a]	Final[b]	R^2	RE%[c] initial	RE%[d] final	K[e] initial	K[f] final	d[g]
B-Prepared	4.44	5.88	0.977	5.8%	7.2%	1.6	1.8	1.51
B-Sieved	4.14	5.44	0.972					1.76
D-Prepared	4.96	6.43	0.986	14.1%	12.4%	3.2	2.9	1.41
D-Sieved	4.34	5.72	0.988					1.51
E-Prepared	**3.97**	**5.23**	0.994	7.8%	4.8%	1.5	1.0	1.66
E-Sieved	**3.69**	**4.99**	0.995					1.60
Kelly-Prepared	4.87	7.11	0.995	16.5%	15.2%	3.6	3.9	1.68
Kelly-Sieved	**4.18**	**6.17**	0.999					1.05
Chung-Prepared	**3.78**	**5.93**	0.987	-2.2%	3.8%	-0.4	0.9	0.96
Chung-Sieved (W/C=0.4)	3.87	5.72	0.929					1.11
Chung-Prepared	5.42	7.43	0.989	11.7%	-3.7%	3.0	-1.2	1.02
Chung-Sieved (W/C=0.5)	4.85	7.72	0.984					0.72

bles 4.3 and 4.4 by the "K-factors" which express the measured difference in setting time between sieved and prepared mortars divided by the ASTM single operator precision. As seen in the Tables, K-factors are 1.5 to 3 for initial setting time and 1 to 3 for final setting time. Kelly's experiment [3] also showed the same pattern of delay in setting times of prepared mortar with slightly larger

difference, 14% to 16% corresponding to K-factors of 3 to 4 times of ASTM C403 precision. The data sets by Chung et al. [4] presented very different results, with little difference between the setting behavior of sieved and prepared mortar. Chung et al. [4] did report, however, that the penetration resistance of their prepared mortar was measured by a screw-driven testing machine, while that for their sieved mortar was tested by portable testing apparatus.

4.4.2 Functions to estimate setting times

ASTM C403-08 [80] requires use of the power function (Eq.(6.2)), although the exponential function (Eq.(6.3)) can sometimes provide a better fit to the data, as shown in Table 4.3 and 4.4.

Popovics [93] had advocated the power function, and more specifically recommended use of a fixed power of 7 for the variable b in ASTM C403 equation 1 (which is Eq.(6.2) in this paper). While ASTM has not adopted that recommendation, the data collected here provide interesting insight to the utility of such a fixed value for the exponent in the power function. Figure 4.5 (a) shows the histogram of b in Eq.(6.2) computed by the best-fit for each available sieved data set, and Figure 4.5 (b) shows the same for the prepared mortars. (These values are reported in the last column of Table 4.3.) One first notices that there is no significant difference between these two populations, as is evidenced by similarity in the 95% confidence intervals on the exponent of [5.5 to 6.3] for sieved, and [5.6 to 6.4] for prepared. These analyses suggest that the exponent obtained from curve-fitting with the power function will most frequently be found in the range of about 5.5 to 6.5 for the types of materials and proportions evaluated

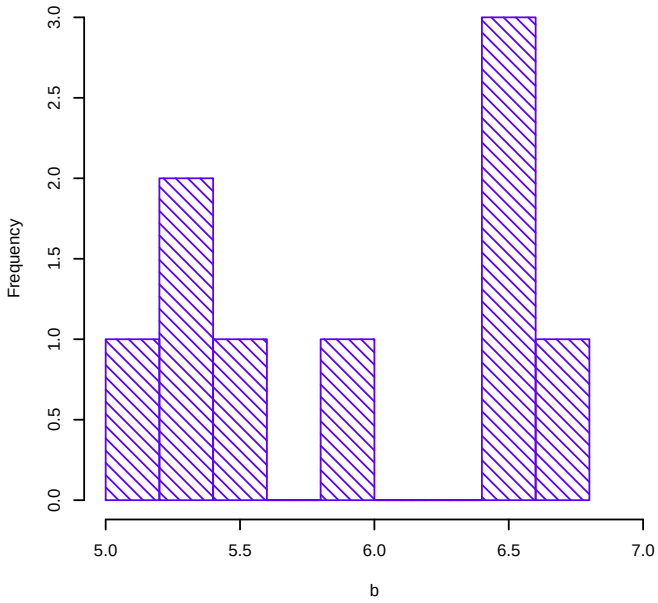

(a) b of Sieved Mortar Data

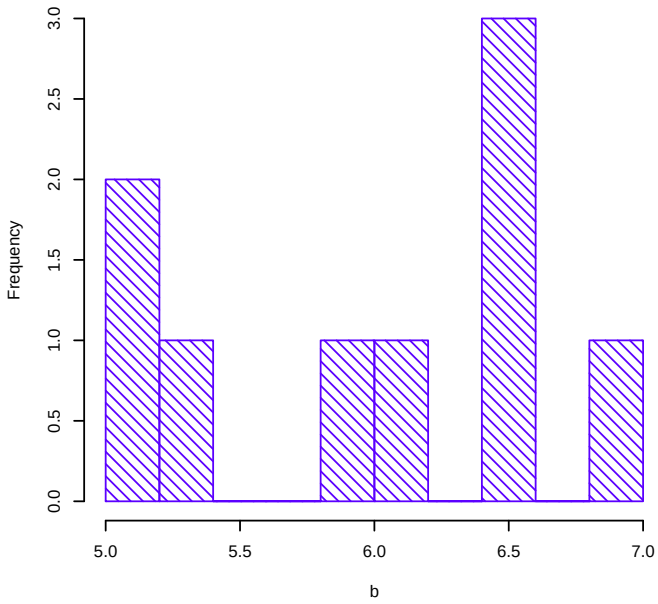

(b) b of Prepared Mortar Data

Figure 4.5: Histogram of best-fit value of exponent (b in Eq.(6.2)) for Power function for all experiments

here.

In regard to the curve-fitting function itself, the data reported in Tables 4.3 and 4.4 demonstrate that for about 1/3 of the data sets the exponential function provided the best-fit. As shown in Tables 4.3 and 4.4, the differences in setting time obtained from the two functions range from 0 to 18 minutes ($0.3\ h$). While the significance of these differences varies, it may be reasonable for ASTM to include the exponential function as a viable alternative to the power function, depending on goodness of fit for curve-fitting.

4.4.3 Estimation of Concrete Setting Times

In the general case the fundamental purpose for performing the C403 test on mortar, sieved or prepared, is to learn about the setting behavior of the parent concrete, as implied by the title of the test method, and as noted earlier by Tuthill and Cordon. For example, it is generally expected that faster-setting mortar will likewise lead to faster-setting concrete, and a series of lab tests would enable a correlation between the two. The practical significance of any difference in the behavior of sieved vs. prepared mortar would be indicated by the impact of that difference on the ability to predict setting behavior of the concrete the mortar represents. In this regard Abel and Hover [94] performed C403 tests simultaneous with observations of concrete placing and finishing operations in the field and suggested that "initial setting[2]" and "final setting[3]" as defined by professional concrete finishers, occurred at about the time that the C403 test indicated a penetration resistance for sieved mortar of approximately $41.4\ kPa$

[2]Professional finishers can stand on freshly placed concrete with a footprint depth of no more than about $6.35\ mm$ ($1/4\ in.$), can float the concrete, and can place a powered float machine on the concrete surface at their definition of "initial setting."

[3]No footprint is left on the surface, and concrete finishing operations can no longer be effectively performed without damage to that surface at a finisher's definition of "final setting."

(6 psi), and 103.4 kPa (15 psi) respectively. Similar threshold values have been suggested by others [95]. Using these numerical criteria, data collected from sieved mortar would lead to predictions of concrete setting times that are up to 0.4 $hours$ earlier than predicted from prepared mortar. The significance of this difference would depend on the application, and could be taken into account with an appropriate correlation as long as one is consistently using either sieved, or prepared mortar exclusively.

4.5 Conclusion

Wet-sieving must be performed to remove coarse aggregates when preparing the specimens in accordance with ASTM C403-08 because of the interference between coarse aggregate particles and the penetrometer probes as discussed by the inventors of the test [81]. It is therefore implicit that the resulting setting behavior of the extracted mortars correlates in some representative way to that of the concrete. Both sieved and prepared mortars are used in various applications, and the results vary between the two. ASTM C403 notes that such differences may be expected, and this study has quantified those differences as follows:

- In general, initial and final setting times of prepared mortars were delayed 5% to 16% as compared with those of sieved mortars based on experiments performed in the research and the data set obtained by Kelly.
- Such differences vary in magnitude from 1 to 3 times the currently reported duration of the ASTM C403 single-operator precision for three samples.

- Therefore, the setting times of a prepared mortar that exactly represents the mortar fraction of a given concrete can be significantly different from those of sieved mortars extracted from a given concrete.
- The difference in setting behavior between Experiments B and D suggests that the type of sieve used may impact the observed setting behavior.
- It is also suggested that the exponential function can be a viable alternative to the power function for fitting setting time data and for computing initial and final set-time intercepts.

CHAPTER 5

THE EFFECTS OF SIEVING AND PASTE CONTENT ON THE SETTING BEHAVIOR OF MORTARS AS MEASURED BY ASTM C403

5.1 Introduction

ASTM C403-08 [80], "Time of Setting of Concrete Mixtures by Penetration Resistance," quantifies the setting behavior of "concrete" by measuring the penetration resistance of mortar sieved from the concrete. (This procedure was adopted by Tuthill and Cordon [81] from the soil testing method for measuring penetration resistance in fine-grained soils for geotechnical applications [82].) To avoid the labor-intensive process of sieving the concrete (in which the mass of concrete sieved must be about twice the mass of mortar required for testing), some users opt to intentionally mix the mortar component of concrete without inclusion of coarse aggregate to study setting behavior of that concrete. The mortar thus obtained is referred to as a "prepared mortar" in contrast to the "sieved mortar" extracted from concrete. ASTM C403 acknowledges this practice and alerts the user that setting times may be increased when using the prepared mortar. Lee et. al. [2] showed that such differences can be larger than the single operator precision in C403 precision statements. They showed that setting times for prepared mortars increased 5% to 14% compared to those of sieved mortars extracted from a given concrete. Figure 5.1 summarizes their compilation beginning with Kelly's data [3] on the left to set the general pattern, with additional similar results on the right. As seen in Figure 5.1, the magnitudes of the "sieving-effect" vary but with the exception of Chung et al. [4], match the pattern first identified by Kelly [3], and thus substantiate the note in ASTM

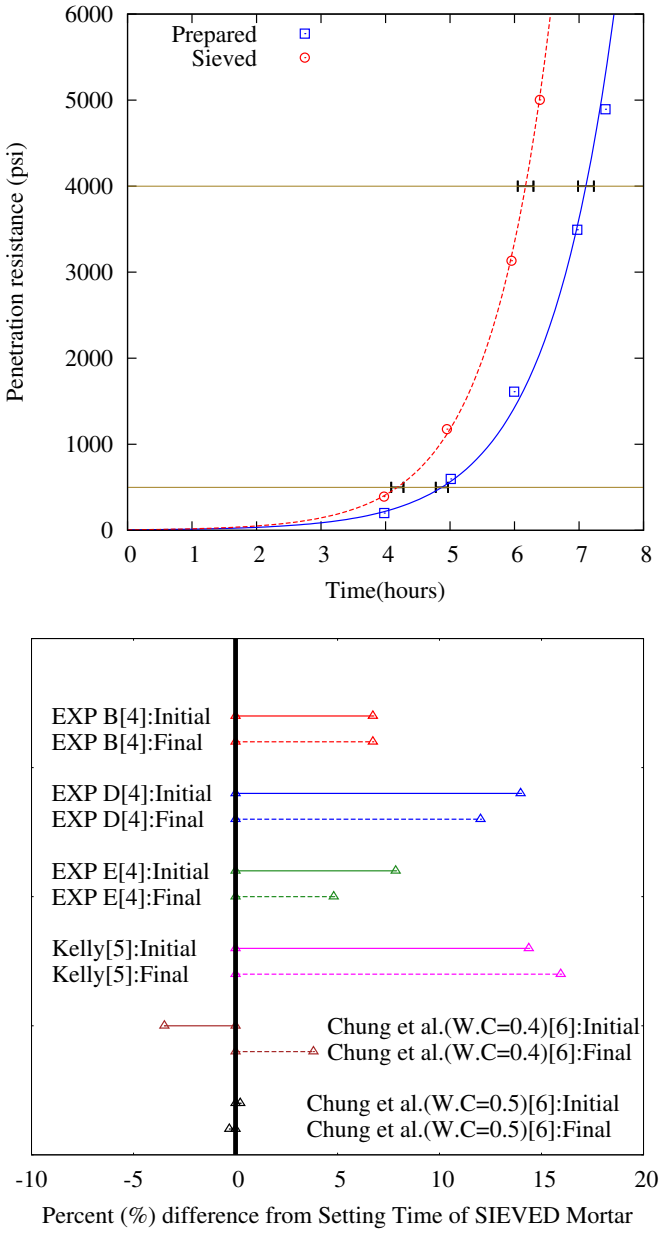

Figure 5.1: Pattern of difference between penetration resistance of sieved and prepared mortars by Kelly [3] (Left panel), and collected percent difference of setting times of prepared mortar relative to sieved mortar from Lee et.al [2] (Right panel)

C403 [80, 5.3]. While neither Kelly [3] nor C403 offer further commentary or explanation for the difference in behavior, the authors pose the hypothesis that the

difference in setting behavior between sieved and prepared mortar is because wet-sieving reduces paste content of the mortar. The rationale for this hypothesis is that coarse aggregates retained on the sieve are observed to be coated with a layer of paste with embedded fine aggregate particles. The primary purpose of this paper is to further investigate this hypothesis as an explanation for the observed impact of sieving on the setting behavior of mortar.

As will be demonstrated here, sieved mortars have lower paste content than prepared mortars, even though both began with the same initial mixture composition. Further, as suggested by Powers [96] and observed by others [4, 86], the reduction of paste content (or increase in aggregate content) in mortar leads to decreased workability, accompanied by a greater force required to achieve a given plastic deformation. In the context of this work that would lead to higher penetration resistance and therefore faster setting times for mortar with a reduced paste content.

5.2 Experiment

Experiments detailed in Lee et. al. [2] compared the C403 penetration resistance between three sets of sieved and prepared mortars, without reference to the changes in paste content induced by the sieving operation itself (reported as Experiments B, D, and E). This paper presents the method for measuring such changes in paste content (developed via Experiment C), and documents those paste changes for Experiments C, D and E. Further, this paper introduces additional setting-time experiments conducted on three mortars intentionally prepared with paste volume-fractions of 48%, 52%, and 55% (Experiment F), to

confirm the effect of changes in paste content on setting behavior.

5.2.1 Materials

Mixture proportions for prepared mortar and concrete for experiments C, D, E and F are summarized in Table 5.1. Details of aggregates properties are shown in Table 5.2. The general targets were to create or represent concrete with 60% mortar volume (Experiments C and D), 55% mortar volume (Experiment E), and 51–60% mortar volume (Experiment F). As shown in Figure 5.2, in every case the paste volume in the concrete was targeted at a fixed 30% with W/C=0.45 (giving the paste a 41% cement volume-fraction) and with the mortar volume fractions adjusted by means of modifying the coarse/fine ratio of the aggregate. Note that Experiment F was conducted with prepared mortar only, representing the composition of the concrete shown in Figure 5.2, but without inclusion of coarse aggregate. Further, the proportions actually realized varied from target values due to the measured air content of about 5 to 7% in the pre-sieved, non-air-entrained mortar. This translates to an air content of 2.5 to 3.8% in the associated non-air-entrained concretes. While the differences in paste and fine aggregate content appear minor in Figure 5.2, it is interesting to note that because a decrease in paste content in mortar is always accompanied by an increase in fine aggregate content, the ratio of paste volume to fine aggregate volume (P/FA) varies from 1.0 to 1.4 across all experiments, as shown in Table 5.1.

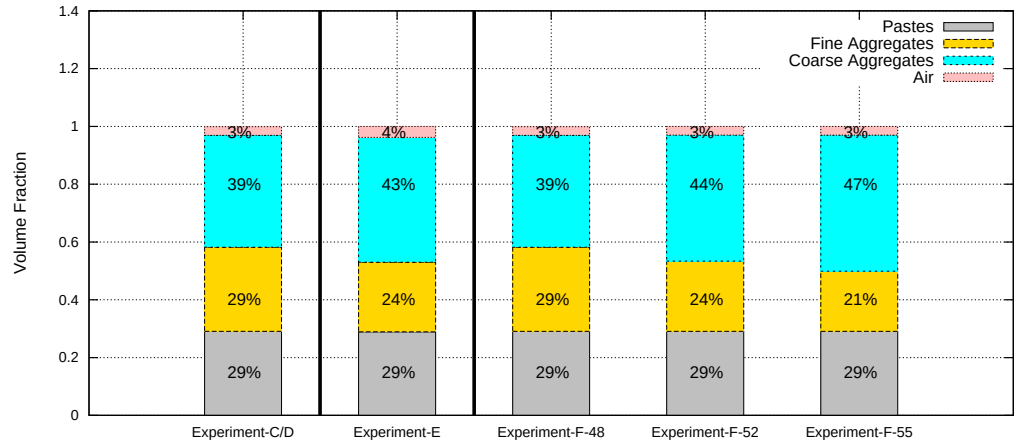

Figure 5.2: Target Volume fractions of Concrete Mixtures for each experiment prior to sieving

5.2.2 Experimental Procedure

As detailed in Lee et. al. [2], all concrete and mortar mixtures were prepared under indoor laboratory conditions at an ambient temperature of $23°C$. The focus of this paper is the method used to analyze the post-sieving mortar composition and post-sieving aggregate grading. This was performed by delicately washing, decanting, separating, and weighing the sieved-mortar and the paste-coated coarse aggregate retained in the mortar sieving operation. Details of this procedure are provided here (with example calculations shown later):

STEP 1: A sample of either sieved mortar or the paste-covered coarse aggregate that was retained on the sieve was retrieved and the as-collected mass determined.

STEP 2: Samples of known mass (about 2–4 kg) were placed on a sieve-stack that included the 75 μm (#200) sieve on top and 32 μm (#450) sieve on the bottom, suspended over a clean bucket. Water was gently sprayed

Table 5.1: Mixture Proportion for mortars for experiment C, D, E, and F (kg per $1\ m^3$ of mortar or concrete)

Ingredients	Experiment C[c], D[b]		Experiment E		Experiment F		
	kg/m^3	kg/m^3	kg/m^3	kg/m^3	kg/m^3		
	mixed	mixed	mixed	mixed	mixed mortar		
	mortar	concrete	mortar	concrete	F-48	F-52	F-55
Cement[a]	620	380	644	377	620	677	724
Water	279	171	290	170	279	305	326
Fine agg.	1260	770	1078	632	1260	1145	1050
Coarse agg.	-	998	-	1151	-	-	-
$V_{paste}/V_{concrete}$[d]	-	29%	-	29%	-	-	-
V_{paste}/V_{mortar}	48%	48%	50%	52%	48%	52%	55%
V_{paste}/V_{fine}[e]	1.0	1.0	1.2	1.2	1.0	1.2	1.4

[a] Type I cement from the same manufacturer was used for all experiments, yet cements for experiments F was from a different production run from that used for experiments C, D, and E.

[b] Concrete was designed and batched; sieved mortar was extracted from the concrete. For comparison, mortar was also prepared with the identical composition of the mortar fraction of the concrete.

[c] Concrete was designed and batched, and sieved-mortar was extracted.

[d] In all cases the term "paste" indicates cement and water only, air is not included. Air is classified as a separate component of the mixtures.

[e] $P/FA = V_{paste}/V_{fine}$

over the sieves until visibly clean water passed from the bottom of the stack, taking care not to eject material from the upper sieve due to the

Table 5.2: Properties of Aggregates Prior to Mixing Concrete

Experiment	Types	Absorption (%)	Specific Gravity	Fineness Modulus
C	Fine	2.2	2.62	2.75
	Coarse	1.5	2.65	7.51
D	Fine	2.2	2.62	2.99
	Coarse	1.5	2.65	7.24
E	Fine	2.2	2.62	2.55
	Coarse	1.5	2.65	7.44
F	Fine	2.8	2.65	2.99

[a] Aggregate properties obtained per ASTM C127-08 [87] and C128-08 [88]

[b] Sieve analyses per ASTM C136-06 [89] for both fine and coarse aggregates before mixing.

[c] Coarse aggregates met grading requirements for ASTM C33 size number 7 [90] with a nominal size of $12.5\ mm$.

[d] All aggregates used in Experiments C, D, and E were taken directly from the aggregate sieves and remixed into the concrete to eliminate sampling error between the sieve analysis and the aggregates actually used. Aggregate used in Experiment F was sampled from the stockpiles.

force of the water stream. At this point, clean coarse and fine aggregates were retained on the two sieves, with dark-gray water with suspended solids was in the lower bucket. The bucket was then tightly covered and set aside to allow gravity-settling. (It had been determined previously that $> 99\%$ of the mass of the cement used passed the $32\ \mu m$ (#450) sieve when wet-sieved with the water spray as described above. Similarly, only 0.2% of the fine aggregate passed the $32\ \mu m$ (#450) sieve, making this sieve a useful separator of cement and aggregate.) The entire mass of washed aggregates retained on the $75\ \mu m$ (#200) and $32\ \mu m$ (#450) sieves was oven-dried, and weighed to determine the mass of aggregate, and by subtraction, the mass of paste in the original sample. Corrections were made to account for absorbed moisture.

STEP 3: A sieve analysis of the washed-and-dried aggregates was determined in accordance with ASTM C136-06 [89]. The resulting grading curves were then compared with those obtained prior to mixing.

STEP 4: In subsequent testing, the water with suspended solids was allowed to gravity-settle for at least one week, decanted, and the wet residue oven-dried. The dried material was therefore a mixture of partially-hydrated cement particles and any minus-#450 aggregate fines. This paper does not include subsequent results of this analysis step.

5.3 Experimental Results

5.3.1 Comparison of Paste Contents before and after sieving

The paste content of sieved mortar was estimated as described above for the sieved mortar obtained in Experiments C, D, and E. In estimating paste volume it was assumed that W/C of the paste was preserved during sieving. Detailed calculations using experiment C as an example are shown in Table 5.3. The same method was implemented to compute the pre- and post-sieving paste contents for experiments D and E.

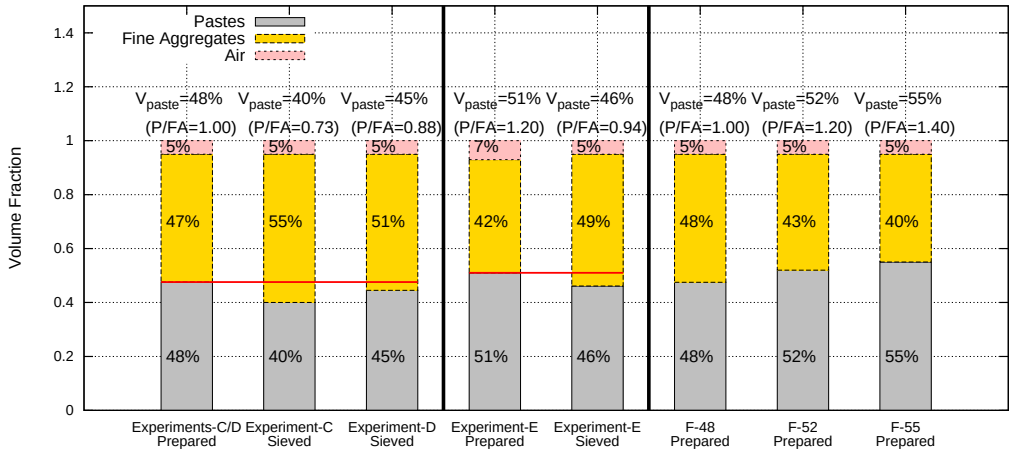

Figure 5.3: Volume fractions of prepared and sieved mortars. Corresponding percent paste volume per unit volume of mortar (V_{paste}) and paste/aggregate volume ratio shown at top of each column.

Figure 5.3 shows the volume fractions of paste, aggregates, and air in both prepared and sieved mortars as tested. The gray proportions indicate relative volume fractions of pastes while the red lines draw attention to the reduction of paste content in sieved mortars for Experiments C, D, and E. For Experiments

Table 5.3: An Example of Estimation of Pastes (Experiment C)

Note	Weight (g)	Volume (mL)
Mortar passing #4 (sieved mortar)	1729	
Washed & decanted aggregates in sieved mortars (Oven Dry)	1119	
Washed & decanted aggregates in sieved mortars (Saturated Surface Dry)	1136[a]	428[a]
Estimated mass of paste in sieved mortar = Difference between mass of freshly sieved mortar and SSD mass of aggregates washed & decanted from that mortar. Air-free paste volume computed from paste mass and $W/C = 0.45$	593	314
Cement in sieved mortars assuming $W/C = 0.45$	409	130
Batch water in sieved mortars assuming $W/C = 0.45$	184	184
Paste volume fraction in the sieved mortar $= 314/(314 + 428)/1.05 = 0.403$ (assuming 5% air as mixed)		
Paste volume in initial, un-sieved, as mixed mortar from mixture proportions $= 0.48$ (assuming 5% air as mixed)		
Reduction of paste volume fraction as a result of sieving operation $= 0.48 - 0.40 = 0.08$		
P/FA initial = air-free paste volume/aggregate volume = 1.0		
P/FA final $= 314/428 = 0.734$, round to 0.73.		

[a] Aggregate properties (absorption and specific gravity) are applied to calculate the weights and volumes of SSD aggregates in the sieved.

C and D, sieving reduced the paste-volume fraction in the mortar from the as-mixed value of 48% to the as-sieved values of 40 and 45%, respectively. (Reduction of paste volume fraction as a result of sieving therefore ranged from 6 to 17% of the pre-sieved volume.) In experiment E the paste-volume fraction was reduced from 50% to 46% (a reduction of 8% of the pre-sieved paste volume). Note also the accompanying changes in P/FA in Figure 5.3.

5.3.2 Sieve Analysis of Aggregates

In addition to the analysis of mortar composition, the effect of sieving on aggregate size distribution was investigated by comparing grading curves of aggregates sampled prior to batching with curves obtained for aggregates that had been washed, decanted, and oven-dried from the collected mortar that had passed through the $4.75\ mm$ (#4) sieve per C403. In experiments C, D and E, the actual aggregate samples used in the pre-mixing sieve analyses were returned to the mixer for incorporation in the concrete. Likewise, aggregates washed from mortar that passed the $4.75\ mm$ sieve in accordance with C403 were then again subjected to the ASTM C136-06 procedure to obtain grading curves. These steps guaranteed that the sieve analyses represented the aggregates actually used in mixing and as affected by sieving, and are not subject to differences due to sampling.

It was first necessary to examine whether the sieving process itself modified the grading of the materials. Samples of coarse and fine aggregate were sieved, collected, weighed, and the same material sieved again a total of three times, with the results reported in Figure 5.4. At this scale the multiple curves are

indistinguishable, and the largest single difference in percent-passing on any sieve was 0.5% for the coarse aggregate and 0.25% for the fine aggregate. It is therefore concluded that for the aggregates used in this study, up to 3 cycles of the sieving process itself did not influence the size distribution.

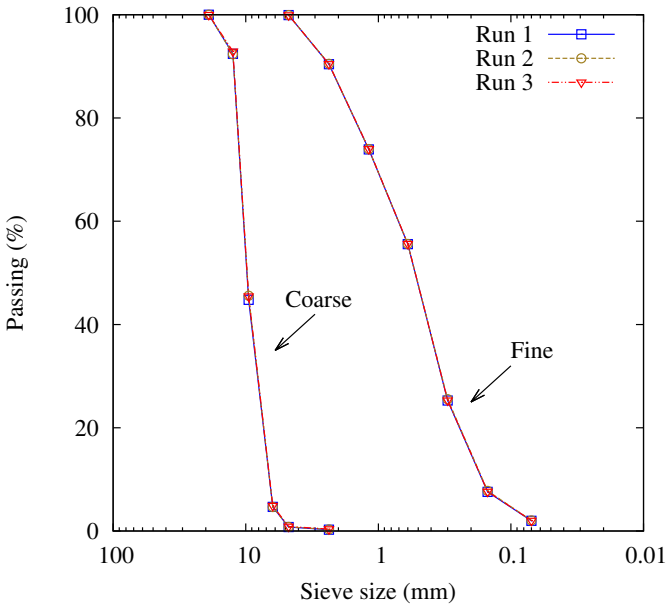

Figure 5.4: Comparison of percent-passing grading curves for coarse and fine aggregates for three repeated analyses of the same samples

Figures 5.5 and 5.6 show particle size distribution curves for the aggregates as-mixed, and again after sieving and washing as described above. For all these curves the values on the Y-axis are obtained by dividing the masses of aggregate retained on each sieve by the total mass of aggregate initially mixed, and normalized across all experiments for an initial combined aggregate mass of $1\ kg$. This reporting technique is different from the conventional method of expressing percent retained based on the total mass of aggregate sieved. The advantage of the method used here is that changes resulting from wet-sieving are immediately apparent. For example, in Figure 5.5 (a), it is seen that 108 grams

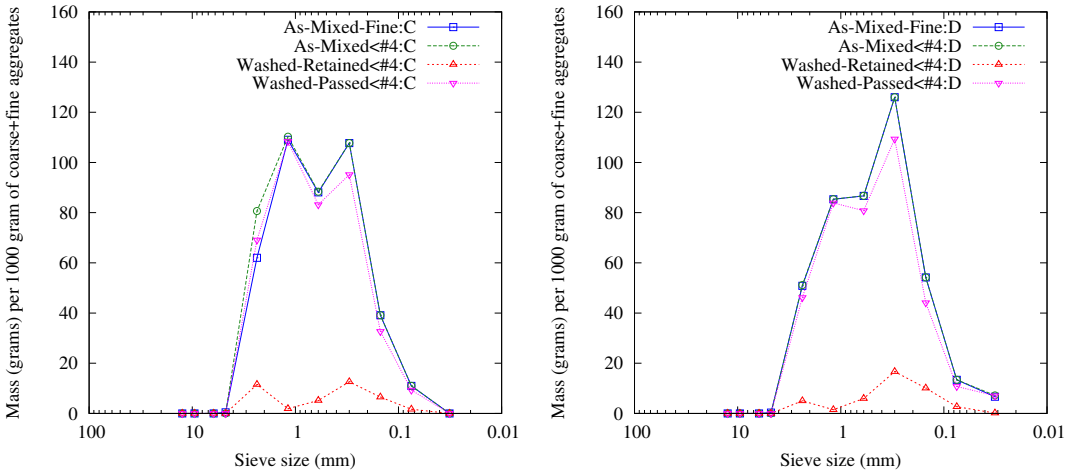

(a) Experiment C

(b) Experiment D

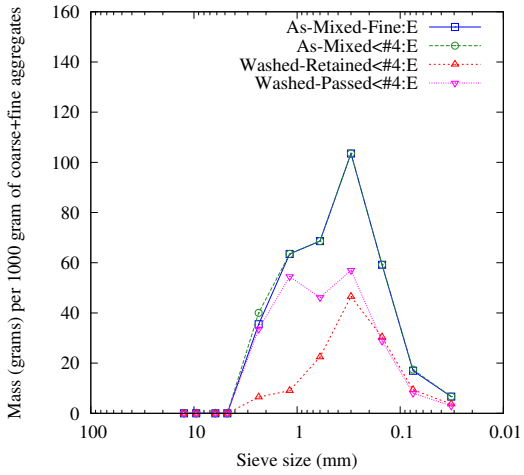

(c) Experiment E

Figure 5.5: Mass grading curves of combined aggregates that smaller than $4.75\ mm$ sieve and as-mixed fine aggregates in experiments C, D, and E

of fine aggregate were retained on the $300\ \mu m$ (#50) sieve, per kg of combined aggregate at the time of batching. After wet-sieving, the mortar that passed the $4.75\ mm$ sieve was washed, dried, and re-sieved, and of the initial $108\ g$ retained at batching, about $95\ g$ were present in the sieved mortar. From this it may be estimated that out of the $105\ g$ of aggregate retained on the #50 sieve at batch-

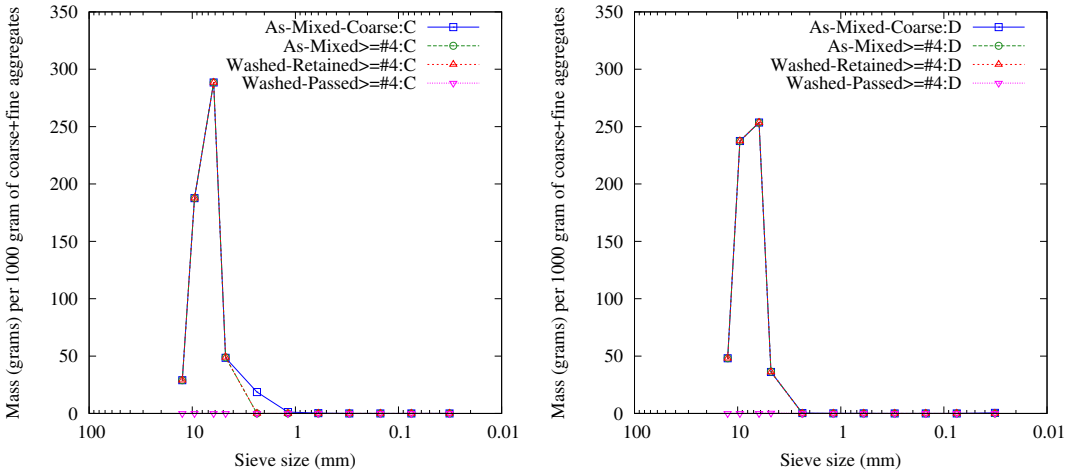

(a) Experiment C

(b) Experiment D

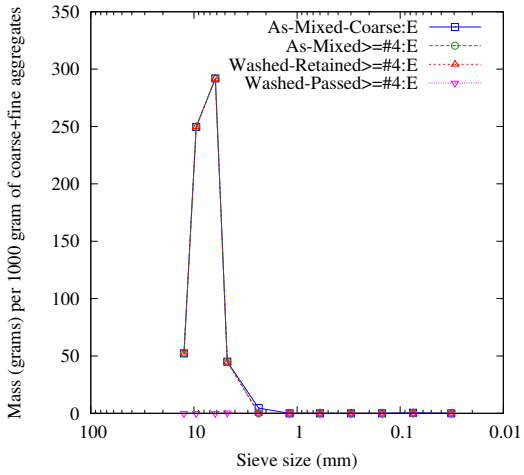

(c) Experiment E

Figure 5.6: Mass grading curves of combined aggregates that greater than $4.75\,mm$ sieve size and as-mixed fine aggregates in experiments C, D, and E

ing, about $13\ g$ remained behind on the #4 wet-sieve, adhering to the coarse aggregate. This is verified in the lowest curve in Figure 5.5 (a), that shows about $13g/kg$ of combined aggregate that was washed from the coarse aggregate removed from the mixture by wet-sieving. For additional clarity, the curves are separated into aggregate sizes below (Figure 5.5) and above (Figure 5.6) the #4

sieve. “As-mixed-fine” and “As-mixed-coarse” in Figures 5.5 and 5.6 denote retained mass distributions of original aggregates. The term “Washed” refers to grading analysis performed on aggregates obtained from wet-sieving the concrete, where “Retained” means material retained above the #4 wet-sieve, and “Passed” means material collected below the #4 wet sieve.

As expected, wet-sieving produced no significant change in aggregate larger than the openings in the #4 sieve in all three experiments as shown in Figures 5.6. However, wet-sieving notably altered the size distribution of fine aggregates in the mortar that passed the #4 sieve, as seen in Figures 5.5 (a), (b), and (c). One observes that fine aggregate particles smaller than the #4 wet-sieve are nevertheless present in the paste-coated aggregate that is retained on the wet-sieve. This is evident in the red lines at the bottom of Figures 5.5 (a), (b) and (c). This is most pronounced for Experiment E which had a concrete slump of less than $38\ mm$, or about half that of the concrete in Experiments C and D, and was more difficult to force through the sieve.

One way to characterize the changes in the sand-grading that resulted from wet-sieving is to compare pre- and post-sieving Fineness Modulus (FM). The as-mixed FM of sand in Experiments C and D was 2.99 and 2.75, shifting to finer values of 2.89 and 2.71 after wet-sieving. On the other hand, for experiment E the FM of sand increased from 2.55 at mixing to 2.87 after wet-sieving. While one cannot generalize on the nature of the changes, it is nevertheless clear that sieving can change the grading of the fine aggregate in the mortar.

While presenting these findings on aggregate grading, the possibility remains that what has been interpreted here as sand-fines in the sieved mortar is actually Portland cement. Recall, however, that washing of the mortar con-

tinued until the water was clear. Further, intentional, preliminary wet-sieving of pure cement always returned zero %-retained on the $75\ \mu m$ (#200) sieve, with a visible but immeasurably small %-retained on the $32\ \mu m$ (#450) sieve. Nevertheless, since grading analysis of all pre-mixed aggregates showed zero percent retained on the #450 sieve, any mass retained on the #450 sieve after washing the sieved mortar was ignored. (This value was typically in the range of 0.1%). It is thus concluded that the results reported above are not significantly complicated by the mass of cement (partially-hydrated or un-hydrated).

5.4 Correlation of Paste Content and Penetration Resistance

5.4.1 Penetration Resistance for Intentional Variations of Paste Content

Given the observed reductions in paste content associated with the C403 sieving procedure, it was useful to develop background data on the effects of intentional variations in paste content on penetration resistance of mortar. In this regard, Experiment F was performed with prepared mortars with paste volume fractions of 48, 52, and 55%, which were subsequently tested per C403 without wet-sieving. The resulting characteristic patterns of penetration resistance versus time are shown in Figure 5.7. As seen in the figure, the effect of changing paste volume by 3 to 4% is to merely translate the entire curves horizontally by a magnitude of approximately 0.4 hours as shown in Table 5.4. This difference exceeds the ASTM C403 "acceptable ranges of three results" for a single operator as observed by Lee et. al. [2]. A clear pattern emerges in which lower paste

contents (i.e., higher aggregate contents) are associated with greater penetration resistance at any time, which is interpreted as more rapid setting. It is interesting to note that in the data from Experiment F, the magnitudes of the differences in paste content, and the magnitudes of the differences in setting times are comparable with the differences noted between the prepared and sieved mortars reported above.

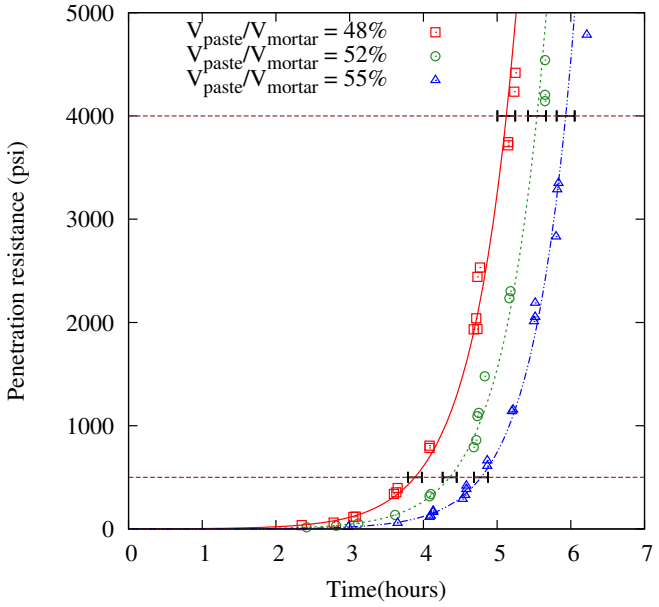

Figure 5.7: Penetration Resistance with Variable Volume Ratio of Pastes from Experiment F (horizontal line segments denote acceptable range of three results for initial and final setting time per C 403)

5.4.2 Reduction in Paste Content Correlated with Setting Behavior

As reported above, sieving reduces the paste content in the mortar that passes the sieve (as is evident from the paste that is observed to adhere to the coarse

Table 5.4: Summary of Setting Times for experiments B, D, E, and F [2] and data collected from literature [3, 4]

Experiments	Initial[a]	Final[a]	R^2	RE%[b] initial	RE%[c] final	K[d] initial	K[e] final	Function for best-fit
B-Prepared	4.3	6.0	0.998	6.7%	6.7%	1.7	1.7	P
B-Sieved	4.0	5.6	0.987					P
D-Prepared	4.8	6.5	0.997	14.0%	12.0%	3.1	2.9	P
D-Sieved	4.2	5.8	0.997					P
E-Prepared	4.0	5.2	0.994	7.8%	4.8%	1.5	1.0	E
E-Sieved	3.7	5.0	0.995					E
F-48-Prepared	3.9	5.1	0.994					E
F-52-Prepared	4.4	5.5	0.996					E
F-55-Prepared	4.8	5.9	0.993					E
Kelly-Prepared	4.8	7.2	0.999	14.3%	15.6%	3.2	4.0	P
Kelly-Sieved	4.2	6.2	0.998					E
Chung-Prepared[f]	3.8	5.9	0.987	-2.2%	3.8%	-0.4	0.9	E
Chung-Sieved[f]	3.9	5.7	0.971					P
Chung-Prepared[g]	5.1	7.6	0.991	0.2%	-0.3%	0.1	-0.1	P
Chung-Sieved[g]	5.1	7.7	0.998					P

[a] Initial and final setting times estimated by either power or exponential function

[b] RE% initial = $|t_{initial\ set,prepared} - t_{initial\ set,sieved}|/t_{initial\ set,sieved} \times 100\%$

[c] RE% final = $|t_{final\ set,prepared} - t_{final\ set,sieved}|/t_{final\ set,sieved} \times 100\%$

[d] K initial=$(t_{initial\ set,prepared} - t_{initial\ set,sieved})/11.4\ min$

[e] K final= $(t_{initial\ set,prepared} - t_{initialset,sieved})/14.6\ min$

[f] Estimated from data set of $W/C = 0.4$ obtained by Chung et al. [4]

[g] Estimated from data set of $W/C = 0.5$ obtained by Chung et al. [4]

aggregates retained in the sieving process). For sieved mortars (with reduced paste contents, therefore) setting times were significantly shorter than for prepared mortars of the same initial composition (but relatively higher paste content). Likewise, mortars in Experiment F with intentionally reduced paste content demonstrated significantly shorter setting times. In each case the term "significant" is justified in comparison to the C403 precision statements. Figure 5.8 shows the influence of paste content on setting times for all experiments, as presented in Table 5.4.

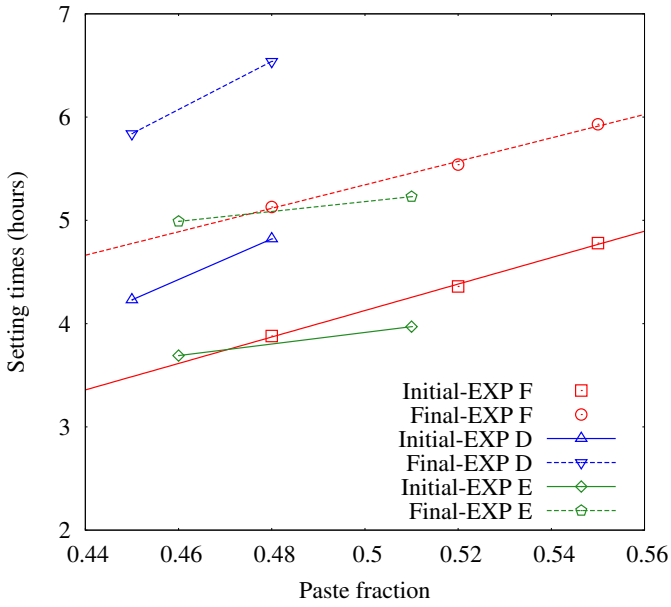

Figure 5.8: Setting Times against Paste Volume Fractions estimated either by exponential or power functions that provided the best-fit

In Figure 5.8 the general trend of increased setting time with increased paste content is evident. The sensitivity of setting behavior to paste content varies; however, with Experiment D showing that an increase in paste content of 1% will extend both initial and final setting times by about 0.20 to 0.23 hours (12 to 14 min.) The least-sensitive mixture was Experiment E, (also the stiffest mix-

ture examined) where an increase in paste content of 1% will delay both initial and final setting times by about 0.04 to 0.06 hours (2 to 4 min.). Experiment F displayed an intermediate behavior.

While general trends are clear in Figure 5.8, slopes and intercepts vary for each mixture for the simple linear models shown. Although the input materials were the same in each mixture, the proportions intentionally varied, sampling of the fine aggregate from the source resulted in differing FM, and although all cement was the same type and from the same producer, each experiment used bagged cement from a different production run. Further, the fluidity of the mixtures generally corresponded to a pre-sieving concrete slump of about $75\ mm$, but the concrete in Experiment E had a slump of less than $38\ mm$. To minimize the influence of these differences, setting times (Y-values) are re-expressed in Figure 5.9 relative to values obtained for mortar in any given experiment with the lowest paste content. In Experiments D and E this means normalizing by the initial and final setting times for sieved mortar, and for Experiment F normalizing by the mortar with the lowest paste content, i.e., prepared mortar F-48. Likewise, paste contents (X-values) are normalized to the smallest paste content for a given experiment.

As seen in Figure 5.9, this normalization method highlights the slopes which indicate the sensitivity of setting time to paste content for the various mortars. These observed sensitivities varied from a minimum increase of 0.44% in final setting time per 1% increase in paste content for Experiment E, to a maximum value of 2.1% increase in initial setting time per 1% increase in paste content for Experiment D. The average for all data is that setting time increased by about 1% for 1% increase in paste content. Conversely, if sieving removes about 5% of

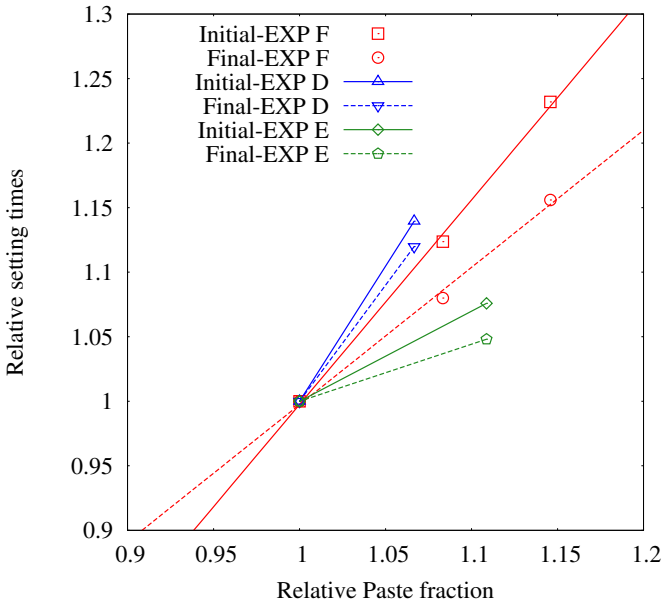

Figure 5.9: Relative setting Time against Relative Paste Fractions

the paste content, setting time will be decreased by about 5%.

5.5 Discussion

5.5.1 The Effects of Sieving on Mixture of Sieved Mortars

Within the relationships between relative setting times and relative paste fractions shown in Figure 5.9, it is evident that other factors are at work beyond paste content alone. One such factor may be the influence of sieving on the grading of the aggregate in the sieved mortar. For example, sieving lowered the FM of fine aggregate in the mortar in experiments C and D, while increasing FM in the sieved mortar in Experiment E.

These changes may be important, because as Mindess et al. [53] have pointed out, the finer the aggregate, the greater the paste volume required to achieve a given level of workability because a larger aggregate surface area must be covered by the paste. Therefore, among mortars with fixed, identical paste content, one incorporating a finer aggregate is expected to be less fluid, and therefore exhibit apparently faster setting times. However, in the experiments reported here, sieving resulted in a dual effect: a reduction in paste content (which reduces workability) combined with the changes in aggregate grading already discussed. From the simple multi-linear model of Eq. (5.1), the resulting "standardized coefficients" [97, 65], shown in Table 5.5 suggest approximately equal weighting for the influence of paste volume and FM of sand. Thus a combination model is proposed in which both the effects of paste-volume and sand fineness are taken into account as follows:

$$\text{Relative setting time} = \beta_0 + \beta_1\,(\%\text{ change in paste content}) + \beta_2\,(\%\text{ change in FM}) \tag{5.1}$$

While this simple model appears promising, the small number of data points

Table 5.5: Standardized Beta for β_1 and β_2 (The resulting R^2 of analysis = 0.9332)

Independent Variables in Eq.(5.1)	Standardized Beta
% change in paste content	0.732
% change in FM	0.739

limits the statistical level of confidence to less than 80%. In the next section a somewhat more physical model of the combined effect of paste volume and aggregate grading is proposed, in which both parameters are used to estimate an equivalent average paste-layer thickness over the surface of all aggregates.

5.5.2 Equivalent Thickness of Pastes Coating around Aggregates

Computing the equivalent average thickness of the paste layer enveloping all aggregates assumes that the entire paste volume is distributed in a layer of uniform thickness over all particles, and that the aggregates are spherical. This is the fundamental model that Powers [96, 98] proposed for paste-layer thickness over air voids when the ratio of paste to air volume is less than or equal to 4.342 (which condition applies here as well with P/FA ranging from 0.7 to 1.2.) As reported by Mindess et. al. [53] and by Neville & Brooks [99], workability is a function of water content divided by aggregate surface area. But, since paste content is proportional to water content for a given value of W/C, workability is therefore proportional to paste content divided by aggregate surface area. This ratio may be envisioned as an equivalent average paste-layer thickness. For the work reported here, computation of aggregate surface area was based on characteristic particle sizes that are the average of the opening size of the sieve upon which the particles were retained, and the opening of the sieve immediately above. Surface area of both coarse and fine aggregates were taken into account for concrete mixtures.

Table 5.6 presents the computed thickness of pastes under the given postulations. For all three experiments shown, the average paste-layer thickness decreased due to sieving, even though FM decreased in C and D and increased in E. This general decrease in layer thickness likewise coincides with the general reduction in setting time observed in all three cases. It is also interesting to note that when modest reductions in paste volume, on the order of 3% to 5% for experiments D and E, are combined with changes to the aggregates, the result is

Table 5.6: Estimated paste-layer thickness around aggregates

	Thickness (μm)	P/FA	Thickness (μm)	P/FA	Thickness (μm)	P/FA
Experiments	Concrete		Prepared Mortar		Sieved Mortar	
C	54	0.90	-	1.0	41	0.73
D	69	0.94	74	1.0	55	0.87
E	64	1.10	76	1.2	61	0.94
	F-55		F-52		F-48	
F[a]	138	1.4	116	1.2	97	1.0

[a] Experiment F implemented only prepared mortars.

a reduction of paste-layer thickness in the range of 20 to 25%. This is because of the powerful impact of very fine aggregate particles on total aggregate surface area.

Figure 5.10 shows the relationship between setting times and computed paste-layer thickness. In Figure 5.11 these same data are normalized to become relative setting time as a function of relative change in paste layer thickness. Once again, this normalization method highlights the sensitivity of setting time to paste-layer thickness for these tests. These sensitivities varied from a minimum increase of 0.3% in initial setting time per 1% increase in paste-layer thickness for Experiment E, to a maximum value of 0.6% increase in initial setting time per 1% increase in paste-layer thickness for Experiment F. The average for all data is that setting time increased by about 0.4% for a 1% increase in paste-layer thickness. Therefore, in a case where sieving reduces paste-layer thickness by about 20% (as seen in Experiment E), setting time would be expected to be

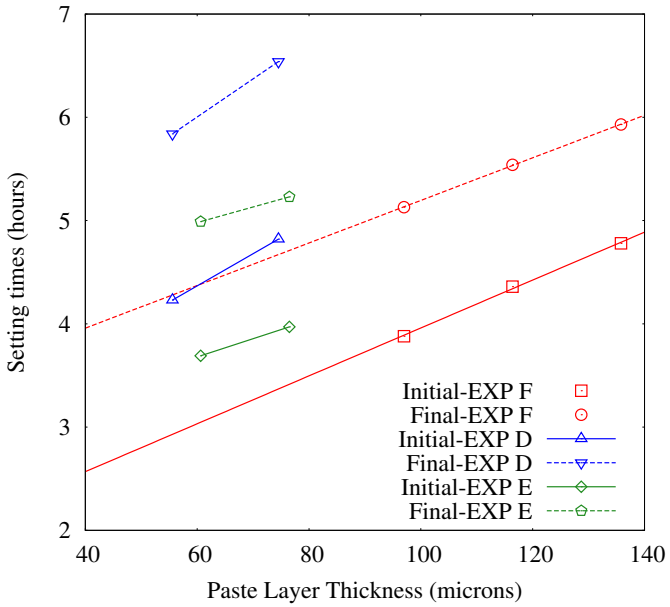

Figure 5.10: Setting Times with paste-layer thickness of paste

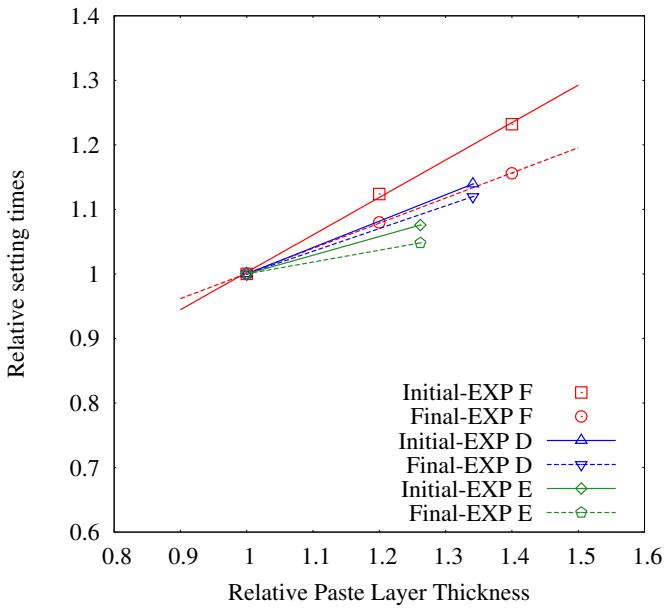

Figure 5.11: Relative Setting Time with Relative paste-layer thickness

decreased by about 8%.

It is of interest to consider that since wet-sieving changes the paste content and the grading of fine aggregate in the mortar, the sample thus acquired in the ASTM C403 test is no longer truly representative of the mortar phase of the concrete in question. The significance of this difference can be taken into account, however, by the fact that predicting concrete behavior from mortar behavior requires some type of correlation in any case.

Finally, it has been observed that the simple, low-energy operation of wet-sieving concrete to produce mortar makes subtle but significant changes in composition and aggregate grading beyond the mere removal of aggregate particles larger than the wet-sieve itself. It may therefore be worthwhile to examine the effects of higher-energy construction operations such as various placing methods, consolidation with vibrators, and a variety of finishing techniques. One may hypothesize that the character and composition of the mortar phase varies spatially in concrete as-placed, consolidated, and finished as influenced by construction processes and mixture properties. If a given construction process locally modifies paste content or aggregate grading, for example, setting behavior might be locally modified as well. In this regard, the methods used in this series of small-scale experiments might be useful to study such larger-scale phenomena.

5.6 Conclusion

This study investigated changes in paste content and aggregate grading that accompany the wet-sieving of concrete for the ASTM C-403 test. As previously

documented [2, 3] this same sieving operation produces mortar with shorter initial and final setting times than measured for prepared mortar of the same initial composition. The work reported here has therefore attempted to correlate these observations as follows:

- Wet-sieving reduced the paste volume fraction by 3% to 8% in mortars that subsequently showed a 5 to 16% reduction in initial and final setting times. (Changes in aggregate grading accompanied the paste reduction.)
- Prepared mortars with intentional reductions in paste volume fraction of 5 to 13% from the control mixture subsequently showed a 8 to 16% reduction in initial and final setting times. (There were no changes to aggregate grading for the prepared mortars.)
- The average for all data is that setting time increased by about 1% for 1% increase in paste content. Conversely, if sieving removes about 5% of the paste content, setting time will be decreased by about 5%.
- Wet-sieving modified the grading of the fine aggregate. In two cases the sand remaining in the mortar after sieving was finer than that used in the initial mixture and in one case the sand became coarser.
- When the effects of paste volume and aggregate fineness were combined via a model of computed paste-layer thickness. Wet-sieving always led to mortar with a reduced paste-layer thickness, with a reduction of 20% to 25%. Due to the impact of the surface area of sand particles retained on the $600\ \mu m$ (#30) and $300\ \mu m$ (#50) sieves, the magnitude of changes in paste-layer thickness is significantly greater than the magnitude of changes to paste content.

- Reductions on paste-layer thickness are associated with reductions in initial and final setting time. The average for all data is that setting time decreased by about 0.4% for a 1% decrease in paste-layer thickness. Therefore, in a case where sieving reduces paste-layer thickness by about 20% (as seen in Experiment E), setting time would be expected to be decreased by about 8%.
- The experimental methods and models introduced here may be useful for evaluating localized changes to the composition of concrete mixtures and mortars resulting from various construction operations.

CHAPTER 6

CLARIFICATION OF SETTING TIMES OF PASTES, MORTARS, AND CONCRETES

6.1 Introduction

This paper explores the correlation between the time-dependent stiffening of concrete as indicated by ASTM C403 [80] (which measures penetration-resistance of mortar sieved from concrete), and the ability to effectively consolidate and finish freshly cast concrete. The need for correlation, or at a minimum, clarification, is demonstrated by potential confusion with use of the terms "initial" and "final setting", which both have clear and quantifiable definition in the context of the ASTM C403 test. These same terms have a less rigorous, semi-quantitative meaning as applied to various construction operations required to finish horizontal concrete surfaces (floors and slabs), as described in detail in ACI 302.1R-04 (Construction of floors) [100]. In fact, ACI 302.1R-04 [100] uses the term "setting" 38 times in the context of the stiffening of concrete, and does not mention, cite, or refer to ASTM C403.

The terms "initial" and "final setting" appear in yet a more generalized context in industry documents such as ACI 308 (Curing) [101], ACI 309 (Consolidation) [102], and ACI 347 (Formwork) [103] to describe non-specific, qualitative stages in the stiffening of concrete, and again, without reference to ASTM C403 [104, 105, 106] ACI technical committee meetings frequently entertain ad hoc debates about whether the ASTM C403 definitions of initial and final setting are always implied when these terms are used. This paper is intended to inform such debates by comparing the setting behavior of paste, mortar, and

concrete as determined by the ASTM C191 Vicat test, the C403 mortar test, and the concrete setting test developed by Abel & Hover. Included in the comparison are the results of several non-standard, field-type indicators of the developing stiffness of freshly cast concrete. These comparisons demonstrate that setting behavior of paste, mortar, and concrete are significantly different from each other, but are nevertheless related. A researcher or practitioner can obtain useful information about the timing of construction operations, or the effects of mixture or environmental variables on the basis of any of several indicators, provided that mixture-, materials-, and environment-specific correlations have been established.

6.2 Research Significance

The rate of stiffening of fresh concrete is critical for effective timing of placing, consolidating, finishing, curing, heating, cooling, and saw-cutting. Failure to initiate and complete these operations in accordance with the changing behavior of concrete can lead to poor consolidation, surface defects, unacceptable flatness or levelness, scaling or delamination, reduced abrasion resistance, or cracking. Providing a quality concrete surface requires management of construction processes and some form of monitoring the continuous stiffening of the concrete over time. This paper addresses standard lab techniques and commonly applied field techniques and rules-of-thumb used to monitor concrete's fluid to solid transition.

6.3 Background

The terms "initial setting" and "final setting" refer to changes in behavior as recently cast concrete stiffens over time. A review of ACI committee documents published in the 2011 Manual of Concrete Practice reveals use of the word "setting" at least 100 times to refer to the stiffening of paste, mortar, or concrete. In many, but not all cases, the term is used in the context of ACI's standard terminology [107] as shown in Table 6.1. Keys to interpreting the standard definitions of initial and final setting are the phrases "empirical value," "resist...penetration," and "to an established degree." Those empirical penetration resistance values have been established for the ASTM C191 [108] "Vicat" and the C266 [109] "Gilmore" tests for cement setting, and the C403 test, which although entitled "Standard Test Method for Time of Setting of Concrete Mixtures by Penetration Resistance," the test is actually performed on mortar that has been wet-sieved from the concrete. Wet-sieving is necessary to remove the coarse aggregate particles which would otherwise interfere with penetration of the probes. For the Vicat and Gillmore tests the applied force and size of probes are fixed and the depth of penetration varies with time. For the C403 test probe diameter and applied force are varied as required to achieve a fixed depth of penetration of $25\ mm$ ($1\ in.$) as the probe is pushed into the mortar. See Table 6.2 for standard tests and criteria. According to C403, "Initial Setting" is reached when penetration resistance is $3.4\ MPa$ ($500\ psi$). When it comes to defining initial set for the purpose of "second-floating" a concrete slab (after bull-floating), ACI 302.1R instructs the finisher to wait until the concrete will sustain foot pressure with only approximately $6\ mm$ ($1/4in.$) indentation." Thus ACI 302's guidance fits the format of the ACI setting time terminology by defining a degree of

Table 6.1: Terminologies of Setting and Setting Times

Term	ACI Definition
Setting	a chemical process that results in a gradual development of rigidity of a cementitious mixture, adhesive, or resin.
Setting Time	(1) time to achieve either initial setting or final setting (2) the length of time required to set or harden resin or adhesive under heat or pressure.
Initial Setting	A degree of stiffening of a cementitious mixture less than final set, generally stated as an empirical value indicating the time required for the cementitious mixture to stiffen sufficiently to resist, to an established degree, the penetration of a weighted test device.
Initial Setting Time	The time required for a freshly mixed cement paste, mortar, or concrete to achieve initial setting.
Final setting	A degree of stiffening of a cementitious mixture greater than initial setting, generally stated as an empirical value indicating the time required for the cementitious mixture to stiffen sufficiently to resist, to an established degree, the penetration of a weighted test device.
Final Setting Time	the time required for a freshly mixed cement paste, mortar, or concrete to achieve final set.

Table 6.2: Comparison of test methods implemented in the research

Test method	ASTM C 191 for Paste	ASTM C 403 for Mortar
Initial setting		
Diameter of probe	1 mm	Variable
Depth and rate of penetration	25 mm in 30 sec	1 $in.$ in 10 sec
Force applied	0.66 lb[a]	Variable
Contact pressure	$\simeq 542$ psi[b]	500 psi
Final setting		
Diameter of probe	1 mm	Variable
Depth and rate of penetration	0 in 30 sec	1 $in.$ in 10 sec
Force applied	0.61 lb	Variable
Contact pressure	$\simeq 542$ psi	4000 psi

[a] It was measured separately.

[b] The pressure is calculated by the applied force (0.61 lb), and the dynamic effect was neglected.

stiffening at which the concrete resists penetration to a prescribed depth of the weighted test device, (a worker's boot with a foot in it) with body weight as the applied force.

According to C403, "Final Setting" is reached when penetration resistance is 27.6 MPa (4000 psi). However, concrete finishers are likely to use the term "final setting" to indicate the point at which the surface of concrete can no longer be

beneficially worked to improve surface texture.

Given that C403 is the only rigorously defined protocol for evaluating setting behavior of mortar and by implication, of concrete, it is useful to review details of its development by Tuthill and Cordon [81]. The C403 test came about as a direct application of the Proctor penetrometer used to evaluate the stiffness of fine-grained soils, without modification of the standard test equipment. Wet-sieving through the $4.75\ mm$ (#4) sieve to obtain mortar was necessary to avoid interference from coarse aggregates since the original geotechnical apparatus was not applicable to granular soils. The developers defined initial set as the degree of stiffness at which "the concrete no longer can again be made plastic by re-vibration." Tuthill wrote that "a running vibrator will not sink of its own weight into concrete that has passed the vibration limit" [81]. The $3.4\ MPa$ ($500\ psi$) initial-set threshold therefore also came to be known as the "Vibration Limit," and this value was in agreement with work by Popovics [110]. (While the term "Vibration Limit" does not appear in recent versions of C403, it is still frequently used in instructional materials and documents with a common interpretation that concrete can be effectively consolidated with a vibrator up until the initial setting time.) Tuthill and Cordon's original (and the current) criterion for final set was established strictly on the basis of the physical limitation of the manually operated device rather than any particularly meaningful characteristic of the mortar being tested. Thus the C403 final setting time is roughly equivalent to the time at which the compressive strength of a given concrete is about $0.7\ MPa$ ($100\ psi$) [81].

In regard to the continuing debate as to whether the results of the C403 mortar penetration test are applicable to concrete setting behavior, Kelly [3] reported

that the setting time determined by Tuthill and Cordon's penetration-resistance method can be used as a convenient reference point for determining relative rates of hardening of concretes on the basis of the relative rates of hardening of their mortar fractions. Other researchers have continued to use C403 results to set a quantitative background against which various concrete behaviors can be compared [94, 95, 111, 112, 113, 114].

On the other hand, Christensen [115], Dodson [116], Malish & Suprenant [95, 111], and Abel and Hover [94] have all cited problems in meaningfully applying the specific initial and final setting times established from C403 mortar data to concrete behavior in the field. In general it has been observed by the time the mortar has reached initial setting, concrete has been placed, consolidated, and finished. After visiting a construction site, Dodson [117] reported that "the concrete finishers had done their job and moved on to another job site some 60 minutes before the [C403 mortar] sample exhibited initial set." This same observation is demonstrated in Figures 6.1 (a), (b), and (c) showing lack of a discernible footprint in the concrete surface (under full body weight) at the time that the maximum penetration resistance in mortar sieved from the same concrete sample was $860\ kPa$ ($125\ psi$), about $45\ min.$ before the mortar specimen had reached C403 "initial set." It must be remembered, however, that Tuthill and Cordon themselves noted that the "... equipment provides an accurate, rapid, and economical method of determining hardening characteristics of concrete mortar which, though not equal to those of corresponding concrete, are of similar character and reliably indicative of what may be expected of the concrete." The developers of the test evidently intended that the similarity of character be established on the basis of some sort of correlation or calibration. Scripture [118] explicitly stated the need for correlation.

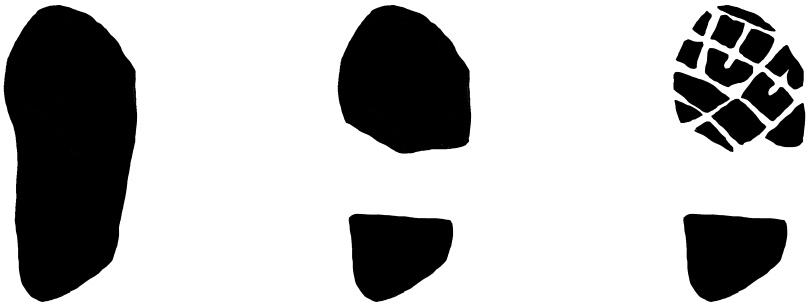

(a) Minimum pressure (b) Medium pressure (c) Maximum pressure

Figure 6.1: Foot print according to possible pressures

In response to the need for a method for evaluating setting behavior of concrete, and without the accompanying need for calibration or the need to sieve mortar (cited as a disadvantage of C403 by Christiansen [115]), Garcia et. al. proposed a concrete setting test in which a standard mass is dropped from a fixed height and the resulting depth of indentation is measured. To the same purpose, and inspired by the ACI 302.1R use of footprint-depth as a meaningful indicator of concrete setting, Malisch and Suprenant [95, 111] have used a weighted boot to create a standard reference in the field. Likewise, Abel and Hover [94] have developed a modified C403 test with a probe in the form of a circular plate with a concrete contact area representative of that of a work boot. The circular plate is embedded to a depth of $6\ mm$ ($1/4\ in.$). As an example of the use of this technique, in observations of finishing operations of outdoor paving slabs, at the time the finisher foreman pronounced that the concrete was ready to receive a hand float finish, the measured penetration resistance with this modified Proctor test averaged about $41.4\ kPa$ ($6\ psi$). When the foreman subsequently pronounced that this same concrete was ready for a "light-broom finish," the average penetration resistance was about $103.4\ kPa$ ($15\ psi$).

6.4 Questions that this study sought to answer; therefore included

- To what degree can setting of concrete in the surface of floors be judged from the results of the C403 test?
- Does the C403 test "initial setting time" for mortar correspond to various concrete finishing operations?
- Can the modified Proctor test of Abel and Hover be used effectively? IS the C403 "Vibration Limit" reliably correlated to a vibration limit in concrete?
- Can the earliest start and the latest finish of concrete floor construction operations be monitored or predicted on the basis of standard or modified tests? Is footprint-depth a reliable indicator of setting behavior?

6.5 Experimental Investigation

The purpose of the experiment was to compare the setting behavior of paste, mortar, and concrete all made from the same set of materials and sequentially batched in the same mixer so as to produce first a paste sample, then a mortar sample, and finally, a concrete sample. ASTM C191 and ASTM C403 penetration tests were used to measure penetration resistance and thus quantify setting behavior for the pastes and mortars, respectively, and the modified Proctor test proposed by Abel and Hover [94] was used to measure penetration resistance of concrete. In addition to penetration resistance testing, non-standard tests were performed to evaluate fresh concrete's response to insertion of a vibrator, indentation of the tread of a worker's boot, and a magnesium-float finish. All results

are graphically compiled and the differences and similarities discussed.

6.5.1 Materials

The sequential paste-mortar-concrete experiment was initiated by designing two different concrete mixtures, C1 and C2, with the same $W/C = 0.45$, paste volume (29%), total air volume (3%) and same total aggregate volume (68%). The fundamental difference as far as the concrete is concerned is that the coarse/fine aggregate volume ratio of mixtures C1 and C2 were 57% and 64%, respectively. The ratio of the volume of air-free paste to fine aggregate in the mortar fraction in C1 (M1) was 1.0. Due to the seemingly modest variation in coarse/fine aggregate distribution, however, the ratio of the volume of air-free paste to fine aggregate in the mortar fraction in C2 (M2) was significantly higher at a value of 1.2. Although the paste component of both concrete mixtures used the same cement and W/C, the two pastes were mixed and tested on different days, and are therefore denoted as P1 and P2. Mixture proportions are summarized in Table 6.3.

Cement was ASTM C150 Type I, manufactured by Saylor division of ESSROC, with Vicat initial and final setting times of 2.4 and 3.0 hours. "Normal Consistency" per ASTM C 187-11 was 25.0%. Both coarse and fine aggregates met the requirements of ASTM C33-13 [90], with specific gravities of 2.57 and 2.65, respectively. Coarse aggregate is categorized as #7 ($1/2\ in.$) by ASTM C33-13, as seen in Figure 6.2; the FM of the fine aggregate was 2.99.

Table 6.3: Mixture proportions of concrete, mortar, and paste for the experiments

Concrete	C1	C2
Cement (kg/m^3 concrete)	380	377
Water (kg/m^3 concrete)	171	170
Fine aggregates (kg/m^3 concrete)	771	638
Coarse aggregates (kg/m^3 concrete)	998	1116
Air (%)	2.9	3.3
Mortar	M1	M2
Paste	P1	P2

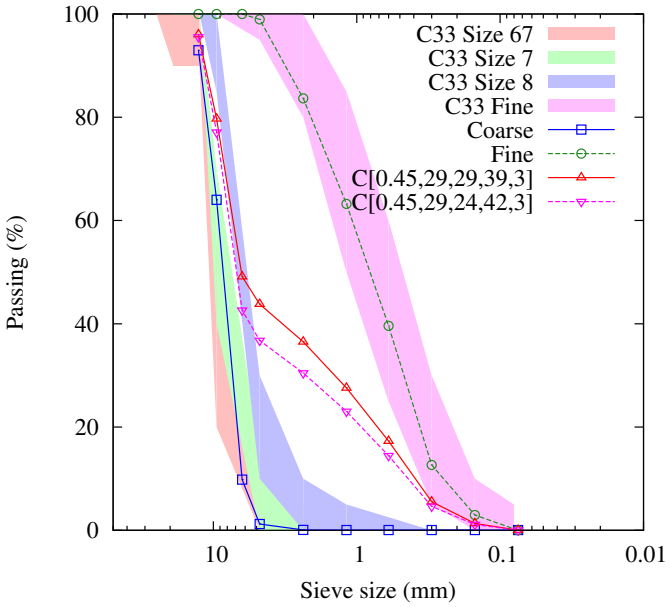

Figure 6.2: Passing grade of fine and coarse aggregates

6.5.2 Continuous Preparation of Specimens

For a given experiment, preparation of specimens began with mixing pastes in accordance with ASTM C305-13 [91]. As soon as a $240\ g$ ($0.53\ lb.$) sample of paste

was extracted for subsequent testing, fine aggregate was added to the remaining paste to create the mortar. After extraction of $67\ kg$ $(147\ lb.)$ of mortar for testing, concrete was produced by adding coarse aggregate. In each case the amount of fine or coarse aggregate added was based on the actual mass of paste or mortar remaining in the mixer. Maximum batch volumes ranged from $0.030\ m^3$ $(1.1\ ft^3)$ for pastes, $0.05\ m^3$ $(1.8\ ft^3)$ for mortars, and $0.030\ m^3$ $(1.1\ ft^3)$ for concrete. To achieve thorough mixing a 4-paddle, $0.17\ m^3$ $(6\ ft^3)$ mason's mixer was used which had been proven effective for up to #7 $(1/2\ in.)$ coarse aggregate. The time-line of preparing specimens is shown in Figure 6.3. Concrete was mixed within approximately 11 minutes after initial contact between cement and water in the preparation of paste.

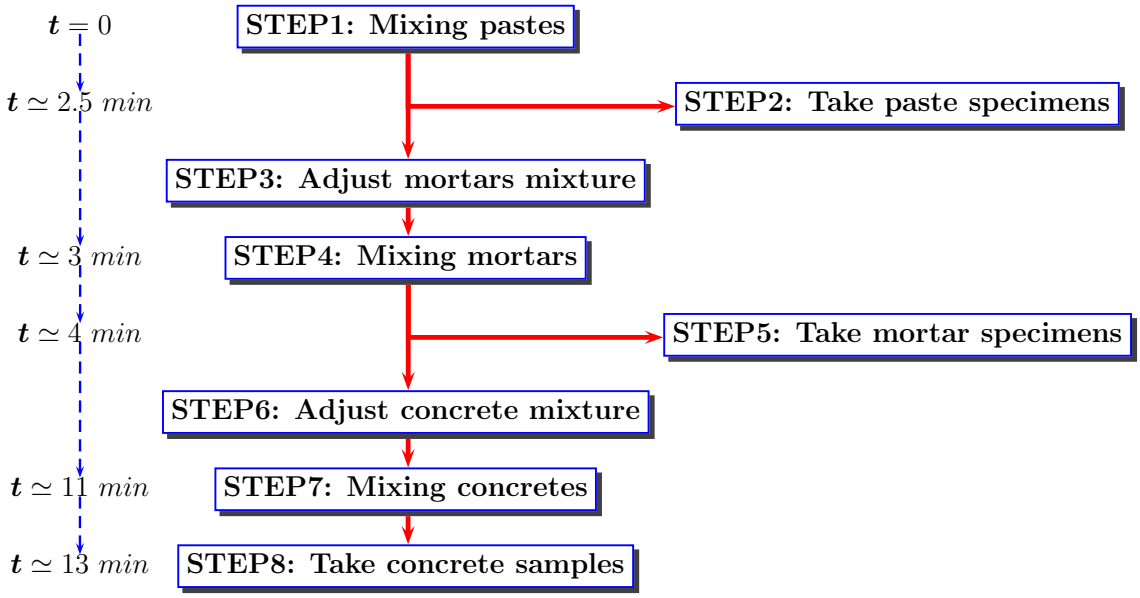

Figure 6.3: Preparation of Pastes, Mortars, and Concretes

6.5.3 Penetration Test

Paste as-mixed with a $W/C = 0.45$ was evaluated by the Vicat needle test (ASTM C191-08) to characterize the paste as actually incorporated in the mortar and concrete [4, 119]. Setting behavior of mortar was evaluated with ASTM C403-08 [80] using the prepared mortar as sampled rather than sieved mortar. Penetration resistance of concrete was experimentally obtained by the method proposed by Abel and Hover [94], in which the C403 Proctor test is modified with a larger probe so that contact pressure on the concrete surface simulates that generated by a worker standing on recently placed concrete. Two "loading plates" are used in the conduct of this test. The larger is $117\ mm$ ($4.6\ in.$) in diameter and permits recording of pressures up to about $41.4\ kPa$ ($6\ psi$). The smaller plate is $70\ mm$ ($2.75\ in.$) in diameter and permits recording of pressures up to about $116\ kPa$ ($17\ psi$). Either plate is pressed into the concrete (over 5 seconds) to a penetration depth of $6\ mm$ ($1/4\ in.$), creating a circular indentation [figure needed]. The resulting indentation from the larger plate has an area of $107.5\ cm^2$ ($16.7\ in^2$), or about the size of the footprint from a large work boot. This is similar in concept to the "weighted boot" of Suprenant and Malisch [113].

Prior to use of the device described above, concrete samples were collected in a plastic mortar bin ($380\ mm \times 470\ mm \times 140\ mm$ ($15\ in. \times 18.5\ in. \times 5.5\ in.$)) rodded 60 times with a typical slump-test-rod, and struck off with a wooden screed with a sawing motion. The penetration test was then conducted on the exposed top surface of the concrete. As a trial for mixture C2 only, it was observed that when the filled mortar-bin was placed on a ($38\ cm \times 40\ cm$ ($15\ in. \times 15 - 3/4\ in.$)) vibrating table operating at $60\ Hz$ for 30 seconds, the concrete slowly self-leveled. This was explored as an effective manner to achieve more uniform compaction

throughout the sample, but the unintended consequence was a densification of the concrete such that when the Proctor device and loading plate were applied, the concrete deformed in a "settlement" mode, as shown in Figure 6.4 (b), rather than the punching- or shearing-mode that replicates a footprint on an ordinary concrete slab, as presented in Figure 6.4 (a). However, this provided additional data on the deformability of freshly cast and consolidated concrete as a function of time, in which the measured force imposed a settlement of $6\ mm$ $(1/4in.)$ from the original concrete surface. Such mode of deformation is more similar to the displacement of concrete against forms that are not stiff or tight enough, as will be discussed later. Table 6.2 summarizes all penetration tests and the associated standard criteria implemented in the research.

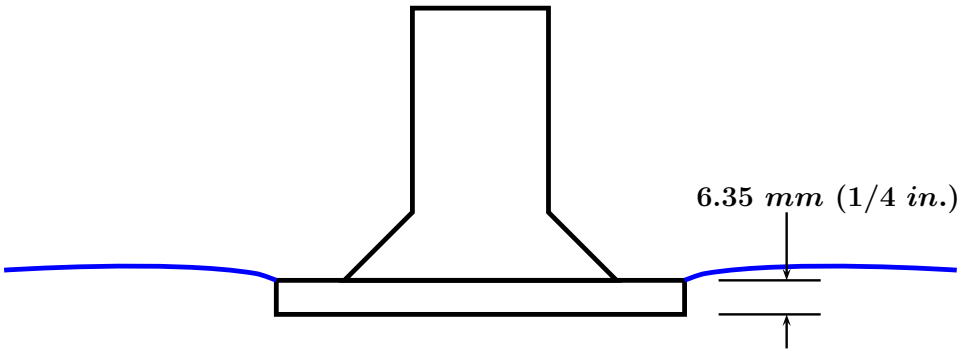

(a) Edge shear

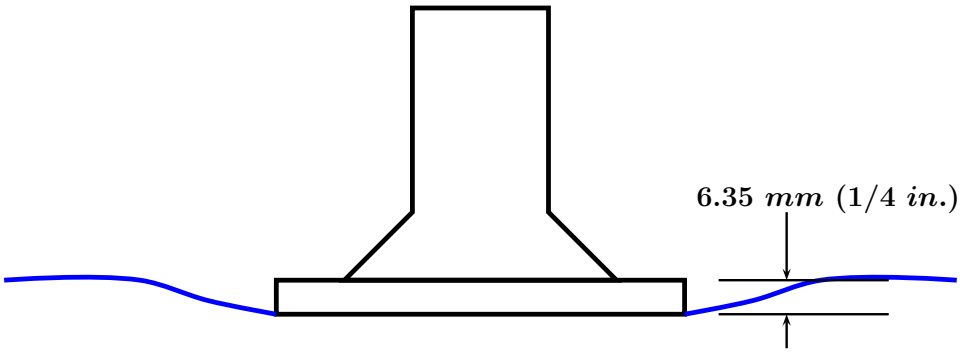

(b) Settlement

Figure 6.4: Schematic comparison of edge shear failure and settlement

6.5.4 Other tests of the deformability of freshly-cast concrete

Simultaneous with conduct of the penetration tests, a number of non-standard procedures were conducted to evaluate the deformability of the concrete. The first of these was determination of the duration of time since batching over which the concrete could still be effectively consolidated with an immersion vibrator. After casting and screeding concrete in the mortar bin (without use of the vibrating table), each time penetration readings were taken (about 20 min. intervals) an immersion vibrator was inserted into the concrete in accordance with ACI 309. The vibrator had a head-diameter of $27\ mm$ ($1.06\ in.$) operating at $1900\ W$ ($2.5\ HP$) with a frequency of $11,000\ VPM$ in air. It was lowered $90\ mm$ into the concrete over a 5 seconds period and immediately withdrawn over another 5 seconds. The concrete was closely observed to determine whether the void created by the vibrator head was closed by the vibration as the tool was withdrawn. For the conditions of this study, if the concrete flowed under vibration such that the void was filled completely the concrete was judged to be sufficiently plastic to be effectively consolidated by the immersion vibrator. This status was termed "Compact-ability" Level 1. As the concrete continued to stiffen, "Level 2" was reached when the void was filled to only about 1/2 of the diameter of the vibrator head. (This would be an unacceptable outcome in the field, and would be beyond what it normally considered to be the "Vibration Limit," but was nevertheless useful in quantifying observed behavior.) Finally, "Level 2" was terminated when the residual void was about the same diameter as the vibrator head indicating virtually no flow of the concrete in response to vibration.

The second measure of deformability was a semi-quantitative (but industri-

ally common) analysis of footprints on the freshly-cast concrete surface. Beginning at the time that the modified Proctor pressure reached $103\ kPa$ ($15\ psi$), the test operator stood on the concrete for 5 seconds. The concrete surface was then inspected to evaluate distinctive details and approximate depth of the resulting footprint. Deformability levels 1 and 2 are defined as having an average depth of more than, or less than 6 mm (1/4 inch), respectively, and level 3 is defined as no visible indentation (although some bleed water was usually expressed by the applied pressure, which left a discernible pattern.) In prior testing [94], it was determined that footprints were consistently deeper than $6\ mm$ ($1/4\ in.$), or Level 1 as defined here, whenever the modified Proctor reading was less than 34 to $41\ kPa$ ($5-6\ psi$). In the experiments reported here, footprint depth was always 1/2 of this depth or less when the modified Proctor reading was greater than 34 to $41\ kPa$ ($5-6psi$). Note that the measured contact pressure under the operator's boot was 34 to $48\ kPa$ (5 to $7\ psi$).

As a final evaluation of deformability, the operator used a $400\ mm$ ($16\ in.$) cast magnesium hand float to attempt to "erase" the footprints and voids left by the vibrator. "Finishability" Level 1 indicates that all surface defects could be erased and the initial surface restored, while Level 2 indicates that while the shallow footprint could be erased, the deeper void or impression left by the vibrator could not be closed. Level 3 indicates that the footprint could not be erased, such that the footprint became a permanent feature of the hardened concrete. For each of these measures of deformability the times associated with each level were recorded. Figure 6.5 is a photo-array of the deformability tests described.

(a) Vibration hole Level I (b) Vibration hole Level II (c) Vibration hole Level III

(d) Foot print Level I (e) Foot print Level II (f) Foot print Level III

(g) Finishing Level I (h) Finishing Level II (i) Finishing Level III

Figure 6.5: Qualitative Levels of Non-Penetration Tests

6.5.5 Calculation of Setting Times

According to ASTM C191, time of initial setting of paste is determined via linear interpolation of the 30-second depth of penetration, at a depth of $25\ mm$ ($1in.$). With greater expediency and no loss of accuracy, the initial setting time is estimated here by fitting the data with Eq. (6.1). In accordance with C191, final set is defined as the elapsed time from initial contact of cement and water to when

"the needle does not sink visibly into the paste."

$$PD(t) = \eta_0 \left[1 - \exp\left[-\left(\frac{\eta_1}{t}\right)^{\eta_2}\right]\right] \tag{6.1}$$

For mortars, initial- and final set-time intercepts (and other key thresholds to be discussed) were determined by curve-fitting with both the power function (proposed by Popovics [93] and adopted by ASTM C403-08 (Eq. (6.2)), and the exponential function (Eq. (6.3). The exponential function has been also effectively used by other researchers [4, 120] and its effectiveness is discussed in reference [2].

$$P(t) = \gamma_0 t^{\gamma_1} \tag{6.2}$$

$$P(t) = \alpha_0 \exp(\alpha_1 t) \tag{6.3}$$

6.6 Experimental Results

6.6.1 Penetration Test Results

Of the multiple tests performed here, only the C191 Vicat and the C403 penetration resistance tests have unambiguously defined criteria for initial and final setting times for paste and mortar. These results are shown in Table 5 and graphed in Figures 6.6 (a) and 6.7 (a). It is observed that initial setting time for M1 occurred about 0.7 hour prior to Vicat initial set of the paste, while the initial setting of M2, which had a higher paste content, occurred at only 0.1 hour prior to Vicat initial set of the paste. Similarly, Mortars M1 and M2 reached C403 final setting time 1.4 and 0.9 hour, respectively, prior to Vicat final setting time. The results of the modified C403 test are superimposed on the paste and mortar data

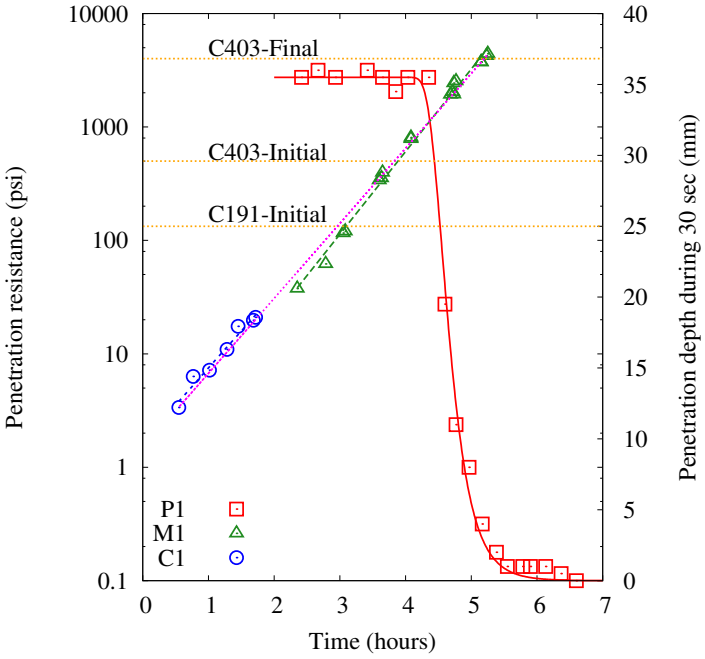

(a) Penetration Tests

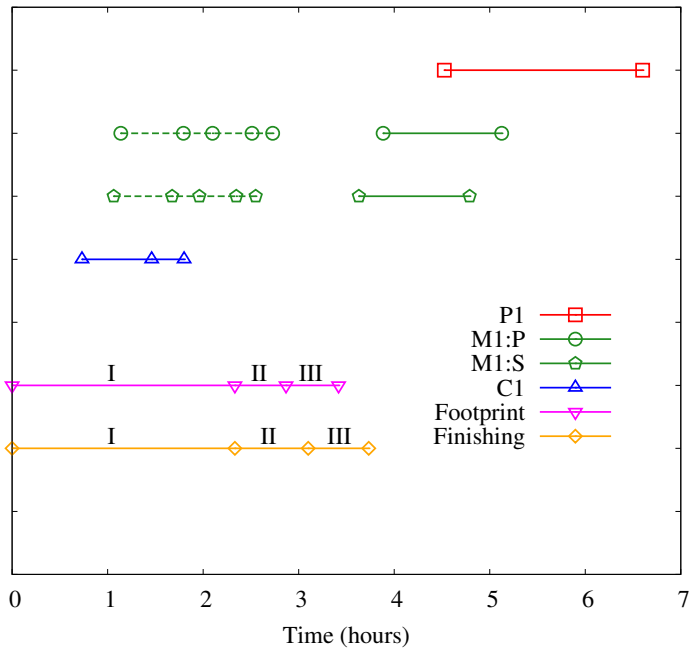

(b) Summary of Events

Figure 6.6: Penetration Tests of C1, M1, and P1 (left panel) and chronological summary of events (right panel)

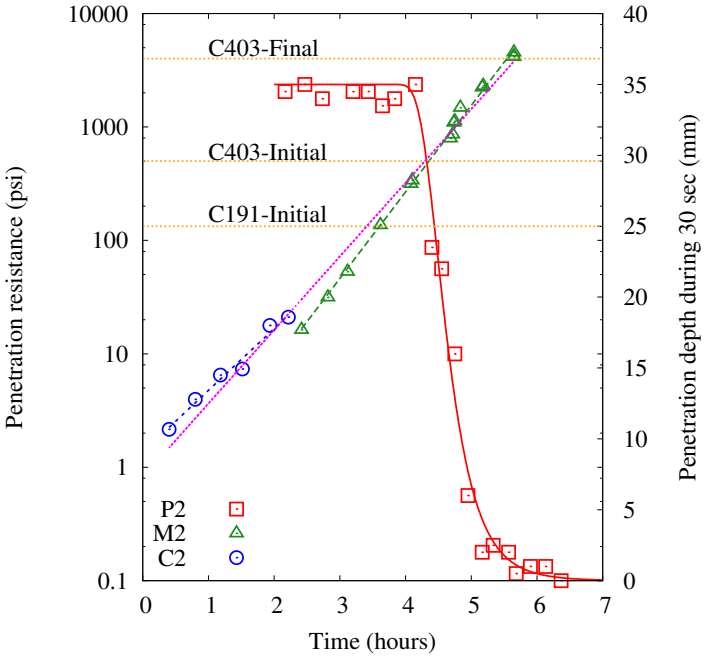

(a) Penetration Tests

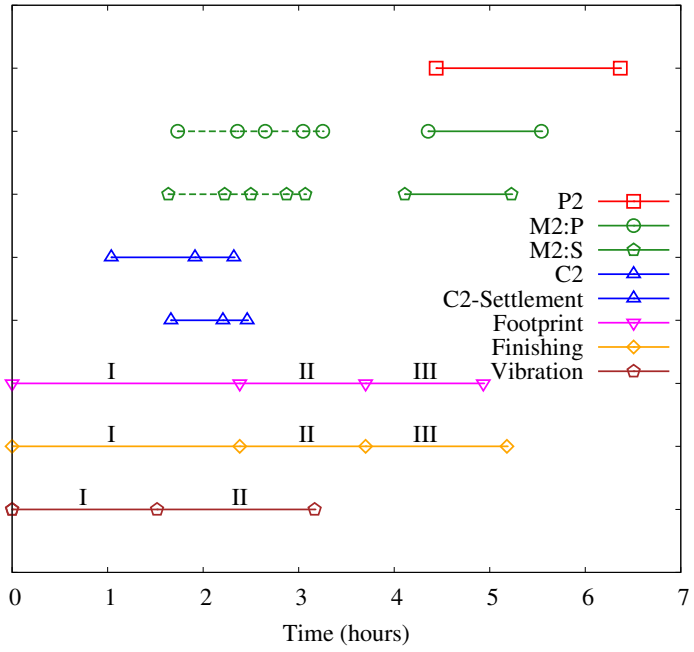

(b) Summary of Events

Figure 6.7: Penetration Tests of C2, M2, and P2 (left panel) and chronological summary of events (right panel)

Table 6.4: Setting Times of Pastes and Mortars

	Criteria	Initial setting (hours)	Criteria	Final setting (hours)
P1	C191-Eq.(6.1)	4.53	C191-Zero penetration	6.60
P2	C191-Eq.(6.1)	4.44	C191-Zero penetration	6.37
M1	C403-Exponential-$500\ psi$	3.88	C403-Exponential-$4000\ psi$	5.13
M1	C403-Power-$500\ psi$	3.77	C403-Power-$4000\ psi$	5.23
M2	C403-Exponential-$500\ psi$	4.36	C403-Exponential-$4000\ psi$	5.54
M2	C403-Power-$500\ psi$	4.22	C403-Power-$4000\ psi$	5.71

in Figures 6.6 (a) and 6.7 (a). Figure 6.6 (a) shows that for C1 (Paste Vol./Sand Vol. = 1.0) the trajectory of the concrete penetration resistance with time aligns well with C403 mortar data. (R^2 for the combined data set = 0.99 for an exponential fit.) This trend is as reported by Abel and Hover [94]. The alignment is visually less striking in Figure 6.7 (a) for C2 (Paste Vol./Sand Vol. = 1.2), but statistically speaking the R^2 remains at 0.99 for an exponential fit of the combined data. This is discussed further in the analysis section. Tables 6.4 and 6.5 include all computed times for arrival at key thresholds of penetration resistance, showing values obtained for both the power and exponential functions. Figures 6.6 and 6.7 only show the best-fit curves.

Table 6.5: Time (hours) at given stress levels of penetration resistance (The values in the parenthesis denote R^2.)

Stress level	34.5 kPa (5 psi)		103.4 kPa (10 psi)		172.4 kPa (25 psi)	
Function	EXP	Power	EXP	Power	EXP	Power
C1	0.73	0.72	1.46	1.43	1.80	1.98
	(0.96)	0.96)	(0.96)	(0.96)	(0.96)	(0.96)
C2	1.03	0.87	1.91	2.00	2.32	2.96
	(0.98)	(0.93)	(0.98)	(0.93)	(0.98)	(0.93)
C2-Settlement	1.66	1.58	2.20	2.37	2.46	2.87
	(0.98)	(0.93)	(0.98)	(0.93)	(0.98)	(0.93)
M1-Prepared	1.14	1.83	1.79	2.17	2.10	2.35
	(0.99)	(0.99)	(0.99)	(0.99)	(0.99)	(0.99)
M2-Prepared	1.73	2.16	2.36	2.54	2.65	2.73
	(0.99)	(0.99)	(0.99)	(0.99)	(0.99)	(0.99)
M1-Sieved	1.06	1.71	1.68	2.03	1.96	2.20
	(0.99)	(0.99)	(0.99)	(0.99)	(0.99)	(0.99)
M2-Sieved	1.64	2.04	2.23	2.39	2.50	2.58
	(0.99)	(0.99)	(0.99)	(0.99)	(0.99)	(0.99)

6.6.2 Non-Penetration Test Results

Figures 6.6 (b) and 6.7 (b) summarize the times at which levels 1, 2 and 3 were reached for the various non-standard indicators of stiffening of the concretes, against the background of standardized setting results. At the top of the chart

is the time interval between Vicat initial and final setting of the paste. This is followed by the C403 initial and final setting times of prepared mortar, with dashed lines to the left indicating other proposed thresholds of mortar penetration resistance to be discussed, ranging from 206.8 to 482.6 kPa (30 to 70 psi). Values for sieved mortar (per C403) are also shown as corrected from the measured values, recognizing that as independently verified for these mixtures and materials, sieved mortar has initial and final setting times that are about 93% of the measured values for prepared mortar [2]. Next are the times at which concrete penetration resistance reached (34.5, 103.4, and 172.4 kPa (5, 15, and 25 psi) as measured by the modified C403 test. Immediately under this, for mixture C2 only, are similar data for the times at which a 6 mm ($1/4in.$) settlement of the concrete (without the shearing deformation associated with penetration tests or the formation of a footprint) required a contact pressure of 34.5, 103.4, and 172.4 kPa (5, 15, and 25 psi). The next diagrams on the chart show the time over which the operator (with a boot/concrete contact pressure of 34.5 to 48.3 kPa ($5-7$ psi)) was able to leave a level 1, 2, or 3 footprint in the concrete surface, and the capability to erase surface defects in the concrete with the magnesium float. Finally, for C2 only, the lowest line on Figure 6.7 (b) shows the time periods over which the concrete could be consolidated with the vibrator, at effectiveness levels 1, 2, and 3.

6.7 Analysis

6.7.1 Effects of Mixture Proportions on Penetration Test

Examination of Figures 6.6 (a) and 6.7 (a) suggests that while mortars M1 and M2 appear to have distinctly different setting characteristics, concretes C1 and C2 behave very similarly to each other. To examine this set of relationships more closely, a multi-linear regression model was developed to determine whether the populations represented by C1 and C2 were significantly different from each other, and to examine a similar distinction between M1 and M2. Key characteristics in these analyses were the slopes and intercepts of the regression lines shown in Figures 6.6 (a) and 6.7 (a). The model is shown as Eq. (6.4).

$$\ln\left(PR(t)\right) = \beta_0 + \beta_1 t + \beta_2\left(\text{MixID}\right) + \beta_3\left(\text{MixID}\right) \times t \tag{6.4}$$

Where:
PR is the penetration resistance with time t, MixID identifies the populations (C1, C2, M1, M2), and β_0, β_1, β_2, and β_3 are regression coefficients (See Table 6.6). The model postulates that the intercept and the slope of the log-transformed lines of penetration resistance are unique for a given MixID.

Table 6.6 summarizes the outcome of these analyses, showing estimated coefficients and the associated probabilities indicating statistical significance for mortars, concretes, and combined mortar and concrete. The essential conclusion is that at the 95% confidence level, M1 and M2 can be interpreted as distinctly different populations on the basis of measured penetration resistance alone, but the same cannot be said of concrete mixtures C1 vs. C2 with the same level of confidence. When the data sets are combined, (M1&C1) and (M2&C2) are seen

Table 6.6: Statistical Analysis Results with Eq.(6.4)

Coeff.	Mortar		Concrete		Combined	
	Estimate	$\Pr(>\|t\|)$	Estimate	$\Pr(>\|t\|)$	Estimate	$\Pr(>\|t\|)$
β_0[a]	5.38	2.06×10^{-5}	1.53	0.223	0.38	0.002
β_1[b]	1.28	1.18×10^{-5}	2.75	0.012	1.52	2.0×10^{-6}
β_2[c]	-5.68	2.07×10^{-5}	-1.02	0.354	-0.58	0.001
β_3[d]	0.40	0.0825	-1.25	0.139	-0.03	0.519
R^2	0.9951		0.9756		0.9908	

[a] Log-transform of penetration resistance at $t = 0$ (Y-intercept).

[b] Slope of regression curve independent of mixture.

[c] Change in Y-intercept due to mixture

[d] Change in slope due to mixture

to have independent intercepts but one cannot judge the slopes to be distinctly different. This means that the rate constant for development of penetration resistance is similar for the two mortar-concrete families, which is not surprising given that both used the same paste. However, when this statistical model was used to evaluate the probability that the penetration resistance data of C1 are from the same population as M1 (early, low-pressure and later, higher-pressure results for the same hypothetical mixture), the model suggests that M1 and C1 may have the same slope (rate constant for stiffening) but different initial penetration resistance values (Y-intercept.) For C2 and M2, both the slopes and intercepts were determined to be unique. Combining C2 and M2 into a single population is therefore not strictly justified at the 95% confidence level.

6.7.2 Penetration Resistance of Sieved and Prepared Mortars

For setting behavior of mortars, this study implemented prepared mortars since it focused on continuation of materials in setting behaviors across pastes, mortars, and concretes. However, ASTM C403 [80] requires to use sieved mortars that extracted from a given concrete. Therefore, the difference of setting behaviors for prepared and sieved mortars are separately investigated by authors [2, 112]. It was observed that for mortar M1, initial and final setting times were both delayed for prepared mortar compared to sieved mortar by 7%. For Mortar M2, initial setting of prepared mortar was delayed 8%, and final setting was delayed 5%, as shown in Figure 6.8. If one were content to measure or predict setting times to an accuracy of $\pm 1\%$, one could generalize that using prepared mortar in lieu of sieved mortar for the C403 test on these mixtures delayed initial and final setting by about 7% of the measured times. In the context of this paper, the work was performed on prepared mortars, so the initial and final setting times for M1 sieved would have been accelerated by 16 and 23 minutes, respectively. Likewise, both initial and final set for M2 sieved would have been accelerated by about 16 minutes. Figures 6.6 (b) and 6.7 (b) therefore include ranges of mortar setting data for both sieved and prepared mortar.

6.7.3 Analysis of Paste Volume and Computed Average Paste Layer Thickness

The authors previously proposed a simplified model that correlated setting behavior of mortars to the average paste volume fraction [112]. On average, a 1% increase in paste volume fraction delayed both initial and final setting time in

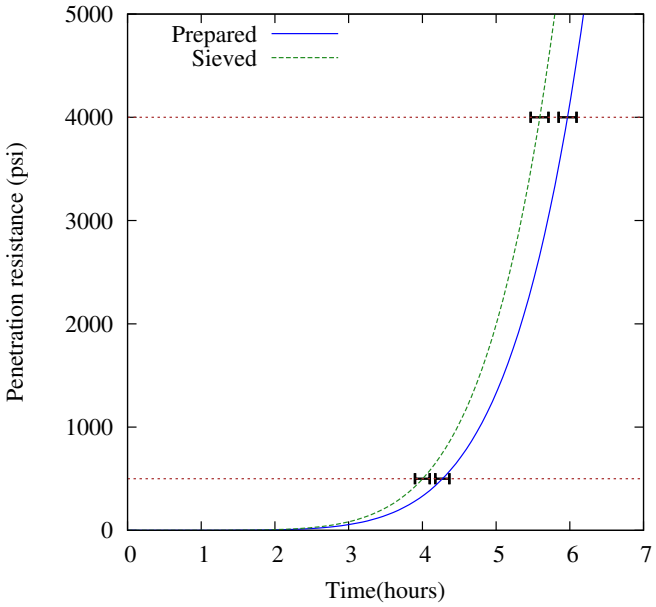

(a) M1

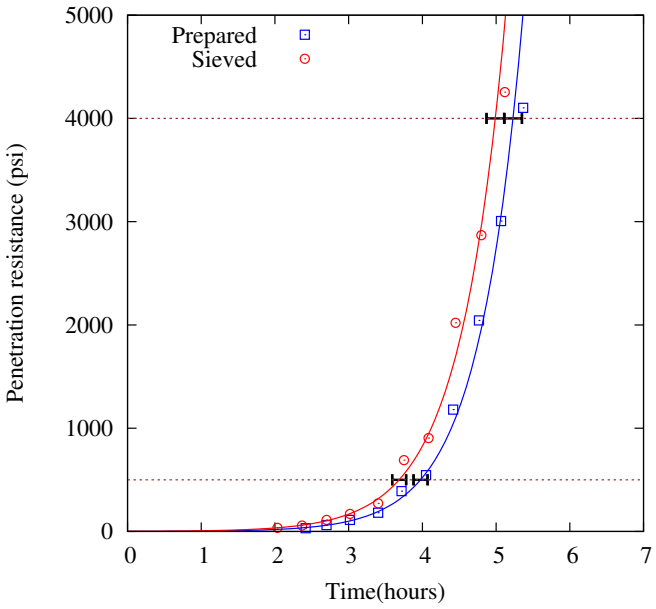

(b) M2

Figure 6.8: Comparison of Penetration Resistance for Sieved and Prepared Mortars

mortar by about 1%. That rule can be tested here by comparing the setting behavior of M1 and M2, for which the increase in coarse aggregate and decrease

in fine aggregate in C2 produced mortar M2 with 54% paste volume compared to M1 at 50% paste volume. Thus the 8% increase in paste volume would predict an 8% increase in setting time. In the same paper, the authors proposed a somewhat more complicated model that correlated setting behavior of mortars to the average thickness of the paste layer surrounding each sand particle, computed by dividing paste volume by the estimated total aggregate surface area. They found that on average, a 1% increase in paste layer increase would delay both initial and final setting time in mortar by about 0.4%. That rule can also be tested here by comparing the setting behavior of M1 and M2, for which mortar M2 had a 20% thicker average paste layer thickness compared to M1. Table 8 summarizes the computed paste thickness layers on the basis of assumption that all aggregates are spherical, and diameters are the average of sieve opening sizes above and of the sieve upon which the aggregates are retained. The computed values also reflect the much greater impact of fine aggregate on surface area compared to the effect of coarse aggregate. For M2 compared with M1, both the paste volume fraction model and the paste layer thickness model predicted an 8%increase in initial and final setting times. The measured increase was 6% for initial setting and 12% for final setting, or an average of 9%. In an attempt to apply these models to setting of concrete, consider that the highest value of penetration resistance that can be reliably measured with the modified proctor apparatus on concrete is about $172\ kPa$ ($25\ psi$). Concrete mixture C2 reached that value at 2.3 hours, which was 29% longer than required to reach the same resistance with C1. Consider also that the proposed models were developed for mortar only, and as such were not intended to apply to predictions of C2 vs C1. Nevertheless, given that C1 and C2 have identical paste volume, no change would have been predicted for the simple model. In regard to paste-

layer thickness, the model would have predicted only a 6% increase in setting time instead of the nearly 30% increase observed. Both mortar-models greatly underestimated the impact of paste characteristics on concrete behavior. At least part of the discrepancy in the models may be in the far shorter concrete setting times compared with mortar setting times.

Table 6.7: Paste layer thickness, paste volume fractions, and aggregate surface areas

	C1	M1	C2	M2
Paste layer Thickness (μm)	87.1	96.8	100.9	116.1
Paste volume fraction per m^3 concrete or mortar	29%	48%	29%	52%
Aggregate surface area m^2 per m^3 concrete or mortar	3395	4914	2937	4470

6.8 Discussion

Looking at Figures 6.6 (b) and 6.7 (b), and starting at the top of each, note that the latest event in both experiments is the Vicat final setting of the paste, occurring at least an hour after the C403 final setting of mortar, and 3 hours (C1) to 1.5 hours (C2) after the latest ability to modify the surface texture of the concrete with foot pressure, vibrator, or finishing tool. Vicat initial setting time of paste falls between the C403 initial and final setting time of mortar. The Vicat data in Figures 6.6 (a) and 6.7 (a) shows that there is no measurable develop-

ment of paste stiffening prior to C403 initial setting of mortar. It is interesting to note that P1 and P2 showed virtually identical Vicat performance, yet the mortars and concretes made from those pastes had varying setting characteristics. These variations are therefore influenced by the mixture proportions and not by changing cement behavior. In this regard, there was no measurable development of paste stiffness until after the time at which the concrete surface could not be indented or restored for C1. On the other hand, by the time that C2 reached this same point, P2 was almost halfway between initial and final setting.

In regard to mortar behavior, observe first the slight shift to the left of the sieved mortar compared to the prepared mortar as discussed earlier. The solid mortar lines represent C403 initial and final set, while the dashed mortar lines show the computed times for the key penetration values introduced earlier. For M1, C403 initial set did not occur until at or beyond the time at which the surface of C1 could no longer be indented or faint footprints removed. C403 final set for M1 occurred about an hour later.

Mortar M2 reached C403 initial set at about the same time that a faint footprint could be made and then erased. Deeper defects such as the vibrator void could not be removed as of C403 initial set. From a contractor's perspective, C403 initial set for M2 occurred about an hour before a concrete finisher would say that C2 had reached final setting. C403 final setting time for M2 is not a bad estimate for a field-based C2 concrete final setting time.

As for the utility of the C403 initial set as a vibration limit, C2 ceased to flow in response to vibration, and hence could not fill the void left by the vibrator head at about 1.5 hours prior to C403 initial setting time for M2. The end of

vibrator effectiveness Level 1 occurred at a computed mortar penetration resistance of less than $5\ psi$, or about the time that the modified Proctor apparatus returned a penetration resistance of about 10 psi. On the basis of these tests the C403 initial setting time is not a useful estimator of the duration of time over which concrete can be effectively consolidated with a vibrator, overestimating the vibration limit by about 1.5 hours.

In a related matter, Dodson [116] discussed the BS (British Standard) 5075-Part I [121] which uses a penetration resistance of $500\ kPa$ ($72\ psi$) for sieved mortar to define the limit for concrete placing and compaction. This value is shown in Figures 6.6 (b) and 6.7 (b) as the rightmost symbol in the dashed lines of computed mortar values. It can be seen that the BS criterion of $500\ kPa$ occurs about 1 hour prior to C403 initial setting time for both M1 and M2, at a time when the depth of footprint is less than $6\ mm$ ($1/4\ in.$) depth. This criterion also aligns with the endpoint of Level 2 vibration, in which the vibrator is able to only partially close the void (the concrete does not flow under vibration at this time). As an endpoint for concrete placing and consolidating, the BS criterion is perhaps more realistic than the C403 initial setting, but it still overestimates the length of time over which the concrete can be effectively vibrated. By preceding the C403 initial set by about an hour it at least moves in the right direction, given Dodson's earlier observation that the finishers were done and gone an hour before C403 initial set had come. Interestingly, BS-5075 also borrows the C403 criterion of 3.5 MPa (500 psi) as a "guide to time available for avoidance of a cold joint." The work reported here does not support the utility of that criterion, since prevention of cold joints is difficult if consolidation by vibration is no longer effective.

Given the traditional connection between setting and foot prints (obvious and handy field indicators, always available) the figures indicate that a footprint depth of about $6\ mm$ ($1/4\ in.$) could be impressed in C1 up until about 2 hours after mixing and up until about 2.5 hours for C2. The $6\ mm$ "impression-point" thus preceded C403 initial setting by about an hour for C1 and by about 2 hours for C2. The $6\ mm$ "impression-point" was reached at a computed penetration resistance of more than $25\ psi$ for M1 and about $15\ psi$ for M2. This agrees with Malisch and Suprenant [95] who reported that "when the finisher first left a 1/4-inch deep footprint in each of the three slabs, the corresponding [C403 mortar] penetration resistance was 15 to $25\ psi$." Using measured rather than computed values for concrete surface penetration resistance, the $6\ mm$ "impression-point" occurred about 1/2 hours after the modified Proctor apparatus reached its maximum value of $25\ psi$. For C2 the $6\ mm$ impression-point the concrete penetration resistance was about $25\ psi$. All of these values generally agree with Bury et al. [114] who observed that what is termed here the "$6\ mm$ impression point" occurred at a C403 mortar penetration resistance of "less than $50\ psi$." Thus the state of concrete stiffness that would often be termed "initial set" in the field often occurs at a mortar penetration resistance of less than 10% of the C403 criterion for initial setting. Given the exponential nature of setting behavior, this corresponds to a time-from-batching that is about 2/3 of the C403 time of initial set.

The figures also show that the finisher has the ability to remove surface defects such as footprints using repeated strokes of the magnesium float for a period of 15 min or less after the latest time that such an impression can be made in the concrete. On the other hand, any time at which a footprint can be impressed in the concrete it can be removed or restored with the float if applied

soon enough and aggressively enough.

Low-pressure penetration resistances for mortar and concrete are in the approximate range from $34.5\ kPa$ to $345\ kPa$ (5 to about $50\ psi$). Mortar values have been extrapolated downwards from the measured C403 data while concrete values are as measured by the modified Proctor apparatus. Note first that these data sets do not align exactly due to the sieved vs. prepared mortar difference described earlier, and due to the slight misalignment of the concrete and mortar curves in Figures 6.6 (a) and 6.7 (a) as discussed in the analysis section above. The concrete values are shifted earlier than the corresponding mortar values by about 1/2 hours, and for both experiments $25\ psi$ in concrete occurred at about the same time as $15\ psi$ in mortar. This difference is large enough to make it necessary that in any discussions of penetration resistance and associated setting behavior it is essential that it be clear whether the pressures debated were obtained from C403 mortar or from the concrete surface (foot pressure, for example.)

Finally, Figure 6.7 (b) shows a dataset labeled "C2-Settlement," indicating the times at which a contact pressure of 5, 15, and $25\ psi$ would deform the concrete surface by about $6\ mm$ ($1/4in.$) but without the punching or shearing mode exhibited by footprints or other defects. Compared with the modified Proctor values on the line immediately above, these times are all shifted to the right by about 20 minutes, indicating that concrete can be deformed without shearing at a given pressure over a slightly extended period of time. One application of this observation is the challenge of adjusting formwork during or after concrete is cast. Re-tightening of bolts or wedges can move form panels, braces, studs, walers, and in the process deform or re-shape the concrete within.

The good news is that the data shown here suggest that at least $6\ mm$ $(1/4in.)$ of re-shaping can happen without shearing or cracking the concrete, for at least up to 2.5 hours after mixing. The bad news is that the pressure required to do this, ignoring any pressure head, varies from 5 psi = 720 lb/ft2 at 1.5 hours after batching to $3600\ lb/ft^2$ at 2.5 hours. ACI 347 (formwork) states that "Even though adjustment of forms can be possible during or after placing, it is not recommended. Any required adjustment should be made before initial set of the concrete." If this reference were intended to pertain to ASTM C403 initial set, and for the data of Figure 6.6 (a), the concrete pressure at C403 initial set of the mortar would be about $200\ psi = 29,000\ lb/ft^2$. Even if it were possible that the concrete remained plastic and deformable to that limit (about 4 hours after batching), it would be difficult in the extreme to bring enough force to bear to move the formwork and the concrete by $6\ mm$ $(1/4\ in.)$

6.9 Conclusion

- The work as summarized in Figures 6.6 (b) and 6.7 (b) establishes a framework for presenting and organizing setting-related data, and permits correlation between of various characteristics and properties obtained in the laboratory, field, or both. Any indicator, rigorous or approximate can be accounted for in this format.
- Standard industry documents make reference to concrete setting in at least three contexts: a) strictly quantitative in accordance with ASTM C403, or some other prescribed standard or non-standard method; b) semi-quantitative as evidenced by typical references to depth of footprints; and qualitative with a broad, general reference to the stiffening of concrete

over time.

- Which of the three contexts described above pertains in any given document is not always clear.
- ACI's formal definition of setting-related terms requires interpreting the phrases "empirical value", "resist...penetration," and "to an established degree." However, defining setting behavior on the basis of depth of a worker's footprint is in accordance with ACI?s definition.
- C403 is the only rigorously defined protocol in the US for evaluating setting behavior of mortar and by implication, of concrete. Other standards, such as BS-5075 are used internationally.
- Even Tuthill and Cordon, developers of the C403 method, noted that the equipment determines hardening characteristics of mortar that are not equal to those of corresponding concrete. Calibration or correlation between C403 results and observed concrete behavior is required for most effective use.
- Several methods have been developed for monitoring setting behavior of concrete. The modified Proctor method of Abel and Hover was evaluated here and found to provide useful information.
- Consolidating concrete in the mortar bin on a vibrating table uniformly densified the concrete and apparently increased shear strength at the surface (C2).
- The traditional method of evaluating surface stiffness by means of foot print depth appears to be quite robust. Different researchers, operating independently over a space of 15 years converged with approximately the same mortar penetration resistance at the time a workers? boot was embedded to a depth of $6\ mm$ ($1/4\ in$).

- While setting data can be fitted with either power or exponential function, the exponential generally gives a better fit and is a more realistic and generally applicable growth model.
- Concrete and mortar penetration curves are similar in form, slope, and intercept, but cannot typically be pooled for detailed statistical analysis. Informally, however, it is clear that the two are related models of the same fundamental behavior.
- The essential conclusion of the analysis of mixture proportions is that at the 95% confidence level, M1 and M2 can be interpreted as distinctly different populations on the basis of measured penetration resistance alone, but the same cannot be said of concrete mixtures C1 vs. C2 with the same level of confidence. When the data sets are combined, (M1&C1) and (M2&C2) are seen to have independent intercepts but one cannot judge the slopes to be distinctly different. Similar slopes suggest that the same rate constants influence setting for both mortar and concrete.
- As shown previously, prepared mortars have delayed setting behavior compared to sieved mortars as required by C403. This difference is shown in Figures 6.6 (b) and 6.7 (b).
- Models previously established by the authors for the influence of paste content and aggregate surface area were effective in predicting the difference in setting behavior between M1 and M2.
- The many observations of the discussion section are not repeated here. Essential conclusions are as follow:
- P1 and P2 showed virtually identical Vicat performance, yet the mortars and concretes made from those pastes had varying setting characteristics.

These variations are therefore influenced by the mixture proportions and not by changing cement behavior.

- The Vicat data in Figures 6.6 (a) and 6.7 (a) show that there is no measurable development of paste stiffening prior to C403 initial setting of mortar.
- For M1, C403 initial set did not occur until at or beyond the time at which the surface of C1 could no longer be indented or faint footprints removed. C403 final set for M1 occurred about an hour later.
- From a contractor's perspective, C403 initial set for M2 occurred about an hour before a concrete finisher would say that C2 had reached final setting. C403 final setting time for M2 is not a bad estimate for a field-based C2 concrete final setting time.
- On the basis of these tests the C403 initial setting time is not a useful estimator of the duration of time over which concrete can be effectively consolidated with a vibrator.
- As an endpoint for concrete placing and consolidating, the BS criterion is perhaps more realistic than the C403 initial setting, but it still overestimates the length of time over which the concrete can be effectively vibrated.
- The work reported here does not support the utility of that criterion, since prevention of cold joints is difficult if consolidation by vibration is no longer effective.
- This work agrees with Malisch and Suprenant and with Bury et. al. on the C403 penetration resistance at which time a worker's boot print is $6\ mm$ ($1/2in.$ deep).

- Any time at which a footprint can be impressed in the concrete it can be removed or restored with the float if applied soon enough and aggressively enough.
- In any discussions of penetration resistance and associated setting behavior it is essential that it be clear whether the pressures debated were obtained from C403 mortar or from the concrete surface (foot pressure, for example.)
- It is doubtful that the reference to "Initial Setting" in ACI 347 is a literal reference to ASTM C403.
- ASTM C403 method is useful for quantifying setting-type behavior, but the criteria for initial and final set do not necessarily coincide with other common interpretations of those same terms.

6.10 Appendix

6.10.1 Pressure Associated with Making a Footprint on the Surface of Concrete

The contact pressure between a worker's boot and the concrete surface varies somewhat as a function of the style of boot, type and depth of tread, how a worker actually steps on the fresh concrete to include dynamic effects and viscoplastic response of the concrete, and ultimately the stiffness of the concrete. In this study, the static foot pressure (the weight of a worker (first-named author) divided by the net area of a single footprint was measured (Lee was standing on

one foot only, as if walking). The net area of the footprint also depends on the depth of indentation any time the sole of the boot has a texture or deep tread, as shown in Figures 6.1 (a), (b), and (c). These figures were generated from image analysis of digital photographs of the footprints in the concrete surface.

The footprint represented by Figure 6.1 (a) was more than $6\ mm$ ($1/4\ in$) deep ("Level 1" criteria) and was pressed into the fresh concrete at about 2 hours after batching when the C403 mortar penetration resistance was about $103\ kPa$ ($15\ psi$) (about 2–1/2 hours before C403 initial setting time of 4–1/2 hours). Because the concrete was soft, the sole of the boot penetrated to the full depth of the treads so that the net area in contact with the concrete (and supported by the concrete) was equal to the full gross area of the sole of the boot $19,700\ mm^2$ ($30.5\ in^2$). The boot/concrete contact pressure was measured to be $35.2\ kPa$ ($5.1\ psi$).

The footprint represented by Figure 6.1 (b) was more than $3.2\ mm$ ($1/8\ in$) deep ("Level 2" criteria) and was pressed into the fresh concrete at about 3–1/2 hours after batching when the C403 mortar penetration resistance was about $1.4\ MPa$ ($200\ psi$) (still about 1 hour before C403 initial setting time). Because the concrete was stiffer and with a higher penetration resistance (analogous to a greater "soil bearing capacity," the concrete was indented only under the ball of the foot and the heel, for a net area $14,500\ mm^2$ ($22.5\ in^2$). Measured contact pressure was $48.3\ kPa$ ($7.0\ psi$).

Finally, the footprint represented by Figure 6.1 (c) was less than $3.2\ mm$ ($1/8\ in$) deep ("level 3" criteria) and was pressed into the fresh concrete at about 5 hours after batching when the C403 mortar penetration resistance was about $8.3\ MPa$ ($1200\ psi$) (about 1/2 hour after C403 initial setting time, but still 1/2

hour before C403 final setting time). Because the concrete was much stiffer with an even higher "soil bearing capacity," the concrete was indented only under the ball of the foot and the heel and not into the spaces between the treads, for a net area $11,400\ mm^2$ ($17.7\ in^2$). Measured contact pressure was $60.7\ kPa$ ($8.8\ psi$).

It is interesting to note that at the instant a worker steps onto the concrete, however gently and approximately flat to the concrete surface, the instantaneous contact pressure is on the order of that shown in Figure 1c. If the concrete is rigid enough to bear that pressure, a shallow indentation is made over a net area that is less than the gross are of the sole of the boot. If, however, the concrete cannot support that pressure the boot sinks deeper, and the net contact area increases until the resulting pressure can be sustained by the concrete. At this point further short-term penetration is prevented.

As introduced above, further complications include the time-dependent effects of how fast the worker is walking, and whether the foot is carefully and deliberately placed down flat to the concrete surface. While it also seems obvious that the average contact pressure should be determined on the basis of full body weight divided by the area of both feet combined, that is actually only valid if the worker is lifted up and gently placed on the concrete. Otherwise, in the action of walking, full body weight (plus dynamic effects) is applied to the area of only one foot. The resulting average pressures reported above are about twice the value reported by Suprenant and Malisch [95], and further inspection of their work reveals use of the combined indented area of both feet. Accounting for this, the single-foot pressure for Lee therefore ranges from $35.2\ kPa$ to $60.7\ kPa$ (5.1 to $8.8\ psi$), the lower bound for Hover is $33.8\ kPa$ ($4.9\ psi$), and

the "single foot" value taken from Malisch and Suprenant is $45.5\ kPa$ ($6.6\ psi$). That these values are all in the same range for 3 different "workers" is actually not surprising, as there is a general correspondence between shoe size and body weight, which is a fundamental principle of forensic criminology [122, 123].

BIBLIOGRAPHY

[1] C. H. Lautz, Estimating compressive strength and thickness of concrete based on surface temperature, Master's thesis, Cornell University, 2004.

[2] C. H. Lee, K. C. Hover, A. Lee, Difference in Setting Behavior between Prepared and Sieved Mortars in the C403 Time of Setting Test, Journal of Testing and Evaluation (In Press) .

[3] T. M. Kelly, Setting Time, in: Significance of Tests and Properties of Concrete and Concrete-Making Materials, ASTM, 102–115, 1966.

[4] C.-W. Chung, M. Mroczek, I.-Y. Park, L. J. Struble, On the Evaluation of Setting Time of Cement Paste Based on ASTM C403 Penetration Resistance Test, Journal of Testing and Evaluation 38 (5) (2010) 1–7.

[5] S. J. Barnett, M. N. Soutsos, S. G. Millard, J. H. Bungey, Strength Development of Mortars containing ground granulated blast-furnace slag: Effect of curing temperature and determination of apparent activation energies, Cement and Concrete Research 36 (3) (2007) 434–440.

[6] G. W. Jones, S. J. Chapman, Modeling Growth in Biological Materials, SIAM Review 54 (1) (2012) 52–118.

[7] Q. Paris, The von Liebig Hypothesis, American Journal of Agricultural Economics 74 (4) (1992) 1019–1028.

[8] J. W. Bullard, H. M. Jennings, R. A. Livingston, A. Nonat, G. W. Scherer, J. S. Schweitzer, K. L. Scrivener, J. J. Thomas, Mechanisms of Cement Hydration, Cement and Concrete Research 41 (12) (2011) 1208–1223.

[9] L. V. Bertalanffy, Quantitative Laws in Metabolism and Growth, The Quarterly Review of Biology 32 (3) (1957) 217–231.

[10] L. V. Pienaar, K. J. Turnbull, The Chapman-Richards Generalization of Von Bertalanffy's Growth Model for Basal Area Growth and Yield in Even-Aged Stands, Forest Science 19 (1) (1973) 2–22.

[11] K. Alagaraja, A. G. Jhingran, Application of Von Bertalanffy's Growth Model to Setipinna Phasa (Hamilton) When Growth is Allometric, Aquaculture 9 (1976) 181–186.

[12] F. Martínez-Jerónimo, Description of the individual growth of Daphnia magna (Crustacea: Cladocera) through the von Bertalanffy growth equation. Effect of photoperiod and temperature, Limnology 13 (1) (2012) 65–71.

[13] V. G. Vaidya, F. J. A. JR., Evaluation of Some Mathematical Models for Tumor Growth, International Journal of Bio-Medical Computing 13 (1) (1982) 19–35.

[14] E. M. Zullinger, R. E. Ricklefs, K. H. Redford, Fitting Sigmoidal Equations to Mammalian Growth Curves, Journal of Mammalogy 65 (4) (1984) 607–636.

[15] F. J. Richards, A Flexible Growth Function for Empirical Use, Journal of Experimental Botany 10 (29) (1959) 290–300.

[16] E. Tjørve, K. M. C. Tjørve, A Unified Approach to the Richards-model Family for Use in Growth Analysis: Why we need only two model forms, Journal of Theoretical Biology 267 (3) (2010) 417–425.

[17] Y. D. Marinakis, Forecasting Technology Diffusion with the Richards Model, Technological Forecasting & Social Change 79 (1) (2012) 172–179.

[18] C. J. Bernhardt, Hardening of Concrete at Different Temperatures, in: Proceedings RILEM Symposium on Winter Concreting, Danish National Institute of Building Research, Copenhagen, 3–20, 1956.

[19] A. International, ASTM C 1074-11: Standard Practice for Estimating Concrete Strength by the Maturity Method, ASTM International, PA 19428-2959, 2011.

[20] F. Hansen, P., J. Pedersen, Maturity computer for controlled curing and hardening of concrete, Nordisk Betong (1977) 19–34.

[21] S. Arrhenius, Über die Reaktionsgeschwindigkeit bei der Inversion von Rohrzucker durch Säuren, Zeitschrift für Physikalische Chemie 4 (1889) 226.

[22] G. Chanvillard, L. D'Aloia, Concrete Strength Estimation at Early Ages: Modification of the Method of Equivalent Age, ACI Materials Journal 94 (6) (1997) 520–530.

[23] J. K. Kim, S. H. Han, K. M. Lee, Estimation of compressive strength by a new apparent activation energy function, Cement and Concrete Research 31 (2) (2001) 217–225.

[24] J. Zhang, D. Cusson, P. Monteiro, J. Harvey, New perspectives on Maturity Method and Approach for High Performance Concrete Applications, Cement and Concrete Research 38 (12) (2008) 1438–1446.

[25] P. Atkins, J. de Paula, Atkins' Physical Chemistry, Oxford University Press, 8th edition edn., 2006.

[26] M. Peleg, M. D. Normand, M. G. Corradini, The Arrhenius Equation Revisited, Critical Reviews in Food Science and Nutrition 52 (9) (2012) 830–851.

[27] J. V. Li, S. W. Johnston, Y. Yan, D. H. Levi, Measuring temperature-dependent activation energy in thermally activated processes: A 2D Arrhenius plot method, Review of Scientific Instruments 81 (3) (2010) 033910.

[28] M. Mozurkewich, S. W. Benson, Negative Activation Energies and Curved Arrhenius Plots. 1. Theory of Reactions over Potential Wells, Journal of Physical Chemistry 88 (25) (1984) 6429–6435.

[29] P. J. H. Sharpe, D. W. Demichele, Reaction Kinetics of Poikilotherm Development, Journal of Theoretical Biology 64 (4) (1977) 649–670.

[30] R. C. Tolman, Statistical Mechanics Applied to Chemical Kinetics, Journal of the Americal Chemical Society 42 (12) (1920) 2506–2528.

[31] A. K. Galwey, M. E. Brown, Application of the Arrhenius equation to solid state kinetics: can this be justified, Thermochimica Acta 386 (1) (2002) 91–98.

[32] L. Huang, A. Hwang, J. Phillips, Effect of Temperature on Microbial Growth Rate-Mathematical Analysis: The Arrhenius and Eyring-Polanyi Connections, Journal of Food Science 76 (8) (2011) E553–E560.

[33] B. Lothenbach, F. Winnefeld, C. Alder, E. Wieland, P. Lunk, Effect of temperature on the pore solution, microstructure and hydration products of Portland cement pastes, Cement and Concrete Research 37 (4) (2007) 483–491.

[34] B. Lothenbach, T. Matschei, G. Mőschner, F. P. Glasser, Thermodynamic modelling of the effect of temperature on the hydration and porosity of Portland cement, Cement and Concrete Research 38 (1) (2008) 1–18.

[35] J. I. Escalante-Garcia, J. H. Sharp, Effect of temperature on the hydration of the main clinker phases in Portland cements: Part I, Neat cements, Cement and Concrete Research 28 (9) (1998) 1245–1257.

[36] F. Vodák, F. Trtík, O. Kapičková, Š. Hošková, P. Demo, The effect of temperature on strength-porosity relationship for concrete, Construction and Building Materials 18 (7) (2004) 529–534.

[37] R. W. Nurse, Steam curing of concrete, Magazine of Concrete Research 2 (1) (1949) 79–88.

[38] A. G. A. Saul, Principles underlying the steam curing of concrete at atmospheric pressure, Magazine of Concrete Research 2 (6) (1951) 127–140.

[39] V. M. Malhotra, N. J. Carino, Handbook on Nondestructive Testing of Concrete, CRC Press, 2nd edn., 2004.

[40] R. K. Niven, $q-$Exponential structure of arbitrary-order reaction kinetics, Chemical Engineering Science 61 (11) (2006) 3785–3790.

[41] J. J. Thomas, J. J. Biernacki, J. W. Bullard, S. Bishnoi, J. S. Dolado, G. W. Scherer, A. Luttge, Modeling and simulation of cement hydration kinetics and microstructure development, Cement and Concrete Research 41 (12) (2011) 1257–1278.

[42] S. Bishnoi, K. L. Scrivener, Studying nucleation and growth kinetics of alite hydration using μic, Cement and Concrete Research 39 (10) (2009) 849–860.

[43] D. P. Bentz, P. V. Coveney, E. J. Garboczi, M. F. Kleyn, P. E. Stutzman, Cellular automaton simulations of cement hydration and microstructure development, Modelling and Simulation in Materials Science and Engineering 2 (4) (1994) 783–808.

[44] S. Garrault, A. Nonat, Hydrated Layer Formation on Tricalcium and Dicalcium Silicate Surfaces: Experimental Study and Numerical Simulations, Langmuir 17 (26) (2001) 8131–8138.

[45] J. W. Bullard, A Determination of Hydration Mechanisms for Tricalcium Silicate Using a Kinetic Cellular Automaton Model, Journal of the American Ceramic Society 91 (7) (2008) 2088–2097.

[46] J. W. Bullard, E. Enjolras, W. L. George, S. G. Satterfield, J. E. Terrill, A parallel reaction-transport model applied to cement hydration and microstructure development, Modelling and Simulation in Materials Science and Engineering 18 (2) (2010) 1–16.

[47] P. W. Brown, J. Pommersheim, G. Frohnsdorff, A Kinetic Model for the Hydration of Tricalcium Silicate, Cement and Concrete Research 15 (2) (1985) 35–41.

[48] M. S. Meddah, S. Zitouni, S. Belâabes, Effect of content and particle size distribution of coarse aggregate on the compressive strength of concrete, Construction and Building Materials 24 (4) (2010) 505–512.

[49] M. Rößler, I. Odler, Investigations on the Relationship between Porosity, Structure and Strength of Hydrated Portland Cement Pastes I. Effect of Porosity, Cement and Concrete Research 15 (2) (1985) 320–330.

[50] I. Odler, M. Rößler, Investigations on the Relationship between Porosity, Structure and Strength of Hydrated Portland Cement Pastes II. Effect of Pore Structure and of Degree of Hydration, Cement and Concrete Research 15 (3) (1985) 401–410.

[51] P. Klieger, Effect of Mixing and Curing Temperature on Concrete Strength, ACI Journal Proceedings 54 (12) (1958) 1063–1081.

[52] S. H. Kosmatka, B. Kerkhoff, W. C. Panarese, Design and Control of Concrete Mitures, Portland Cement Association, Skokie, Illinois, 14th edn., 2002.

[53] S. Mindess, J. F. Young, D. Darwin, Concrete, Pearson Education, Inc., NJ 07458, 2nd edn., 2003.

[54] R. G. Duggleby, Regression Analysis of Nonlinear Arrhenius Plots: An Empirical Model and A Computer Program, Computers in Biology and Medicine 14 (4) (1984) 447–455.

[55] N. J. Carino, The Maturity Method: Theory and Application, Cement, Concrete, and Aggregates 6 (2) (1984) 61–73.

[56] H. Eyring, The Activated Complex in Chemical Reactions, Journal of Chemical Physics 3 (2) (1935) 107–115.

[57] W. F. K. Wynne-Jones, H. Eyring, The Absolute Rate of Reactions in Condensed Phases, Journal of Chemical Physics 3 (8) (1935) 492–502.

[58] A. L. Petrou, The Free Energy of Activation as the critical factor in geochemical process, Chemical Geology 308–309 (2012) 50–59.

[59] K. J. Laidler, A Glossary of Terms Used in Chemical Kinetics, Including Reaction Dynamics, Pure & Applied Chemistry 68 (1) (1996) 149–192.

[60] W. Stiller, Arrhenius Equation and Non-Equilibrium Kinetics, Teubner Verlagsgesellschaft, Leipzig, Berlin, 1989.

[61] P. H. Fang, Kohlrausch and Arrhenius analysis for some solid and liquid materials, Journal of Non-Crystalline Solids 354 (10–11) (2008) 989–993.

[62] M. I. Ojovan, K. P. Travis, R. J. Hand, Thermodynamic parameters of bonds in glassy materials from viscosity-temperature relationships, Journal of Physics: Condensed Matter 19 (41) (2007) 1–12.

[63] G. B. West, J. H. Brown, B. J. Enquist, A general model for ontogenetic growth, Nature 413 (2001) 626–631.

[64] E. A. Mitscherlich, Das Gesetz vom Minimum und das Gesetz des abnehmenden Bodenertrages, Landwirtschaftliche Jahrbücher 38 (1909) 537–552.

[65] R Core Team, R: A Language and Environment for Statistical Computing, R Foundation for Statistical Computing, Vienna, Austria, URL `http://www.R-project.org/`, 2013.

[66] H. Akaike, A New Look at the Statistical Model Identification, IEEE Transactions on Automatic Control 19 (6) (1974) 716–723.

[67] A. Damasceni, L. Dei, E. Fratini, F. Ridi, S.-H. Chen, P. Baglion, A Novel Approach Based on Differential Scanning Calorimetry Applied to the Study of Tricalcium Silicate Hydration Kinetics, Journal of Physical Chemistry B 106 (44) (2002) 11572–11578.

[68] F. Ridi, luigi Dei, E. Fratini, S.-H. Chen, P. Baglioni, Hydration Kinetics of Tri-calcium Silicate in the Presence of Superplasticizers, Journal of Physical Chemistry B 107 (4) (2003) 1056–1061.

[69] L. D'Aloia, G. Chanvillard, Determining the "apparent" activation energy of concrete E_a-Numerical simulations of the heat of hydration of cement, Cement and Concrete Research 32 (8) (2002) 1277–1289.

[70] H. Kada-Benameur, E. Wirquin, B. Duthoit, Determination of apparent activation energy of concrete by isothermal calorimetry, Cement and Concrete Research 30 (2) (2000) 301–305.

[71] V. Aquilanti, K. C. Mundim, S. Cavalli, D. D. Fazio, A. Aguilar, J. M. Lucas, Exact activation energies and phenomenological description of quantum tunneling for model potential energy surfaces. The $F + H_2$ reaction at low temperature, Chemical Physics 398 (4) (2012) 186–191.

[72] H. S. Bamufleh, Y. A. Alhamed, M. A. Daous, Furfural from midribs of date-palm trees by sulfuric acid hydrolysis, Industrial Crops and Products 42 (2013) 421–428.

[73] N. J. Carino, H. S. Lew, The Maturity Method: From Theory to Application, in: P. C. Chang (Ed.), 2001 Structures Congress & Exposition, American Society of Civil Engineers, Reston, Virginia, 1–19, 2001.

[74] N. J. Carino, R. C. Tank, Maturity Functions for Concretes Made with Various Cements and Admixtures, ACI Materials Journal 89 (2) (1992) 188–196.

[75] H. Bisswanger, Enzyme Kinetics, Wiley-VCH Verlag GmbH & Co. KGaA, 2nd edn., 2008.

[76] R. D. Holtz, W. D. Kovacs, An Introduction to Geotechnical Engineering, Prentice-Hall Civil Engineering and Engineering Mechanics Series, New Jersey, USA, 1981.

[77] J. M. Plowman, Maturity and the strength of concrete, Magazine of Concrete Research 8 (22) (1956) 13–22.

[78] R. A. Olson, B. J. Christensen, R. T. Coverdale, S. J. Ford, G. M. Moss, H. M. Jennings, T. O. Mason, E. J. Garboczi, Interpretation of the impedance spectroscopy of cement paste via computer modelling, Journal of Materials Science 30 (20) (1995) 5078–5086.

[79] H. F. W. Taylor, Cement Chemistry, Thomas Telford Publishing, New York, 2nd edn., 1997.

[80] A. International, ASTM C 403-08: Standard Test Method for Time of Setting of Concrete Mixtures by Penetration Resistance, ASTM International, PA 19428-2959, 2008.

[81] L. H. Tuthill, W. A. Cordon, Properties and Uses of Initially Retarded Concrete, ACI Journal Proceedings 52 (11) (1955) 273–286.

[82] A. International, ASTM D 1558-10: Standard Test Method of Moisture Content Penetration Resistance Relationships of Fine-Grained Soils, ASTM International, PA 19428-2959, 2010.

[83] A. International, ASTM E11-09: Standard Specification for Woven Wire Test Sieve Cloth and Test Sieves, ASTM International, PA 19428-2959, 2009.

[84] A. International, ASTM C 172/C 172M-10: Standard Practice for Sampling Freshly Mixed Concrete, ASTM International, PA 19428-2959, 2010.

[85] A. International, Research Report C09-1032: Interlaboratory Study to Establish Precision Statements for: ASTM C403/C403 M, Test Method for Time of Setting of Concrete Mixtures by Penetration Resistance and Proposed ASTM C WK2302-as of January 2007, Test Method for Determination of Setting Time of Concrete by the Temperature Method, Tech. Rep., ASTM International, PA 19428-2959, 2007.

[86] J. J. Assaad, J. Harb, E. Chakar, Relationships Between Key ASTM Test Methods Determined on Concrete and Concrete-Equivalent-Mortar Mixtures, Journal of ASTM International 6 (3) (2009) 1–13.

[87] A. International, ASTM C 127-08: Standard Test Method for Density, Relative Density (Specific Gravity), and Absorption of Fine Aggregate, ASTM International, PA 19428-2959, 2008.

[88] A. International, ASTM C 128-08: Standard Test Method for Density, Relative Density (Specific Gravity), and Absorption of Coarse Aggregate, ASTM International, PA 19428-2959, 2008.

[89] A. International, ASTM C 136-06: Standard Test Method for Sieve Analysis of Fine and Coarse Aggregates, ASTM International, PA 19428-2959, 2006.

[90] A. International, ASTM C33/C33M-13: Standard Specification for Concrete Aggregates, ASTM International, PA 19428-2959, 2013.

[91] ASTM, ASTM C 305-13: Standard Practice for Mechanical Mixing of Hydraulic Cement Pastes and Mortars of Plastic Consistency, ASTM International, PA 19428-2959, 2013.

[92] ASTM, ASTM C 192-07: Standard Practice for Making and Curing Concrete Test Specimens in the Laboratory, ASTM International, PA 19428-2959, 2007.

[93] S. Popovics, Fundamentals of Portland Cement Concrete: A Quantitative Approach, John Wiley & Sons, INC, 1982.

[94] J. D. Abel, K. C. Hover, Field Study of the Setting Behavior of Fresh Concrete, Journal of Cement, Concrete and Aggregates 22 (2) (2000) 95–102.

[95] B. A. Suprenant, W. R. Malisch, Diagnosing slab delaminations: The role of top-down stiffening, Concrete Construction 43 (3) (1998) 277–283.

[96] T. C. Powers, The Properties of Fresh Concrete, John Wiley & Sons, INC., 1968.

[97] D. C. Montgomery, Design and Analysis of Experiments, John Wiley & Sons, INC, USA, 5th edn., 2001.

[98] T. C. Powers, The Air Requirement of Frost-Resistant Concrete, in: Proceedings of the Twenty-Ninth Annual Meeting of the Highway Research Board, 203–211, 1949.

[99] A. M. Neville, J. J. Brooks, Concrete Technology, Longman Scientific & Technical / John Wiley, Essex, England, 1987.

[100] A. C. 302, Guide for Concrete Floor and Slab Construction, American Concrete Institute, Michigan, 1994.

[101] A. C. 308, Guide to Curing Concrete, American Concrete Institute, Michigan, 1991.

[102] A. C. 309, Guide for Consolidation of Concrete, American Concrete Institute, Michigan, 1995.

[103] A. C. 347, Guide to Formwork for Concrete, American Concrete Institute, Michigan, 2004.

[104] A. García, D. Castro-Fresno, J. A. Polanco, Evolution of penetration resistance in fresh concrete, Cement and Concrete Research 38 (5) (2008) 649–659.

[105] N. Robeyst, E. Gruyaert, C. U. Grosse, N. D. Belie, Monitoring the setting of concrete containing blast-furnace slag by measuring the ultrasonic p-wave velocity, Cement and Concrete Research 38 (10) (2008) 1169–1176.

[106] N. Robeyst, C. U. Grosse, N. D. Belie, Measuring the change in ultrasonic p-wave energy transmitted in fresh mortar with additives to monitor the setting, Cement and Concrete Research 39 (10) (2009) 868–875.

[107] ACI, ACI Concrete Terminology, American Concrete Institute, Michigan, 2013.

[108] ASTM, ASTM C 191-08: Standard Test Method for Time of Setting of Hydraulic Cement by Vicat Needle, ASTM International, PA 19428-2959, 2008.

[109] ASTM, ASTM C 266-08: Standard Test Method for Time of Setting of Hydraulic-Cement Paste by Gillmore Needles, ASTM International, PA 19428-2959, 2008.

[110] S. Popovics, Material aspects of concrete consolidated by vibration, Materials and Structures 5 (3) (1972) 143–150.

[111] B. A. Suprenant, W. R. Malisch, The True Window of Finishability: Do finishers have adequate quidelines for hitting the gap between premature and late finishing?, Concrete Construction 43 (10).

[112] C. H. Lee, K. C. Hover, A. Lee, The effects of sieving and paste content on the setting behavior of mortars, Cement and Concrete Composites (In Press) .

[113] B. A. Suprenant, W. R. Malisch, Where to place the vapor retarder, Concrete Construction 43 (5).

[114] M. A. Bury, J. R. Bury, D. Martin, Testing Effects of New Admixtures on Concrete Finishing, Concrete International 16 (1) (1994) 26–31.

[115] B. J. Christensen, Time of Setting, in: J. F. Lamond, J. H. Pielert (Eds.), Significance of Tests and Properties of Concrete and Concrete-Making Materials, ASTM, 86–98, 2006.

[116] V. H. Dodson, Time of Setting, in: P. Klieger, J. F. Lamond (Eds.), Significance of Tests and Properties of Concrete and Concrete-Making Materials, ASTM, 77–87, 1994.

[117] V. Dodson, Concrete Admixtures, Van Nostrand Reinhold, New York, NY 10003, 1990.

[118] J. E. W. Scripture, Setting Time, in: Significance of Tests and Propeties of Concrete and Concrete Aggregates, ASTM, 53–60, 1955.

[119] L. Struble, T.-Y. Kim, H. Zhang, Setting of Cement and Concrete, Cement, Concrete, and Aggregates 23 (2) (2001) 88–93.

[120] M. Polivka, A. Klein, Effect of Water-Reducing Admixtures and Set-Retarding Admixtures as Influenced by Portland Cement Composition, in: Symposium on Effect of Water-Reducing Admixtures and Set-Retarding Admixtures on Properties of Concrete, ASTM, 124–139, 1959.

[121] BSI, Concrete admixtures Specification for accelerating admixtures, retarding admixtures and water reducing admixtures, British Standards Institution, 1982.

[122] D. Atamturk, I. Duyar, Age-Related Factors in the Relationship Between Foot Measurements and Living Stature and Body Weight, Journal of Forensic Sciences 53 (6) (2008) 1296–1300.

[123] H. Ozden, Y. Balci, C. Demirüstü, A. Turgut, M. Ertugrul, Stature and sex estimate using foot and shoe dimensions, Forensic Science International 147 (2–3) (2005) 181–184.